Manuel Maria Brás Pereira Mascarenhas

Licenciado em Ciências da Engenharia Electrotécnica e de Computadores

Speed Control of Induction Machine based on Direct Torque Control Method

Dissertação para obtenção do Grau de Mestre em

Engenharia Electrotécnica e de Computadores

Orientador: Prof. Doutor Stanimir Stoyanov Valtchev
Faculdade de Ciências e Tecnologia,
Universidade Nova de Lisboa

Júri:

Presidente: Prof. Doutor Fernando José Almeida Vieira do Coito

Arguente: Prof. Doutor Luis Filipe Figueira de Brito Palma

Vogal: Prof. Aurelian Craciunescu

FACULDADE DE CIÊNCIAS E TECNOLOGIA
UNIVERSIDADE NOVA DE LISBOA

Março 2013

Speed Control of Induction Machine based on Direct Torque Control Method

Acknowledgements

To my supervisor, Prof. Dr. Stanimir Stoyanov Valtchev, I am grateful for the opportunity of carrying out this work and for his academic excellence in guiding this dissertation.

To my family I would like to thank for the friendship, the love and the support they have always given me.

To my friends I would like to express my appreciation for the strength they gave me, for the words of support and for all the moments we share.

Resumo

Os inversores multinivel têm sido alvos de muita atenção no últimos anos e são considerados como uma das melhores escolhas para uma ampla variedade de aplicações de média tensão. Estes permitem comutações com tensões substancialmente reduzidas e uma melhoria do espectro harmónico sem ser necessário a ligação em série de vários dispositivos, o que é a grande vantagem destas estruturas.

A utilização inversores multinivel contribui para a melhoria dos desempenhos do controlo da máquina de indução. Na verdade, o uso de inversores de três niveis (ou inversor multinível) associado ao controlo DTC pode contribuir para uma maior redução de distorções harmónicas , da ondulação do torque e têm um alto nível de tensão na saída.

Uma variação de DTC-SVM com um inversor Neutral Point Clamped é proposta e discutida nesta tese. O objetivo deste projeto é estudar, avaliar e comparar, através de simulações, o DTC e o DTC-SVM proposto quando aplicado a máquinas de indução. As simulações foram realizadas utilizando o programa de simulações MATLAB / SIMULINK. A avaliação foi feita com base no desempenho da unidade, que inclui binário dinâmico e as respostas do fluxo, a viabilidade e a complexidade dos sistemas.

Palavras-chave: Máquina de indução, Inversor multinivel, Neutral Point Clamped, Direct Torque Control, Space Vector Modulation.

Abstract

Multi-level converters have been receiving attention in the recent years and have been proposed as the best choice in a wide variety of medium voltage applications. They enable a commutation at substantially reduced voltages and an improved harmonic spectrum without a series connection of devices, which is the main advantage of a multi-level structure.

The use of multi-level inverters contributes to the performances amelioration of the induction machine control. In fact, the use of three level inverter (or multilevel inverter) associated with DTC control can contribute to more reducing harmonics and the ripple torque and to have a high level of output voltage.

A variation of DTC-SVM with a three level neutral point clamped inverter is proposed and discussed in the literature. The goal of this project is to study, evaluate and compare the DTC and the proposed DTC-SVM technique when applied to induction machines through simulations. The simulations were carried out using MATLAB/ SIMULINK simulation package. Evaluation was made based on the drive performance, which includes dynamic torque and flux responses, feasibility and the complexity of the systems.

Keywords: Induction Machine, Multi-level Inverter, Neutral Point Clamped, Direct Torque Control, Space Vector Modulation.

Contents

List of Figures

List of Tables

ABBREVIATIONS

2L	Two Level
3L	Three Level
AC	Alternating Current
ADC	Analog-to-Digital Converter
DAC	Digital-to-Analog Converter
DC	Direct Current
DSP	Digital Signal Processor
DTC	Direct Torque Control
EMI	Electromagnetic Interference
EV	Electric Vehicle
FLC	Flying Capacitor
FOC	Field Oriented Control
FFT	Fast Fourier Transformation
GTO	Gate Turn-off Thyristor
I/O	Input/Output
IM	Induction Machine
IGBT	Insulated-Gate Bipolar Transistor
KCL	Kirchhoff's Current Law
KVL	Kirchhoff's Voltage Law
NPC	Neutral Point Clamped
PI	Proportional-Integral
PID	Proportional-Integral-Derivative
PMSM	Permanent Magnet Synchronous Machine
PWM	Pulse Width Modulation
SCHB	Series Connected H-Bridge
SISO	Single Input Single Output
SPWM	Sine Wave Pulse Width Modulation
SVM	Space Vector Modulation
THD	Total Harmonic Distortion
VSC	Voltage Source Converter
VSI	Voltage Source Inverter

SYMBOLS

Variable	Meaning	Units
S_{ki}	Switching state	
Y_k	State of inverter arm , (k=1,2,3)	
$(E_{off} + E_{on})$	Switch-on and switch-off energy	W
$\vec{\psi}_s$	Stator flux	Wb
$\hat{I}$	Peak current	A
I_0	Output current	A
I_{avg}	Average current	A
I_{rms}	Root mean square current	A
K_p	Proportional gain in the PI controller	
K_p	Integral gain in the PI controller	
L_m	Magnetizing inductance	H
L_s	Stator inductance	H
N_{se}	Stator windings number of curves	
P_{cap}	Capacitor losses	W
P_{cond}	Conduction losses	W
P_{loss}	Total converter losses	W
P_{sw}	Switching losses	W
R_s	Stator resistance	Ω
T_{em}	Electromagnetic torque	N.m
T_s	Sampling time	S
U_{Ci}	Capacitors voltage (i=1,2)	V
U_f	Forward voltage	V
U_i	Output voltage in arm I , (i=1,2,3)	V
V_{DC}	DC Source voltage	V
$cos\,\varphi$	Power factor	
d_j	Dwell time (j=1,2,3)	S
$f_{as}(\theta, t)$	Magnetomotive force	A
f_s	Sampling frequency	Hz
f_{sw}	Switching frequency	Hz
i_{dr}	Rotor current in the real axis	A
i_{ds}	Stator current in the real axis	A
i_{qr}	Rotor current in the imaginary axis	A
i_{qs}	Stator current in the imaginary axis	A
r_f	Forward resistance	Ω
u_{ds}	Stator voltage in the real axis	V
u_{qs}	Stator voltage in the imaginary axis	V
$u_{\alpha r}$	Rotor voltage in the real axis (stationary)	V
$u_{\beta r}$	Rotor voltage in the imaginary axis (stationary)	V
z_0	Impedance of the DC voltage	Ω
α_s	Angle between real axis and stationary system	Rad
ρ_s	Angles of the flux linkage and the stator current in stationary frame	Rad
Ixs	Stator phase currents (x=a,b,c)	A
M	Modulation index	
p	Number of pole pairs	
θ	Spatial angle	Rad
ωs	Angular speed	Rad/s

α	Angle between the vectors of the spatial flux linkage and stator current	Rad
σ	Standard deviation	
φ	Phase difference between output current and voltage	Rad

1

INTRODUCTION

This thesis approaches the theme of resorting to a multilevel power converter to drive a system with adjustable speed of an induction machine, which could serve as a basis for a future traction block of an electric vehicle.

1.1 Motivation

Due to issues ranging from environmental concerns to fluctuating oil prices continue to push consumers from combustion engines toward alternatives. It is time to restructure the global economy with an intensive addition of renewable sources of energy and solutions that make use of this energy. The electric vehicle can contribute to build a future with sustainable development. Through research and technological advances, electric powered cars are capable of becoming a feasible alternative for the combustion engine vehicles.

The development of electric vehicles will offer many opportunities and challenges to the power electronics industry, especially in the main traction drive. The advances in improved efficiency are driven by semiconductor development, better controls, cooling, new materials etc. With multilevel converters the number of switch functions is increased, power ratings can be increased, while synthesizing almost a sinusoidal voltage waveform with little or no filter requirements. As multilevel converters provide redundancy and has a high reliability, low losses, while the component cost reduce even further, while steel and copper prices increase.

The main objectives of this thesis are to perform a study of the direct torque control with and without space vector modulation of an induction machine, using a neutral point clamped multilevel inverter. The specific goals of this thesis are:

- Survey of multilevel topologies;
- Modeling and simulation of neutral point clamped;
- Voltage and current total harmonic distortion analysis;
- Loss calculation;
- Steady and transient state simulation under different load scenarios.

1.2 Thesis Organization

Besides this introductory chapter this thesis is composed by five more chapters. In Chapter 2 the most relevant bibliographic concepts to this thesis are presented, including different control methods, a survey of multilevel inverters and their respective modulation.

Chapter 3 is devoted to the neutral point clamped voltage source inverter and its characteristics. Besides the mathematical model of the inverter, voltage and current harmonic distortion is verified, as well as loss calculations of two converters available in the market.

In Chapter 4 two kind of control schemes for an induction machine are presented, direct torque control with and without space vector modulation. Also, an analysis and synthesis of digital flux and torque estimators and respective controllers approach are given.

In Chapter 5 simulation results of both control schemes – direct torque control with and without space vector modulation- proposed and studied are presented.

In the sixth and last chapter, the results obtained previously, are discussed and the conclusions of this work are presented.

2

STATE OF ART

In this chapter is made a review of the most relevant concepts to the development of this thesis. The principal electric motors available to drive an electric vehicle and their control methods are compared. Also a survey of most common multi-level voltage source converters and their respective modulation is made.

2.1 Electrical Machines for Electric Vehicle

Electric vehicle need an electrical machine to transform electrical power to mechanical torque on the wheels. The electrical machine needs to be controlled accurately (control of speed and/or torque) and the only machine that initially could fulfill these demands was the DC motor. Due to high weight and a short lifetime the DC motor was gradually replaced by the induction machine (IM).

The induction machine is a robust, well-known device and, with the development of new power electronics (like the IGBT transistor), many new methods of controlling three phase machines have been developed. In order to increase the energy efficiency of the EV, all parts of it have to be very efficient and, as an alternative, machines of the permanent magnet type have become a serious challenger to the IM [6].

The following table lists the main benefits and drawbacks of different motor types.

Table 2.1 – Comparison of PMSM and IM

	PMSM	IM
Benefits	Smooth torque	High speed operation
	High efficiency	Low price
	High torque/volume	Simple construction
	Good heat dissipation	Durable
Drawbacks	Expensive	Complicated control
	Demagnetization of the magnets	Low efficiency with lighter loads

In vehicle drives, induction machines properly designed for the application can have efficiencies substantially higher than those of permanent magnet machines, even if the single point efficiency of the induction machine is lower than the single point efficiency of the permanent magnet.

The power density of permanent magnet machines together with the high cost of permanent magnets makes these machines less attractive for EV applications. The maintenance-free and low-cost induction machines became a good attractive alternative to many developers.

However, high-speed operation of induction machines is only possible with a penalty in size and weight. Three-phase squirrel cage-rotor induction motors are best suited to electric vehicle drive applications thanks to its well-known advantage of simple construction, reliability and low cost [1].

2.2 Control

The IM advantages have determined an important development of the electrical drives, with induction machine as the execution element, for all related aspects: starting, braking, speed reversal, speed change, etc. The dynamic operation of the induction machine drive system has an important role on the overall performance of the system of which it is a part. There are two fundamental directions for the induction motor control:

1. *Analogue*: direct measurement of the machine parameters (mainly the rotor speed), which are compared to the reference signals through closed control loops;
2. *Digital*: estimation of the machine parameters in the sensorless control schemes, with the following implementation methodologies:
    - Slip frequency calculation method;
    - Speed estimation using state equation;
    - Flux estimation and flux vector control;
    - Direct torque and flux control;
    - Observer-based speed sensorless control;
    - Model reference adaptive systems;
    - Kalman filtering techniques;
    - Sensorless control with parameter adaptation;
    - Neural network based sensorless control;
    - Fuzzy-logic based sensorless control.

Another classification of the control techniques for the induction machine is made by Holtz from the point of view of the controlled signal [2]:

1. Scalar control - These techniques are mainly implemented through direct measurement of the machine parameters.
2. Vector control -These techniques are realized both in analogue version (direct measurements) and digital version (estimation techniques).

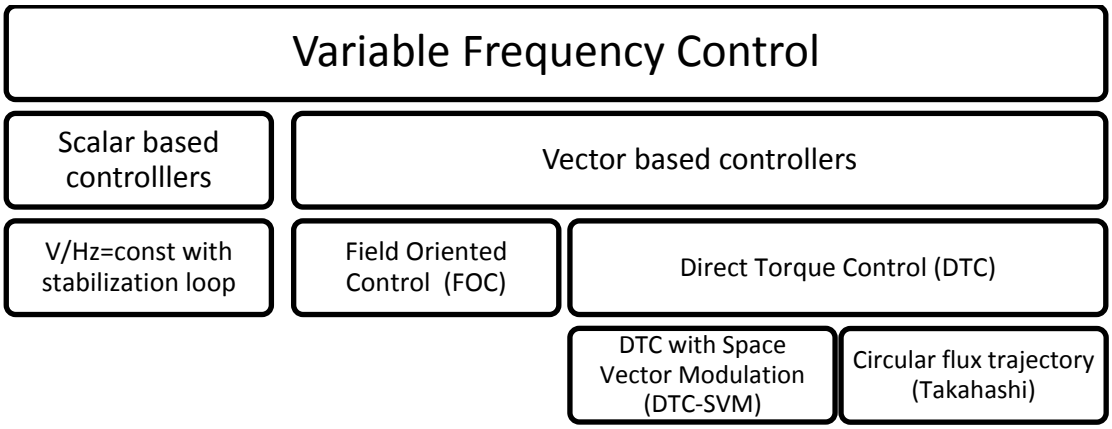

Figure 2.1- Holtz classification of control techniques

The scalar control is based on a relation valid for steady states, only the magnitude and frequency (angular speed) of voltage, currents, and flux linkage space vectors are controlled. Thus, the control system does not act on space vector position during transient. Therefore, this control is dedicated for application, where high dynamics is not demanded.

In search of a simpler and more robust high performance control system a new vector control called direct torque control (DTC) was developed. It allows direct control flux and torque quantities without inner current control loops. Using hysteresis controllers for flux and torque control loops made this control concept very fast and not complicated.

However, the main disadvantage of DTC is fast sampling time required and variable switching frequency, because of hysteresis based control loops. In order to eliminate above disadvantages and kept basic control rules of classical DTC, a new developed control technique called direct torque control with space vector modulator (DTC-SVM) has been introduced.

This control employed instead of hysteresis controller as for classical DTC, the PI controllers and a space vector modulator (SVM). It allows achieving fixed switching frequency, what considerably reduce switching losses as well as torque and current ripples. Also requirement of very fast sampling time is eliminated. Therefore, this method is subject of this thesis. In spite of many control strategies there isn't one which may be considered as standard solution.

2.2.1 Field Oriented Control

Field oriented control method, known popularly as vector control is widely used in modern industrial systems. The field oriented control method of the motor is realized for current components in dq rotating coordinate system [3].

In the field oriented control system a stator current d-component adjusts the rotor flux in the motor, while the combination of d and q- components adjusts the motor torque. By applying the decoupling block in the particular d and q control parts the control of flux and torque can be done independently.

2.2.2 Direct Torque Control

The field-oriented control is an attractive control method but it has a serious drawback: it relies heavily on precise knowledge of the motor parameters. The rotor time constant is particularly difficult to measure precisely, and to make matters worse it varies with temperature.

A more robust control method consists first in estimating the machine stator flux and electric torque in the stationary reference frame from terminal measurements.

The estimated stator flux and electric torque are then controlled directly by comparing them with their respective demanded values using hysteresis comparators. The outputs of the two comparators are then used as input signals of an optimal switching table [4],[7[,[8].

2.2.3 Direct Torque Control with Space Vector Modulation

The main disadvantage of DTC is that a fast sampling time is required and variable switching frequency, because of hysteresis based control loops. In order to eliminate these disadvantages and keep the basic control rules of classical DTC, a different control technique called direct torque control with space vector modulator (DTC-SVM) has been introduced [9].

When this method is employed, the hysteresis controllers and the look-up tables present in DTC are replaced by PI controllers and a space vector modulator, thus achieving a fixed switching frequency, reducing considerably the switching losses as well as torque and current ripples. Also the requirement of very fast switching time is eliminated [10].

In DTC with multi-level inverters there will be more voltage vectors available to control the flux and torque. Therefore, a smoother torque can be expected. However, more power switches are needed to achieve a lower ripple, which will increase the system cost and complexity.

According to the analysis, the DTC strategy is simpler to implement than the field oriented control method essentially because it does not require voltage modulators. Despite the undesired torque ripple introduced when using DTC, through multi-level inverters this effect can be minimized. Therefore, both DTC and DTC-SVM methods are subject of study in this thesis.

2.3 Voltage Source Multilevel Inverters

Multi-level converters have been receiving attention in the recent years and have been proposed as the best choice in a wide variety of medium voltage (MV) applications [11]. They enable a commutation at substantially reduced voltages and an improved harmonic spectrum without a series connection of devices, which is the main advantage of a multi-level structure.

Other advantages of these topologies are better output voltage quality, reduced electromagnetic interference (EMI) problems, and lower overall losses in some cases. However, today they have a limited commercial impact due to their disadvantages such as high control complexity and increased power semiconductor count when comparing the 2L-VSC with the 3L-NPC VSC.

Multilevel inverter structures are becoming increasingly popular for high power applications, because their switched output voltage harmonics can be considerably reduced by using several voltage levels while still switching at the same frequency. As well, higher input DC voltages can be used since semiconductors are connected in series for multilevel inverter structures, and this reduces the DC voltage each device must withstand [12],[13].

2.3.1 History

The concept of utilizing multiple small voltage levels to perform power conversion was presented by an MIT researcher over twenty years ago. Advantages of this multilevel approach include good power quality, good Electro-Magnetic Compatibility (EMC), low switching losses and high voltage capability. The main disadvantages of this technique are the larger number of semiconductor switches required than the 2-level solution and the capacitor banks or insulated sources needed to create the voltage steps on the DC busses [14].

The first topology introduced was the series H-bridge design. This was followed by the diode-clamped converter which utilizes a bank of series capacitors to split the DC bus voltage. The flying-capacitor (or capacitor clamped) topology followed diode-clamped after few years: instead of series connected capacitors, this topology uses floating capacitors to clamp the voltage levels. Several combinatorial designs have also emerged, implemented cascading the fundamental topologies; they are called hybrid topologies. These designs can create higher power quality for a given number of semiconductor devices than the fundamental topologies alone due to a multiplying effect of the number of levels, however, the complexity of the control in these topologies also increases [15].

The most interesting applications of these structures include renewable energy sources, electrical machines, electrical power distribution and power quality. However, given the significant price reduction of the power semiconductor and of the microprocessor is expected that the use of multilevel topologies also extends to the low power applications.

2.3.2 Concept

The concept of multilevel inverter consists in utilizing an array of series switching devices to perform the power conversion in a small increase of voltage steps by synthesizing the staircase voltage from several levels of DC capacitor voltages.

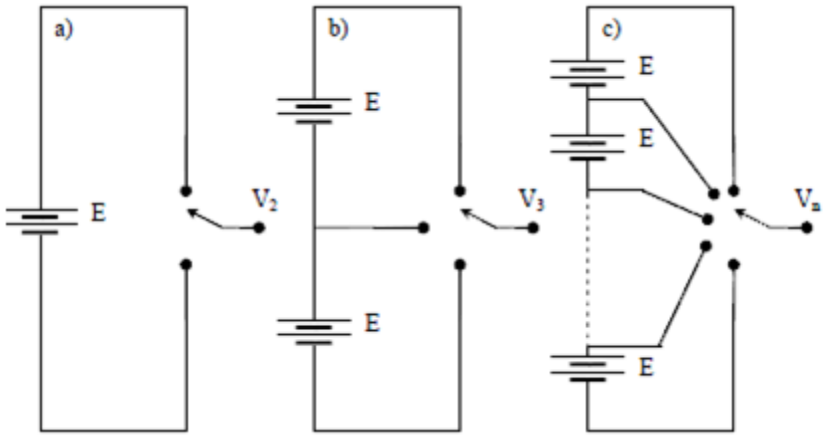

Figure 2.2 – Inverter phases. a) 2-level inverter, b) 3-level inverter, c) n-level inverter

Conventional two-level inverters, are mostly used today to generate an AC voltage from a DC source. The two-level inverter can only create two different output voltages for the load, $V_{DC}/2$ or $-V_{DC}/2$ (when the inverter is fed with V_{DC}). To build up an AC output voltage these two voltages are usually switched with PWM. Though this method is effective it creates harmonic distortions in the output voltage, EMI and high dv/dt. This may not always be a problem but for some applications there may be a need for a lower distortion in the output voltage.

Some of the most attractive features in general for multilevel inverters are that they can generate output voltages with very low distortion and dv/dt , generate smaller common-mode voltage and operate with lower switching frequency compared to the more conventional two-level inverters. With a lower switching frequency the switching losses can be reduced.

There are different kinds of topologies of multilevel inverters that can generate a stepped voltage waveform and that are suitable for different applications. By designing multilevel circuits in different ways, topologies with different properties have been developed.

2.3.3 Survey of fundamental topologies

Among the high-power multi-level converters, three topologies have been successfully implemented as standard products for medium voltage industrial drives: the Neutral Point Clamped Voltage Source Converter (NPC VSC), the Flying Capacitor Voltage Source Converters (FLC VSC), and the Series Connected H-Bridge Voltage Source Converters (SCHB VSC). These topologies can be classified by the type their respective number of DC sources, as it is displayed in figure 2.3.

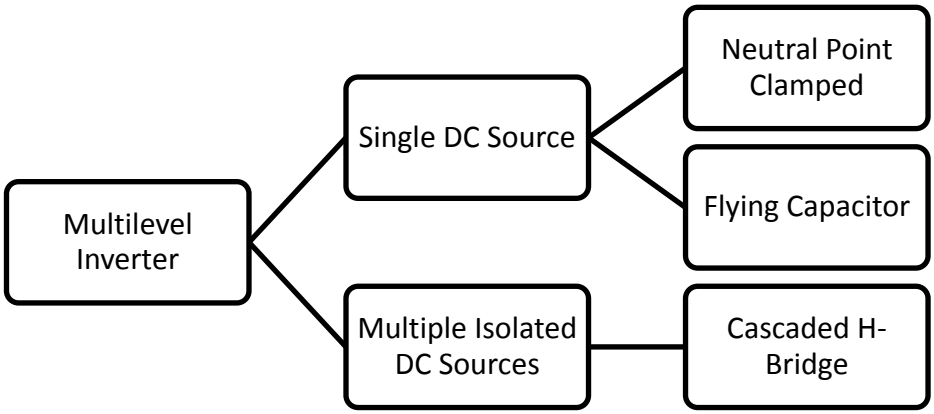

Figure 2.3 – Classification of multi-level voltage source converters

2.3.3.1 Neutral Point Clamped / Diode Clamped Inverter

The main concept of this inverter is to use diodes to limit the power devices voltage stress. The voltage over each capacitor and each switch is *Vdc*. An *n* level inverter needs (*n*-1) voltage sources, 2(*n*-1) switching devices and (*n*-1) (*n*-2) diodes.

2.3.3.1.1 Operation Principle

This topology known by NPC (Neutral clamped Point) or DCI (Diode-clamped Invert) consists of a chain of power semiconductors connected in series, in parallel with a chain of capacitors also in series. The capacitors allow the division of the voltage in a range of voltage levels by generating a set of continuous voltage sources, arranged in series. These two chains are joined by means of diodes, which connect the semiconductor top and bottom arm.

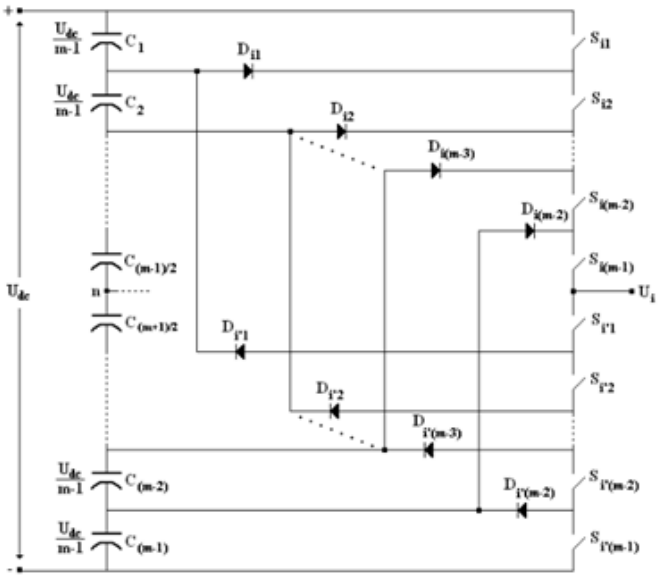

Figure 2.4 – Multilevel NPC converter

The converter of diodes connected to the neutral point of m levels, shown in figure 2.4 is obtained at the expense of m-1 capacitors in the DC bus and 2 × (m-1) power semiconductors for each arm of the converter, which can synthesize m levels in the output Ui.

Assuming the use of equal connecting diodes, the converter requires the use of (m-1) × (m-2) diodes per arm. This structure results in a quadratic increase in the number of diodes in relation to the number of levels, making it impractical to implement this system to a high number of levels.

One of the most used topologies in multilevel converter arm structure consists of two semiconductor diodes connected to the neutral point of three levels represented in Figure 2.5.

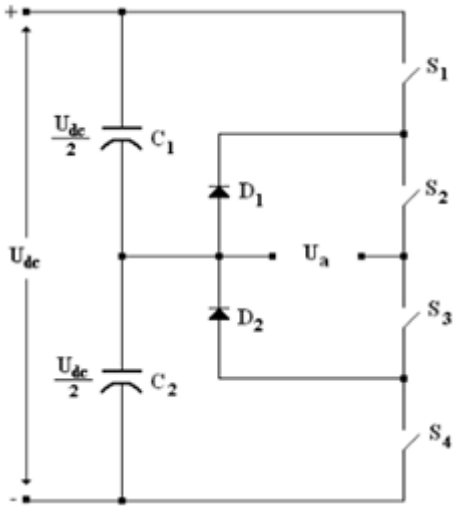

Figure 2.5 – Monophasic three-level NPC converter

The two capacitors, act almost as a DC voltage, and shall allocate the supply voltage Udc equally, allowing each arm of the multilevel converter to present a three-level output voltage: Udc / 2, -Udc / 2 and zero.

In this converter, S1 and S2 or S3 and S4 are used to control the switches of the converter and the two diodes connected to the neutral point of the two capacitors, acting as a capacitive voltage divider, can be regarded as free-wheeling diodes (clamping diodes) creating a path for current flow when the output voltage has the value 0.

The states of the switches pairs in the upper branch (S1 and S2) are complementary to the states of the lower branch switches (S3 and S4), so when S1 is on S3 is off, verifying the same for S2 and S4.

It is relatively easy to generalize the working principle of these topology converters to n voltage levels. The extension to n levels involves the use of 2 × (n-1) of semiconductor with controlled cutting, of which n-1 switch simultaneously, so as to obtain different levels of voltage. To eliminate concurrency problems in command and properly distribute the tension by semi-conductors should only be allowed transitions between adjacent levels.

The increase in the number of voltage levels can add more steps to the wave of output voltage, approaching that of a sine wave with minimum harmonic distortion. In an extreme case, a zero harmonic distortion in the output voltage waveform could be obtained with a converter with an infinite number of levels.

However, increasing the number of voltage levels, also corresponds to an increase in the number of semiconductors used, increasing the complexity and difficulty of the vector control for correcting the imbalance in the voltages of the capacitors.

2.3.3.1.2 Characteristics

Diode-clamped converter presents some peculiarities which other multilevel topologies do not have. First of all, it is quite simple to control. Indeed, a simple extension of a traditional analog PWM control can directly gate the switches without any switching table in between. The main problems related to its control came from the digital controller which are suited for traditional 2-level converters and may not have outputs enough to drive all the semiconductors in the leg.

Diode-clamped does not require insulated DC sources to create the voltage level, but exploits several capacitors to equally split a single DC source. This is a great advantage because makes the circuitry topology suitable to substitute a traditional system in all kinds of application: to upgrade an existing system it is necessary only to design a proper diode-clamped, take out the old converter and use the new one in its place.

Furthermore, when this kind of converter is connected in a back-to-back configuration, a proper synchronization between inverter and rectifier controls is sufficient to keep the capacitors balanced.

Advantages

- The increase in the number of levels allows to reduce the harmonic content of the alternating voltages, avoiding the use of filters when the number of levels is sufficiently high;
- High income because semiconductors are switched to relatively low frequencies;
- Ability to control reactive power;
- Simple control methods for rectifier / inverter systems (back-to-back system).

Disadvantages

- Excessive increase in the number of clamping diodes by increasing the number of levels;
- Difficulty in controlling the energy transit in real time.

2.3.3.2 Flying-Capacitor

This inverter uses capacitors to limit the voltage of the power devices. The configuration of the flying capacitor multilevel inverter is like a diode clamped multilevel inverter except that capacitors are used to divide the input DC voltage.

2.3.3.2.1 Operation Principle

The Flying-capacitor multilevel converter comprises a series of capacitors connected between the arms of the semiconductor converter acting as a source of DC voltage, sharing the common voltage equally in order to create different voltage levels.

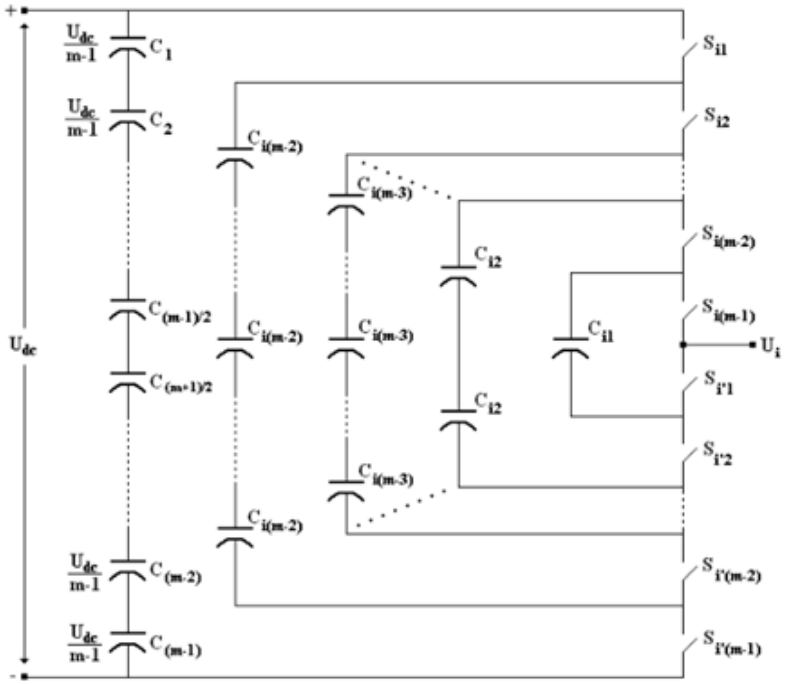

Figure 2.6 – Multilevel flying-capacitor converter

For a configuration of m levels, shown in figure 2.6, are used 2 × (m-1) power semiconductors and (m-1) × (m-2) / 2 floating capacitors for each arm of the converter, besides the m-1 capacitors connected in series in the DC bus, allowing synthesizing m levels of the converter output voltage (Ui).

As in the NPC converter topology, each arm of a floating capacitor converter can be used alone, producing m voltage levels, in full-bridge, producing a 2m-1 voltage levels, or in a combination of three arms , generating a three-phase voltage with m levels per phase.

Although the voltage levels produced by this converter are similar to the NPC converter, this topology provides greater flexibility in the synthesis of these levels.

Also, as happened with the NPC topology, in this converter the switches states of the upper branch are complementary to the states of the switches of the lower branch. In addition to the difficulty of balancing the voltage on the floating capacitors, the major problem that this converter presents is the need to use a large number of capacitors. However, it is possible to balance the voltage on these capacitors using the redundant combinations of voltage levels intermediate to the detriment of the switching frequency.

2.3.3.2.1 Characteristics

The main disadvantage of flying-capacitor architecture is capacitors balance. In a 3-level converter there is only one capacitor to keep balanced and the implementation of the control algorithm is quite easy. When the number of level rises, the voltages to keep controlled increase: a greater number of voltage sensors and a more complicated control are needed.

Even for this topology, the switch average currents could be different because they strictly depend on the control choice of redundant states. Some estimations of this value can be done, but is difficult to rate each switch for the exact current value. Like in diode-clamped implementation, a not fully exploitation of some switch is preferred.

Advantages

• The large number of floating capacitors provides greater flexibility in the synthesis of the output voltage levels;
• Redundant switching combinations allows the balancing of the voltages of the floating capacitor;
• Low harmonic content, for structures with a sufficiently high number of levels, eliminating the use of filters;
• The ability to control the active and reactive power, making its use possible DC transmission systems.

Disadvantages

• Need excessive floating capacitors when the number of levels is high;
• Complex control and high switching frequency and switching loss.

2.3.3.3 Cascaded H-Bridge

The concept of this inverter is based on connecting H-bridge inverters in series to get a sinusoidal voltage output. The output voltage is the sum of the voltage that is generated by each cell. The number of output voltage levels are 2*n*+1, where *n* is the number of cells. The switching angles can be chosen in such a way that the total harmonic distortion is minimized. An *n* level cascaded H-bridge multilevel inverter needs 2(*n*-1) switching devices where *n* is the number of the output voltage level.

2.3.3.3.1 Operation Principle

This multilevel converter structure is based on the cascade association of several full-bridge converters, for generating m output voltage levels. Although each converter uses an independent source of DC voltage, this topology avoids the use of extra floating capacitors or diodes when the number of levels of the converter increases.

Figure 2.7 illustrates the basic structure of a single-phase m levels bridge inverter using converters connected in cascade. In this type of structure, the AC terminals of the converters are connected in series.

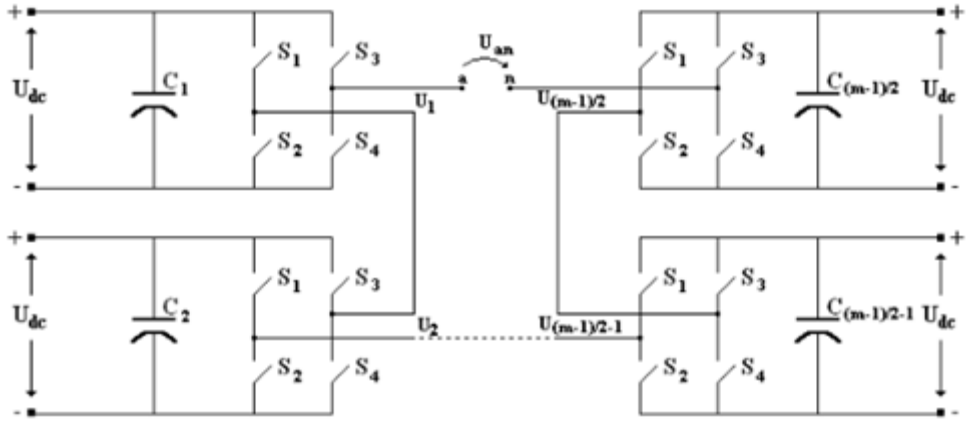

Figure 2.7 – Multilevel h-bridge converter

The output voltage of the converter with m levels is synthesized by summing the output voltages of several converters connected in series, that is, *Uan=U1+U2+…+U(m-1)/2-1+U(m-1)/2*. As each full-bridge converter can generate three voltage levels, *+Udc*, *0* and *–Udc* , the output voltage levels are obtained by the combination of (m-1) / 2 converters.

Means that the number of levels of the converter is defined by m = 2s +1, where m is the number of voltage levels and s is the number of independent sources of DC voltage.

2.3.3.3.2 Characteristics

Cascade H-bridge converter is a very modular solution based on a wide commercialized product. This has a good repercussion on the reliability and the maintenance of the system since the cells have high availability, intrinsic reliability and a relatively low cost.

The main disadvantage of this converter consists in requiring several insulated sources that are not available in all applications. At the same time, this disadvantage makes cascade converters more suitable for photovoltaic or battery fed applications than the other types. Indeed, photovoltaic panels can easily be rearranged in several insulated sources to feed cascade H-bridge cells. A similar operation can even be done with battery banks.

There are other several application dependent ways to exploit intra-phase redundancy proper of this converter. As an example, considering a three-phase system and a vector modulation, control can choose among the redundant configurations the one which needs the fewest commutations to be reached.

While there are no limitations on the level of diode-clamped or flying-capacitor, which can be even or odd, cascade H-bridge can have only odd numbers of levels; indeed the first cell gives three levels whereas the others always add two levels more.

Advantages

- requires fewer components compared to other multilevel converter structures, for the same number of levels;
- Allows modular structures since all levels have the same structure, not requiring a diode connection or extra floating capacitors;
- Techniques may be used for soft switching avoiding the need for the use of snubbers.

Disadvantages

- Requires independent voltage sources for each converter structure thereby limiting its use in some applications.

2.3.3.4 Other Topologies

2.3.3.4.1 Cascaded H-Bridge with Unequal DC Sources

The cascaded H-Bridge with Unequal DC sources has exactly the same structure as the regular cascaded H-Bridge except, as the name implies, it has unequal DC voltage sources.

This structure has the advantage of being able to generate more levels with fewer sources. The disadvantage is that the inverter will see unequal power losses and heat distribution. The inverter also still requires more than one DC source, giving it many of the same limitations as the original cascaded H-Bridge.

2.3.3.4.2 Cascaded H-Bridge with a Single DC Source

Another set of topologies that have been proposed recently are single source cascaded H-Bridge inverters. These topologies replace all but one of the DC sources with capacitors, incorporating control techniques to keep the DC voltage levels intact. Variations of this scheme also include topologies that replace the traditional H-Bridge modules with NPC modules. The drawback is that the control schemes used to balance the DC voltages especially during active power conversion place restrictions and limits on the inverters' operating range.

2.3.4 Comparison of Topologies

At this point it should be clear that one of the major advantages of a multilevel converter, regardless of topology, is increased power rating. A converter need not be limited in size by the prevailing semiconductor technology, since a multilevel converter allows the voltage and/or the current to be shared among a number of switches. This advantage has traditionally justified the extra complexity of multilevel converters [16].

The applications of MLIs include induction machine and motor drives, active filters, renewable energy sources interconnection to grid, flexible AC transmission systems (FACTS), and static compensators (STATCOM).

Each topology has its own mixture of advantages and disadvantages for any particular application, one topology will be more appropriate than the others. Although the choice of the multilevel topology is directly linked to the application and the list of specifications, in order to minimize losses, volume and costs, the number of components plays a very important role. Therefore, in order to provide some guidelines for selecting the proper multilevel topology, Table 2.2 summarizes the number of semiconductors and passive components required by the most common topologies [30].

Table 2.2 – Number of components required for each topology

Topology	Levels	Switches	Clamping Diodes	Floating Capacitors	Dc-link Capacitors	Isolated DC Sources
Neutral Point Clamped	3	12	6	0	2	1
	5	24	36	0	4	1
	m	6(m-1)	3(m-1)(m-2)	0	m-1	1
Flying Capacitor	3	12	0	3	2	1
	5	24	0	18	4	1
	m	6(m-1)	0	(3/2)(m-1)(m-2)	m-1	1
H-Bridge	3	12	0	0	6	1
	5	24	0	0	12	2
	m	6(m-1)	0	0	3(m-1)	(m-1)/2

For a three-level approach, the analysis shows that the Neutral-Point Clamped (NPC), Flying Capacitor (FC) and Cascaded H-Bridge converters require the same number of switches (12), however they differ on the clamping elements and number of dc sources needed.

For applications where only one dc source is available, the NPC and FC topologies have advantageous against the Cascaded H-Bridge system, which requires a complex transformer to provide the various independent dc sources. On the other hand, when multiple dc sources are available the Cascaded H-Bridge topology might be considered a reasonable solution since it requires the least number of components.

Therefore the most suitable three-level topology for electric vehicle drive application is the diode clamped inverter, mainly because compared to the h-bridge has less DC sources and in relation to the FC topology, has a simpler control.

2.4 Multilevel Modulation Techniques

The distinction between multilevel modulation and multilevel control is the following, multilevel modulations are meant to produce an average output voltage proportional to the reference given by some external algorithm, while multilevel controls are meant to apply an output voltage calculated by themselves, like Direct Torque Control (DTC) [26].

There are several ways to classify modulation techniques. The switching frequency can subdivide multilevel modulations into three classes: fundamental, mixed and high switching frequency. Fundamental switching frequency modulations produce switch commutations at output fundamental frequency and can be aimed to cancel some particular low frequency harmonic. In this class there are Space Vector Control (SVC) and selective harmonic elimination.

In Space Vector Control (SVC) the complex plain is divided in several hexagonal zones defining the proximity of the reference to the nearest generable vector which is definitely applied. In selective harmonic elimination the output is a staircase wave with steps duration optimized to cancel the specified harmonics; however the number of harmonics which can be eliminated at the same time is proportional to the number of converter levels. Mixed switching frequency modulations are those in which switches commutate at different frequency, like hybrid multilevel modulation, and are particularly suited for hybrid converters: different cells can easily commutate at different frequencies.

High switching frequency modulations are the adaptation of standard PWM to multi-levels and they are meant to switch at very high frequency, about 10 to 20 kHz. Among them, there are Space Vector PWM (SVPWM) and Phase Shifted PWM (PSPWM) and a subclass called level shifted PWM. Phase Opposition (PO), Opposition Disposition (OD) and Alternate Opposition Disposition (AOD) modulations belong to this last level. SVPWM is the extension of the standard 2-level Space Vector Modulation to a greater number of levels. In PSPWM several phase-shifted references are used to generate the control pulses. PO, OD and AOD exploit only one reference waveform which is compared with carries covering all the range of reference variation. The number of used carriers is equal to $n-1$.

3

NEUTRAL POINT CLAMPED

This chapter presents a model that describes the dynamics of a three level neutral point clamped converter used in a synchronous inverter application. The highly nonlinear model, originally in *abc*-coordinates, is also expressed in its *dq*-coordinates. Simulations are presented to validate the proposed model.

Conduction and switching losses of semiconductor devices occurred in three-level NPC inverter during its performance are discussed in this chapter. In addition, along with loss behaviour of the inverter, calculation methods used to assess amount of losses and its implementation in the simulation model are also discussed here.

3.1 Mathematical Model

The neutral point converter (NPC) can be constituted by three monophasic arms identical to that shown in figure 3.2. This converter is reversible, can transfer energy from the alternating to the continuous side or vice versa, keeping unaltered its topology for various operating modes, changing only the magnitudes to be controlled, the type of applied loads and sources of the circuits adjacent to the converter [28].

In order to characterize the behavior of the electrical quantities of the converter, in this chapter a nonlinear and time variant model state space is deduced, by applying variables that define the switching state of neutral point clamped converter.

Assuming the converter in figure 3.1 is composed of ideal components, the state variables are usually currents in the alternating side and the voltages on the capacitors of the continuous side.

The alternating voltages and the current I_0 provided by the Udc source are considered vector components of the system input, allowing the study of the converter operating as an inverter or as rectifier, since the current I_0 can be considered a load current (I_0 <0) or supply current (I_0 > 0).

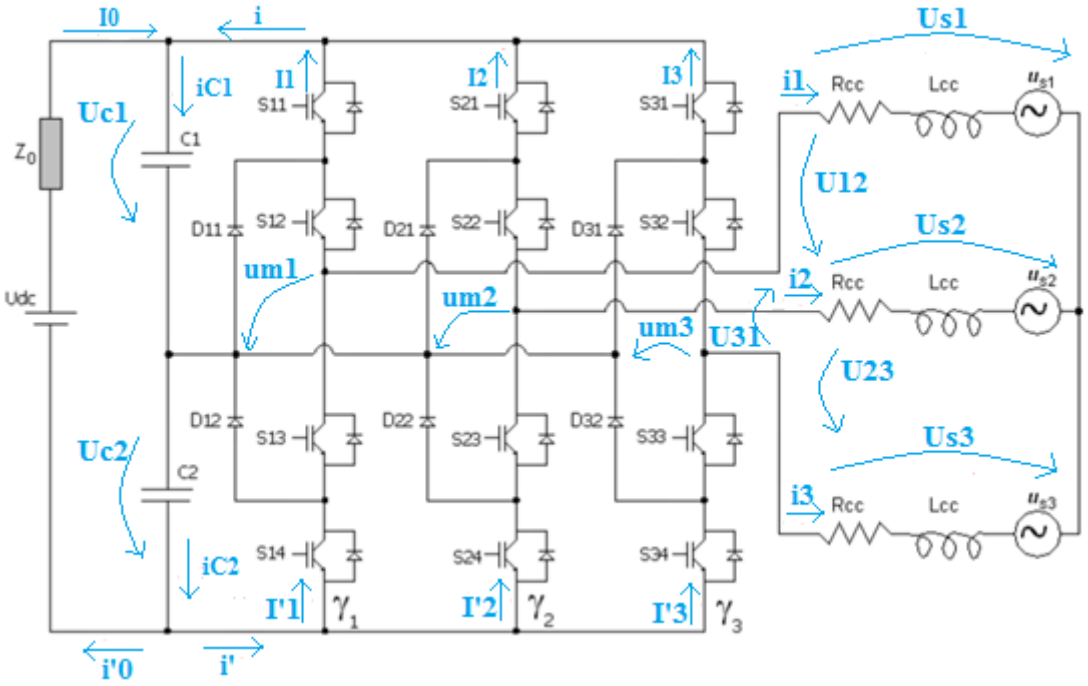

Figure 3.1 – Three-level NPC inverter

The three-level NPC comprises two capacitors connected in series on the continuous side with three arms. Each arm, represented in figure 3.2, consists of four switches and two diodes connecting to each neutral point. Each switch comprises a power semiconductor with an antiparallel diode in order to guarantee the bidirectional current [21],[24].

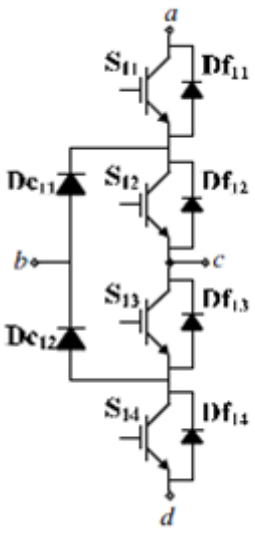

Figure 3.2 – NPC monophasic arm

The two capacitors used in this topology (C1 and C2) function is to perform the division of DC supply voltage *Vdc* to approximately half its value, allowing each arm to forward voltage levels +*Vdc* / 2, 0 and -*Vdc* / 2 between its output and the converter neutral point (Umk) for the various configurations of the semiconductor arm.

3.1.1 Switching variables

Each arm of the inverter is characterized by a variable Υ_k, which quantifies the state of the respective arm (Υ_1, Υ_2, Υ_3), and the state of each switch is characterized by the control variable S_{ki}.

The control of the output voltages or currents of each arm is performed by switching the switches S_{ki}. Each switch has associated two possible states, open (S_{ki}= 0) or closed (S_{ki}= 1), being the maximum number of combinations of $2^{12} = 4096$.

The switches (S11, S14), (S21, S24), (S31, S34) are operating as main switches for PWM, and (S12, S13,), (S22, S23) and (S32, S33) are auxiliary switches to clamp the output terminal potentials to the neutral point potential, together with (D11 – D32).

In three-level inverter, the mid-point of the DC bus provides the third level in the output waveform with the conduction of neutral point diodes.

During these periods, current is drawn from the neutral point. If this point is not connected directly to the supply neutral, then the current is drawn through DC link capacitors, causing one capacitor to charge whilst the other to discharge. Under normal operation, the mean current drawn from the neutral point potential remains constant.

However, during transient operation or if there is any imbalance in the output switching pattern a non-zero mean current will be drawn from the mid-point, resulting in variation of the neutral point voltage.

In fact there are many situations that are not desirable or possible because they violate the topological constraints of circuits theory (short circuit voltage sources, current sources open), thus there are only three combinations between the switches of each arm that allows the three possible voltage levels between the arm of the inverter and neutral point (table 3.1). We obtain this way, $3^3 = 27$ distinct states that allow the control of three-phase converter.

Table 3.3 – Available combinations for each arm

Υ_k	S_{k1}	S_{k2}	S_{k3}	S_{k4}	u_{mk}
1	1	1	0	0	U_{C1}
0	0	1	1	0	0
-1	0	0	1	1	$-U_{C2}$

Due to topological constraints on the operation of the converter, the switches of each arm must be controlled in a complementary way according to the following relationships:

$$\begin{cases} S_{k3} = \overline{S_{k1}} \\ S_{k4} = \overline{S_{k2}} \end{cases} \tag{3.1}$$

Additionally, the control signals must ensure that the voltage across each arm of the converter suffers only transitions between adjacent levels, the voltage cannot pass in each arm from the voltage level $U_{DC}/2$ to $-U_{DC}/2$ without passing through the intermediate voltage level 0.

According to the constraints given by (3.1), representing up to a three-level system the relationship between the state of the command switches (S_{ki}) and the value of the variable that characterizes the state of each arm of the three-phase multilevel inverter (Υ_k).

$$\Upsilon_k = \begin{cases} 1 \ \ se\ S_{k1} \cap S_{k2} \ \text{"Open"}\ and \ \ S_{k3} \cap S_{k4} \ \ "Close" \\ 0 \ \ se\ S_{k2} \cap S_{k3} \ \text{"Open"}\ and \ \ S_{k1} \cap S_{k4} \ \ "Close" \\ -1 \ \ se\ S_{k3} \cap S_{k4} \ \text{"Open"}\ and \ \ S_{k1} \cap S_{k2} \ \ "Close" \end{cases} \tag{3.2}$$

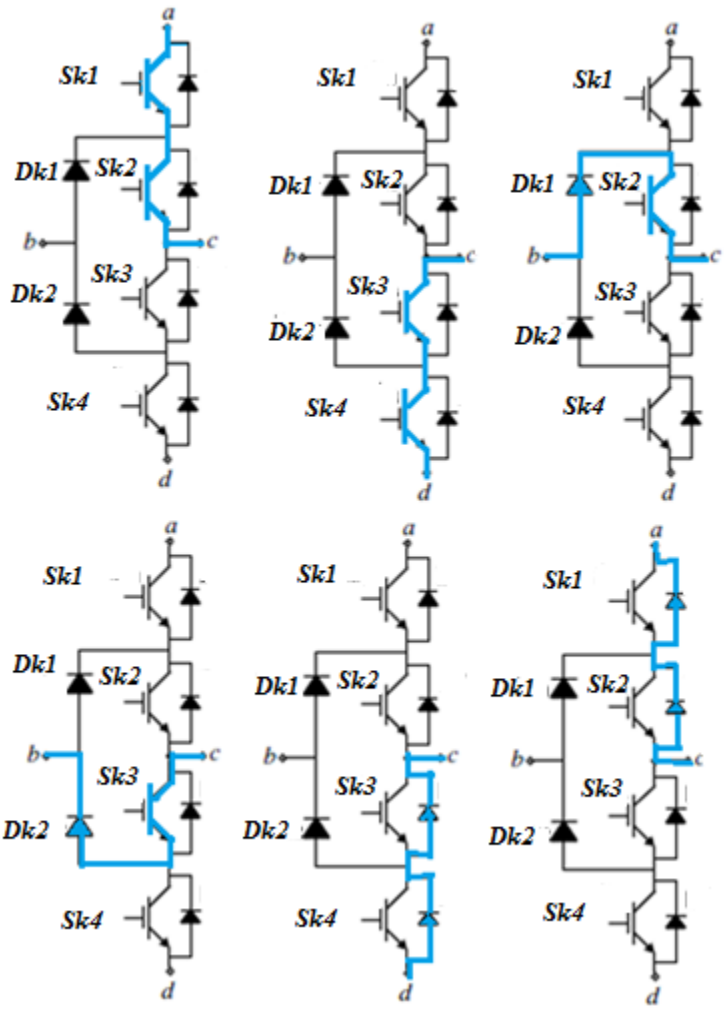

Figure 3.3 – 3L-NPC conduction path

Table 3.2 shows which switches are conducting in the structure of the three-level NPC depending on the current signal and the voltage level at the load.

Table 3.2 – Switching commutations

State	Voltage Level	S_{k1}	$D_{f_{k1}}$	S_{k2}	$D_{f_{k2}}$	S_{k3}	$D_{f_{k3}}$	S_{k4}	$D_{f_{k4}}$	D_{k1}	D_{k2}
Positive Phase Current											
+	U_{dc}/2	x		x							
0	0			x						x	
-	-U_{dc}/2						x		x		
Negative Phase Current											
+	-U_{dc}/2		x		x						
0	0					x					x
-	U_{dc}/2					x		x			

Switching losses are originated by the commutation processes between the different switch states.

For a positive phase current, the commutation from "+" towards "-" (+ → 0 → –) is named “forced commutation”. The contrary natural commutation (– → 0 → +) realizes a positive output power gradient. They are initiated by an active turn-on transient.

For the following discussion of commutations, a positive phase current is assumed. Only turn-on and turn-off losses of active switches and recovery losses of diodes are considered. For a positive phase current, the commutation (+ → 0) is initiated by the turn-off of $S_{k1}$and the current is forced from S_{k1} to $D_{S_{k1}}$. After a dead time (to ensure that S_{k1}has completely turned off), S_{k3} is turned on. The switches S_{k2} and S_{k4} stay on and off respectively.

Table 3.3 – Switch commutations during transitions

State	S_{k1}	$D_{S_{k1}}$	S_{k2}	$D_{S_{k2}}$	S_{k3}	$D_{S_{k3}}$	S_{k4}	$D_{S_{k4}}$	D_{k1}	D_{k2}
Positive Phase Current										
+↔0	x								x	
0↔-			x					x		
Negative Phase Current										
+↔0		x			x					
0↔-							x			x

Only two switches and diodes are involved in this commutation: $S_{k1}$and $D_{S_{k1}}$. Essential turn-off losses occur in S_{k1}. Though the switch S_{k3} *is* turned on, it does not experience losses since it does not take over any current after the commutation.

For the reverse commutation (0 → +), all switching transitions take place in the reverse order. S_{k3} is turned off first, followed by turning on S_{k1} after the dead time. Turning off S_{k3} does not affect the phase current. It only returns to the positive rail after the turn-on of S_{k1}. Recovery losses occur in D_{k1}, and S_{k1} experiences turn-on losses.

The situation for this pair of commutations is visualized in figure 3.4, where the current path of the switching active device is marked bold and the current path of the switching passive device is marked with a dashed line.

Four devices are involved in the commutation (0 → –). It is started by the active turn-off of the switch S_{k2}, forcing the current from its path through $D_{k1}$and S_{k2} to $D_{S_{k2}}$and $D_{S_{k3}}$. S_{k3} has already been in the on state before; S_{k4} is turned on after a dead time. S_{k2} faces turn-off losses.

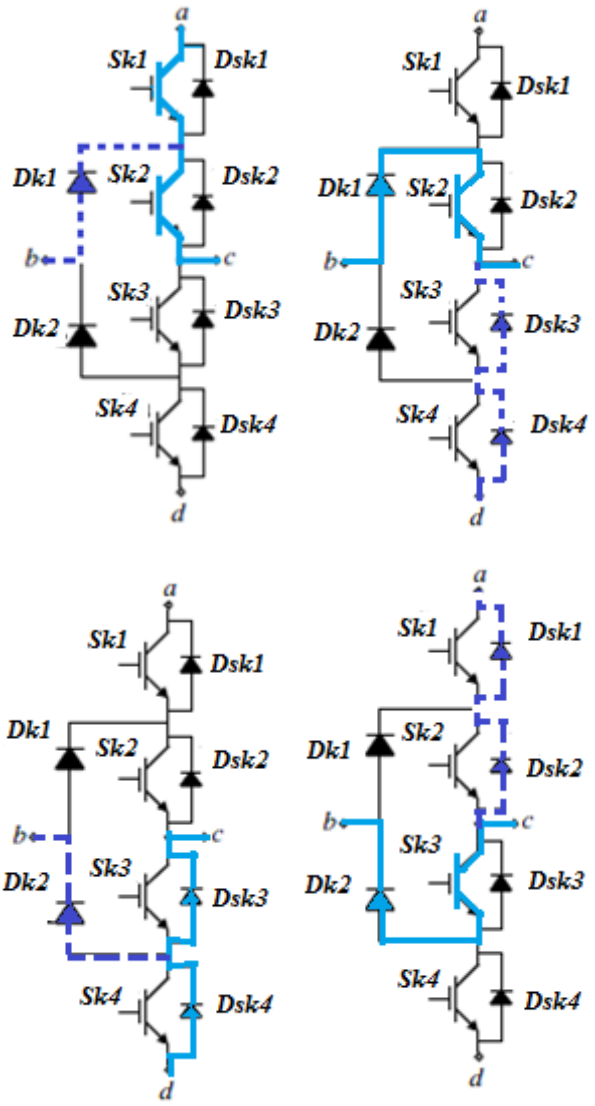

Figure 3.4 – 3L-NPC switching transitions

Although the diode D_{k1} in series with S_{k2} is turned off too, it does not experience notable recovery losses since it does not take over voltage after the commutation. Again, for the reverse commutation (– → 0), all switching transitions take place in the reverse order. S_{k4} is turned off, and S_{k2} is turned on after a dead time. After triggering S_{k2}, the phase current commutates from $D_{S_{k4}}$ and $D_{S_{k3}}$back to D_{k1} and S_{k2}. Both diodes in series $D_{S_{k4}}$and $D_{S_{k3}}$are turned off, but only $D_{S_{k4}}$ takes over blocking voltage. Thus, only $D_{S_{k4}}$ experiences recovery losses. S_{k2} faces turn-on losses.

Table 3.4 – Switching transitions losses

Switching transition	Turn-on losses	Turn-off losses	Recovery losses
Positive phase current			
+↔0	-	S_{k1}	–
0↔+	S_{k1}	–	D_{k1}
0↔-	-	S_{k2}	–
-↔0	S_{k2}	–	$D_{S_{k4}}$
Negative phase current			
+↔0	S_{k3}	–	$D_{S_{k1}}$
0↔+	-	S_{k3}	–
0↔-	S_{k4}	–	D_{k2}
-↔0	-	S_{k4}	–

The distribution of the switching losses is summarized in Table 3.3. It is important to note that all commutations in the NPC VSC can be explained by the basic commutation cell, comprising one active switch and one diode.

3.1.2 Voltage and current equations of the converter

By analyzing the circuit of Figure 3.1, we get the following relationships for the AC voltage u_{mk} and currents $I_k$and $I_k^{'}$ of the arm k as a function of the switching variableΥ_k.

$$u_{mk} = \begin{cases} U_{c1} \ if \ \Upsilon_k = 1 \\ 0 \ if \ \Upsilon_k = 0 \\ -U_{c2} \ if \ \Upsilon_k = -1 \end{cases} \quad (3.3)$$

$$I_k = \begin{cases} -i_k \ if \ \Upsilon_k = 1 \\ 0 \ if \ \Upsilon_k \neq 1 \end{cases} \quad (3.4)$$

$$I_k^{'} = \begin{cases} -i_k \ if \ \Upsilon_k = -1 \\ 0 \ if \ \Upsilon_k \neq -1 \end{cases} \quad (3.5)$$

Given the relationships (3.3), (3.4) and (3.5) we obtain the following u_{mk} voltage and current $I_k$and $I_k^{'}$ equations of the converter as function of Υ_k.

$$u_{mk} = \frac{\Upsilon_k}{2} \times (1 + \Upsilon_k) \times U_{c1} + \frac{\Upsilon_k}{2} \times (1 - \Upsilon_k) \times U_{c2} = \Gamma_{1k} \times U_{c1} + \Gamma_{1k} \times U_{c2} \quad (3.6)$$

$$I_k = -\frac{\Upsilon_k}{2} \times (1 + \Upsilon_k) \times i_k = -\Gamma_{1k} \times i_k \tag{3.7}$$

$$I_k^{'} = -\frac{\Upsilon_k}{2} \times (1 - \Upsilon_k) \times i_k = -\Gamma_{2k} \times i_k \tag{3.8}$$

Where:

$$\begin{cases} \Gamma_{1k} = \frac{\Upsilon_k}{2} \times (1 + \Upsilon_k) \\ \Gamma_{2k} = \frac{\Upsilon_k}{2} \times (1 - \Upsilon_k) \end{cases} with \begin{cases} \Gamma_{1k} \in \{0\,,1\} \\ \Gamma_{2k} \in \{-1\,,0\} \end{cases} \tag{3.9}$$

3.1.3 Dynamic equations of the converter

By applying the Kirchhoff's law to the converter of figure 3.1, one obtains the following equations for the currents in the capacitors C1 and C2:

$$\begin{cases} i_{C1} = i_0 + i = i_0 + \sum_{k=1}^{3} I_k = i_0 + I_1 + I_2 + I_3 \\ i_{C2} = i_0 + i' = i_0 + \sum_{k=1}^{3} I_k^{'} = I_0 + I_1' + I_2^{'} + I_3' \end{cases} \tag{3.9}$$

Given (3.7) and (3.8) the system of equations (3.10) can be written as a function of switching variables:

$$\begin{cases} i_{C1} = i_0 - \Gamma_{11} \times i_1 - \Gamma_{12} \times i_2 - \Gamma_{13} \times i_3 \\ i_{C2} = i_0 - \Gamma_{21} \times i_1 - \Gamma_{22} \times i_2 - \Gamma_{23} \times i_3 \end{cases} \tag{3.10}$$

Considering that,

$$\begin{cases} i_{C1} = C_1 \times \frac{dU_{C1}}{dt} \\ i_{C2} = C_2 \times \frac{dU_{C2}}{dt} \end{cases} \tag{3.11}$$

Then the equations (3.11) can be written in function of the voltage on the capacitors:

$$\begin{cases} C_1 \times \frac{dU_{C1}}{dt} = i_0 - \Gamma_{11} \times i_1 - \Gamma_{12} \times i_2 - \Gamma_{13} \times i_3 \\ C_2 \times \frac{dU_{C2}}{dt} = i_0 - \Gamma_{21} \times i_1 - \Gamma_{22} \times i_2 - \Gamma_{23} \times i_3 \end{cases} \tag{3.12}$$

The system can be written as:

$$\frac{d}{dt}\begin{bmatrix}U_{C1}\\U_{C2}\end{bmatrix}=\begin{bmatrix}-\frac{\Gamma_{11}}{C_1} & -\frac{\Gamma_{12}}{C_1} & -\frac{\Gamma_{13}}{C_1} & -\frac{1}{C_1}\\ -\frac{\Gamma_{21}}{C_2} & -\frac{\Gamma_{22}}{C_2} & -\frac{\Gamma_{23}}{C_2} & -\frac{1}{C_2}\end{bmatrix}\times\begin{bmatrix}i_1\\i_2\\i_3\\i_0\end{bmatrix} \tag{3.13}$$

Where the current i_0 is given by:

$$i_0=\frac{U_{dc}-U_{C1}-U_{C2}}{z_0} \tag{3.14}$$

z_0 represents the internal impedance of the DC voltage source U_{dc}.

The voltages between the arms of the converter (Uij) relate to the simple voltages (Usk) and the voltages between each arm and the neutral point (Umk) by the following equations:

$$\begin{cases}U_{ij}=U_{Si}-U_{Sj}\\U_{ij}=u_{mi}-u_{mj}\end{cases} \tag{3.15}$$

Solving the system of equations as a function of the simple voltages (Usk) so as to eliminate the voltages between the arms of the converter (uij), we obtain the following system of equations:

$$\begin{cases}U_{S1}=\frac{1}{3}\times(2\times u_{m1}-u_{m2}-u_{m3})\\U_{S2}=\frac{1}{3}\times(-u_{m1}+2\times u_{m2}-u_{m3})\\U_{S3}=\frac{1}{3}\times(-u_{m1}-u_{m2}+2\times u_{m3})\end{cases} \tag{3.16}$$

By replacing (3.6) in (3.16) we obtain the system (3.17) which relates the voltages applied on the alternating side with the voltages of the capacitors.

$$\begin{cases}U_{S1}=\frac{1}{3}\times[(2\times\Gamma_{11}-\Gamma_{12}-\Gamma_{13})\times U_{c1}+(2\times\Gamma_{21}-\Gamma_{22}-\Gamma_{23})\times U_{C2}]\\U_{S2}=\frac{1}{3}\times[(-\Gamma_{12+}+2\times\Gamma_{12}-\Gamma_{13})\times U_{c1}+(-\Gamma_{22+}+2\times\Gamma_{22}-\Gamma_{23})\times U_{C2}]\\U_{S3}=\frac{1}{3}\times[(-\Gamma_{11}-\Gamma_{12}+2\times\Gamma_{13})\times U_{c1}+(-\Gamma_{21}-\Gamma_{22}+2\times\Gamma_{23})\times U_{C2}]\end{cases} \tag{3.17}$$

The system of equations (3.17) can be represented by matrix system (3.18):

$$U_{Sk} = \Xi \times \begin{bmatrix} U_{C1} \\ U_{C2} \end{bmatrix} \tag{3.18}$$

Where the matrix Ξ is given by:

$$\Xi = \begin{bmatrix} \Xi_{11} & \Xi_{12} \\ \Xi_{21} & \Xi_{22} \\ \Xi_{31} & \Xi_{32} \end{bmatrix} = \frac{1}{3} \times \begin{bmatrix} 2 \times \Gamma_{11} - \Gamma_{12} - \Gamma_{13} & 2 \times \Gamma_{21} - \Gamma_{22} - \Gamma_{23} \\ -\Gamma_{12+} + 2 \times \Gamma_{12} - \Gamma_{13} & -\Gamma_{22+} + 2 \times \Gamma_{22} - \Gamma_{23} \\ -\Gamma_{11} - \Gamma_{12} + 2 \times \Gamma_{13} & -\Gamma_{21} - \Gamma_{22} + 2 \times \Gamma_{23} \end{bmatrix} \tag{3.19}$$

3.1.4 Space vectors

To determine the set of space vectors of the three-level NPC, consider the ideal situation in which the capacitors C1 and C2 of the multilevel converter can be viewed as two voltage sources of equal value:

$$U_{C1} = U_{C2} = \frac{U_{dc}}{2} \tag{3.20}$$

In this situation, the voltage at the neutral point between the capacitors C1 and C2 is Udc / 2 and neglecting the variation of the voltage on the capacitors, it is found that the relation between the voltages between each arm and the neutral point (Umk) is given by:

$$u_{mk} = \Upsilon_k \times \frac{U_{dc}}{2} \tag{3.21}$$

The relation (3.21) shows that each arm of the converter can provide between its output and neutral point converter one of three possible voltage values: Udc/2, 0 and -Udc/2.

By replacing the equation (3.21) in (3.16) gives the following relationship between the line voltages, measured between two arms of the converter, and the control variables of each arm:

$$\begin{cases} U_{12} = (\Upsilon_1 - \Upsilon_2) \times \frac{U_{dc}}{2} \\ U_{23} = (\Upsilon_2 - \Upsilon_3) \times \frac{U_{dc}}{2} \\ U_{31} = (\Upsilon_3 - \Upsilon_1) \times \frac{U_{dc}}{2} \end{cases} \equiv \quad U_{ij} = (\Upsilon_i - \Upsilon_j) \times \frac{U_{dc}}{2} \tag{3.22}$$

Substituting into equation (3.20) the command variables (Υ_i and Υ_j) for their possible states (1, 0, -1), we obtain various levels of output voltage between two arms of the converter (Table 3.5).

Table 3.5 – Output voltage levels

Υ_i	Υ_j	U_{ij}
-1	-1	0
-1	0	$-U_{dc}/2$
-1	1	$-U_{dc}$
0	-1	$U_{dc}/2$
0	0	0
0	1	$-U_{dc}/2$
1	-1	U_{dc}
1	0	$U_{dc}/2$
1	1	0

Table 3.5 shows that the line voltages between two arms of the converter, can take over five voltage levels, according to the state of each command variable.

Substituting equation (3.21) in the system (3.17), one obtains the relation between the simple voltages (Usk) and the control variables of each arm of the converter:

$$\begin{cases} U_{S1} = \frac{1}{3} \times (2 \times \Upsilon_1 - \Upsilon_2 - \Upsilon_3) \times \frac{U_{dc}}{2} \\ U_{S2} = \frac{1}{3} \times (-\Upsilon_1 + 2 \times \Upsilon_2 - \Upsilon_3) \times \frac{U_{dc}}{2} \\ U_{S3} = \frac{1}{3} \times (-\Upsilon_1 - \Upsilon_2 + 2 \times \Upsilon_3) \times \frac{U_{dc}}{2} \end{cases} \quad (3.23)$$

The system (3.22) can also be represented as matrix (3.23).

$$\begin{bmatrix} U_{S1} \\ U_{S2} \\ U_{S3} \end{bmatrix} = \begin{bmatrix} \frac{2}{3} & -\frac{1}{3} & -\frac{1}{3} \\ -\frac{1}{3} & \frac{2}{3} & -\frac{1}{3} \\ -\frac{1}{3} & -\frac{1}{3} & \frac{2}{3} \end{bmatrix} \times \begin{bmatrix} \Upsilon_1 \\ \Upsilon_2 \\ \Upsilon_3 \end{bmatrix} \times \frac{U_{dc}}{2} \quad (3.23)$$

By applying the Concordia transformation matrix to the system (3.23) one obtains the vector of output voltages in the α, β components as function of the control variables of each arm in the inverter:

$$\begin{bmatrix} U_{S\alpha} \\ U_{S\beta} \end{bmatrix} = \sqrt{\frac{2}{3}} \times \begin{bmatrix} 1 & -\frac{1}{2} & -\frac{1}{2} \\ 0 & \frac{\sqrt{3}}{2} & -\frac{\sqrt{3}}{2} \end{bmatrix} \times \begin{bmatrix} \Upsilon_1 \\ \Upsilon_2 \\ \Upsilon_3 \end{bmatrix} \times \frac{U_{dc}}{2} \quad (3.24)$$

The system (3.23) allows to obtain the 3 ^ 3 = 27 distinct states that enable the control of the converter. For each combination of control variables of the arms of the converter, corresponds to a certain vector and consequently the application of a voltage to the converter output.

In table 3.6 are represented twenty-seven vectors provided by the converter three-level NPC in accordance with the state of the arms of the converter, represented by the variable Υ_k.

It is based on the suitable choice of the value of the control variables that performs control of the quantities desired by applying the proper voltage level. In the control process it is necessary to ensure that the voltage level on the arms of the converter does not transit from one level to the other without passing through intermediate levels, ensuring that the terminals of each switch is not a potential difference applied over a step level voltage.

Table 3.6 – Switching states

Switching State	Υ_1 Υ_2 Υ_3	*Voltage Vector*	u_{m1}	u_{m2}	u_{m3}	u_{12}	u_{23}	u_{31}
S1	-1-1-1	V0	$-U_{dc}/2$	$-U_{dc}/2$	$-U_{dc}/2$	0	0	0
S2	000	V0	0	0	0	0	0	0
S3	111	V0	$U_{dc}/2$	$U_{dc}/2$	$U_{dc}/2$	0	0	0
S4	0-1-1	V1	0	$-U_{dc}/2$	$-U_{dc}/2$	$U_{dc}/2$	0	$-U_{dc}/2$
S5	00-1	V2	0	0	$-U_{dc}/2$	0	$U_{dc}/2$	$-U_{dc}/2$
S6	-10-1	V3	$-U_{dc}/2$	0	$-U_{dc}/2$	$-U_{dc}/2$	$U_{dc}/2$	0
S7	-100	V4	$-U_{dc}/2$	0	0	$-U_{dc}/2$	0	$U_{dc}/2$
S8	-1-10	V5	$-U_{dc}/2$	$-U_{dc}/2$	0	0	$-U_{dc}/2$	$U_{dc}/2$
S9	0-10	V6	0	$-U_{dc}/2$	0	$U_{dc}/2$	$-U_{dc}/2$	0
S10	100	V1	$U_{dc}/2$	0	0	$U_{dc}/2$	0	$-U_{dc}/2$
S11	110	V2	$U_{dc}/2$	$U_{dc}/2$	0	0	$U_{dc}/2$	$-U_{dc}/2$
S12	010	V3	0	$U_{dc}/2$	0	$-U_{dc}/2$	$U_{dc}/2$	0
S13	011	V4	0	$U_{dc}/2$	$U_{dc}/2$	$-U_{dc}/2$	0	$U_{dc}/2$
S14	001	V5	0	0	$U_{dc}/2$	0	$-U_{dc}/2$	$U_{dc}/2$
S15	101	V6	$U_{dc}/2$	0	$U_{dc}/2$	$U_{dc}/2$	$-U_{dc}/2$	0
S16	10-1	V7	$U_{dc}/2$	0	$-U_{dc}/2$	$U_{dc}/2$	$U_{dc}/2$	$-U_{dc}$
S17	01-1	V8	0	$U_{dc}/2$	$-U_{dc}/2$	$-U_{dc}/2$	U_{dc}	$-U_{dc}/2$
S18	-110	V9	$-U_{dc}/2$	$U_{dc}/2$	0	$-U_{dc}$	$U_{dc}/2$	$U_{dc}/2$
S19	-101	V10	$-U_{dc}/2$	0	$U_{dc}/2$	$-U_{dc}/2$	$-U_{dc}/2$	U_{dc}
S20	0-11	V11	0	$-U_{dc}/2$	$U_{dc}/2$	$U_{dc}/2$	$-U_{dc}$	$U_{dc}/2$
S21	1-10	V12	$U_{dc}/2$	$-U_{dc}/2$	0	U_{dc}	$-U_{dc}/2$	$-U_{dc}/2$
S22	1-1-1	V13	$U_{dc}/2$	$-U_{dc}/2$	$-U_{dc}/2$	U_{dc}	0	$-U_{dc}$
S23	11-1	V14	$U_{dc}/2$	$U_{dc}/2$	$-U_{dc}/2$	0	U_{dc}	$-U_{dc}$
S24	-11-1	V15	$-U_{dc}/2$	$U_{dc}/2$	$-U_{dc}/2$	$-U_{dc}$	U_{dc}	0
S25	-111	V16	$-U_{dc}/2$	$U_{dc}/2$	$U_{dc}/2$	$-U_{dc}$	0	U_{dc}
S26	-1-11	V17	$-U_{dc}/2$	$-U_{dc}/2$	$U_{dc}/2$	0	$-U_{dc}$	U_{dc}
S27	1-11	V18	$U_{dc}/2$	$-U_{dc}/2$	$U_{dc}/2$	U_{dc}	$-U_{dc}$	0

3.2 Power Semiconductors

System performance highly depends on the semiconductors incorporated. This directly affects efficiency, heat transfer, system voltage and finally cost. It is desirable to use Insulated Gate Bipolar Transistors (IGBT) which is emerging in high power medium voltage applications.

The specific cost increases with rated blocking voltage. Moreover, low voltage switches need more current carrying capability, what requires more silicon, to reach the same switching power as high voltage switches. Therefore it can be concluded that a single high voltage chip is more expensive than a low voltage one. Another major indication in chip technology is the specific switching losses.

When using low voltage IGBTs to have less switching losses and lower cost, this will also imply increased conduction losses and increased mechanical and thermal stress on bus bars, cables and protection equipment (circuit breakers etc.). Hence follows that a trade-off needs to be figured out.

3.2.1 Power loss comparison

In general, power losses of any power electronic equipment comprise of power losses of all components contained in the equipment. In electrical components the power losses caused in the resistances of these components, so power losses, by nature, means heating of the component. Such an undesirable in the most of applications heating limits the load capabilities and affects either efficiency of the inverter or efficiency of the whole system. In addition, if the temperature of any component of the system exceed a certain acceptable limit due to untransfered heat or overload of the component, it could be finally damaged, which in its turn might cause the failure of the whole system.

For comparison of power losses in a three-level inverter it is enough to compare the maximum power losses. In efficiency point of view, the power losses are averaged over the whole period of the output voltage. The losses are calculated assuming sinusoidal PWM is used.

Most of the power loss occurs in the switches, but there is also some power loss in the DC-link capacitor. The total power loss $P_{loss}$is:

$$P_{loss} = 3 \times P_{cond} + 3 \times P_{sw} + P_{cap} \tag{3.25}$$

where P_{cond} is the conduction loss of one phase, P_{sw} is the switching loss of one phase, and P_{cap} is the power loss in the DC-link capacitor.

The evolution of temperature in IGBT modules is a direct consequence of the total losses and imposes the maximum power that can be delivered by power devices or the maximum switching frequency. The following hypotheses were considered to calculate the total losses[1] in power devices:

- the load current is sinusoidal;
- the current and voltage ripples are neglected;
- the dead times of IGBT modules are neglected.

[1] The total losses are made of total conduction and switching losses.

3.2.1.1 Conduction Losses

The conduction losses P_{cond} are comprised of losses in the IGBTs and diodes. The conduction losses for each switch can be calculated with equation (3.26).

$$P_{cond} = U_f \times I_{avg} + r_f \times I_{rms}^2 \tag{3.26}$$

Where U_f is the forward voltage drop with zero current, r_f is the forward resistance, I_{avg} is the average current and I_{rms} is the root-means-square of the current. The currents for IGBTs S_{k1} and S_{k4} are:

$$I_{avg} = \frac{M \times \hat{I}}{4 \times \pi} \times [\sin|\varphi| + (\pi - |\varphi|) \times \cos\varphi] \tag{3.27}$$

$$I_{rms}^2 = \frac{M \times \hat{I}^2}{4 \times \pi} \times \left[1 + \frac{4}{3} \times \cos\varphi + \frac{1}{3} \times \cos(2 \times \varphi)\right] \tag{3.28}$$

Where $\hat{I}$ is the peak current of the output voltage, φ is the phase difference between the output current and voltage and *M* is the modulation index. The currents for S_{k2} and S_{k3} are:

$$I_{avg} = \frac{\hat{I}}{\pi} - \frac{M \times \hat{I}}{4 \times \pi} \times [\sin|\varphi| - |\varphi| \times \cos\varphi] \tag{3.29}$$

$$I_{rms}^2 = \frac{\hat{I}^2}{4} - \frac{M \times \hat{I}^2}{4 \times \pi} \times \left[1 - \frac{4}{3} \times \cos\varphi + \frac{1}{3} \times \cos(2 \times \varphi)\right] \tag{3.30}$$

The currents for the diodes D_{k1} and D_{k2} are:

$$I_{avg} = \frac{\hat{I}}{\pi} - \frac{M \times \hat{I}}{4 \times \pi} \times \left[\cos\varphi + \frac{2}{\pi} \times \sin|\varphi| - \frac{2}{\pi} \times \cos\varphi\right] \tag{3.31}$$

$$I_{rms}^2 = \frac{\hat{I}^2}{4} - \frac{M \times \hat{I}}{2 \times \pi} \times [1 + \frac{1}{3} \times \cos(2 \times \varphi)] \tag{3.32}$$

3.2.1.2 Switching Losses

Switching losses are created by the commutation processes between different switch states. These commutation processes can be classified into natural or inductive commutations, which are characterized by turn-on losses of active switches and recovery losses of diodes, and forced or capacitive commutations, which are contrarily characterized by turn-off losses of active switches. Turn-on losses of diodes are usually small and can be neglected [21], [23].

The switching losses can be calculated with the following equation:

$$P_{sw} = \frac{k \times f \times \hat{\imath}}{\pi} = \frac{(E_{off} + E_{on}) \times f \times \hat{\imath}}{\pi} \tag{3.33}$$

The constant *k* can be acquired from the module datasheet. For IGBTs it comprises of the switch-on energy and the switch-off energy.

The switching losses for the diodes D_{k1} and D_{k2} can be calculated with the same equation (3.33) taking into account there is only switch off energy, which is expressed in the constant *k*.

In general, it can be concluded that, in principle, any switching losses calculation technique is a geometrical method by nature. It should be kept in mind that linearized methods of approximation and estimation of losses may be not accurate, as switching transient waveforms usually have a complex shape. However, in practice the accuracy of such methods is appropriate enough even with certain assumptions.

Thus, the aim of any calculation approach is to find as accurate approximation of commutation current and voltage waveforms as possible. On the other hand it should be not very complicated, as feasibility of the method is also important.

3.3 Voltage and current THD analysis

In this section, a FFT analysis will be performed in order to estimate the impact of operating at different switching frequencies and with different modulation indexes in the total harmonic distortion (THD), which is defined as the root mean square (RMS) value of the total harmonics of the signal, divided by the RMS value of its fundamental signal [29].

This model represents a 50 kW, 380 V, 50 Hz, three-phase neutral point clamped inverter. The IGBT inverter uses PWM technique, to convert DC power from a +/-200 Vdc source to 220 V AC, 50 Hz.

The inverter feeds a R-L load without filter because the primary objective of these simulations is to observe the trend of the THD when different values of carrier frequency and modulation indexes are set. Thus, it is expected relatively high values of harmonic distortion.

The 12 inverter pulses required by the inverter are generated by the "Discrete 3-phase PWM Generator" block (found in the Extras/Discrete Control Blocks library). The NPC converter is demonstrated in Figure 3.6, and the model to perform this simulation is presented in Figure YY bellow.

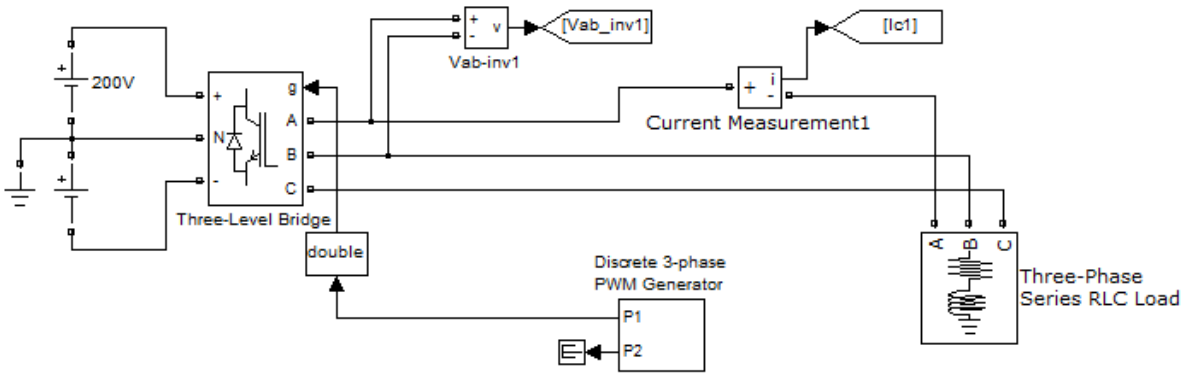

Figure 3.5 – Simulink scheme for THD analysis

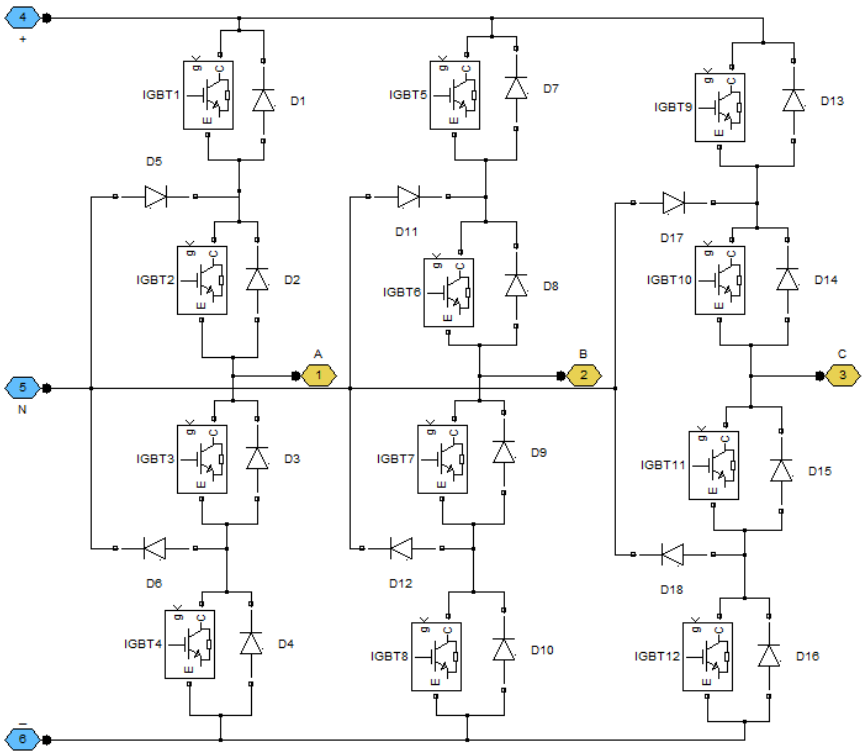

Figure 3.6 – Simulink implementation of three-level NPC

3.3.1 Simulation Results

Both current and voltage THD obtained for different values of switching frequency as function of the modulation index are presented in the table 3.7. Also, these results are displayed in two separate graphics in order to better understand the THD trend.

Table 3.7 – THD simulation results

Modulation Index	***Total Harmonic Distortion***					
	Phase Current			Line Voltage (Vab)		
	10 kHz	*15 kHz*	*20 kHz*	*10 kHz*	*15 kHz*	*20 kHz*
0,1	0,155	0,08932	0,1293	3,061	2,914	3,056
0,2	0,08944	0,06175	0,0582	1,725	1,755	1,728
0,3	0,07729	0,05064	0,04596	1,274	1,261	1,274
0,4	0,06474	0,04427	0,03499	0,9381	0,8471	0,9384
0,5	0,05677	0,03882	0,03098	0,7124	0,7057	0,7126
0,6	0,04765	0,03236	0,02544	0,4992	0,5057	0,4988
0,7	0,04068	0,0275	0,02119	0,4514	0,4516	0,4518
0,8	0,03307	0,02295	0,01768	0,4282	0,4274	0,4289
0,9	0,0219	0,01689	0,01174	0,3573	0,3578	0,3575
1	0,02722	0,01881	0,01483	0,3972	0,3973	0,398

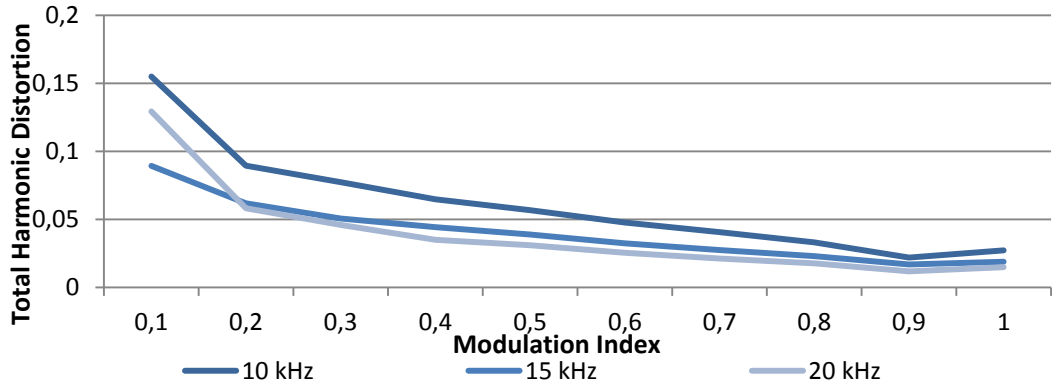

Figure 3.7 – Current THD

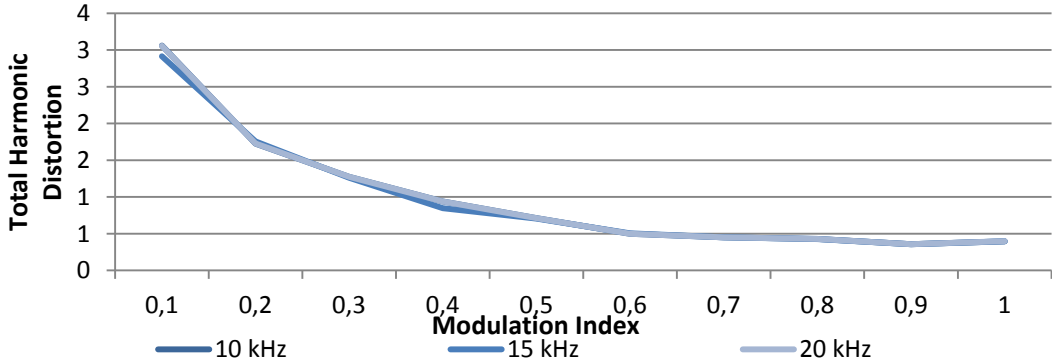

Figure 3.8 – Line Voltage THD

Considering the results for the phase current obtained, it is possible to reach the conclusion that the total harmonic distortion is lower when the modulation index is between 0.7 and 0.9. Furthermore, according to table 3.7 decreases with a higher carrier frequency. On the other hand, in the case of the results obtained regarding the line voltage, the carrier frequency doesn't seem to affect the THD, but similarly to the current phase current, the distortion is at its lowest point when the modulation index is between 0.7 and 0.9.

The frequency of the carrier wave is equal to the switching frequency of the converter. This frequency is depending on the application. A high switching frequency implies a faster and more accurate control of the controlled quantities, and in many applications, a switching frequency higher than 20 kHz is used since the human ear does not perceive frequencies higher than 20 kHz. The problem with a high switching frequency is that the switching losses are proportional to the switching frequency, i.e. selecting switching frequency for an application is a tradeoff between high frequency in order to get an accurate control of the system and switching losses.

The following figures show the aspect of the phase current and the line voltage when three different modulation indexes are set with a carrier frequency of 15 kHz.

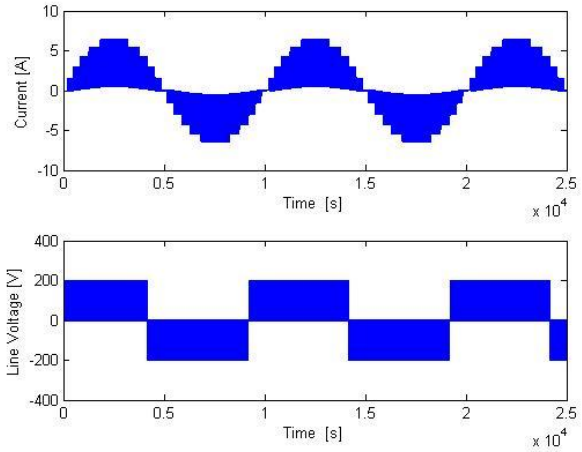

Figure 3.9 – Phase current and line voltage for m=0.2

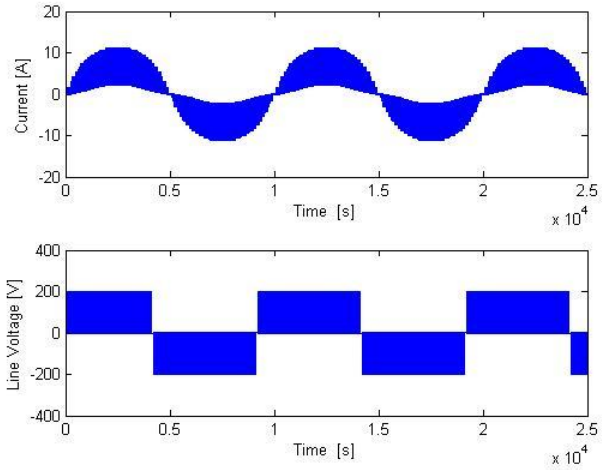

Figure 3.10 – Phase current and line voltage for m=0.5

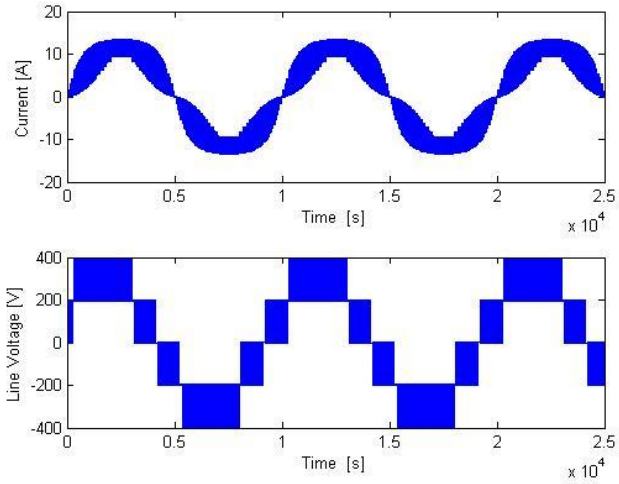

Figure 3.11 – Phase current and line voltage for m=0.8

3.4 Loss calculation of two similar converters available in the market

In the this section, considering the modulation indexes that granted the lower THD in the previous simulations, the overall losses as function of the switching frequency are examined. This will help understand how the switching and conduction losses vary in both converters, when different modulation indexes and switching frequencies are set.

The 3L-NPC topology is symmetrical. As a result, it is enough to analyze only the losses in three switches: S_{k1}, S_{k2} and D_{k1}, and since there are only two commutations per output period in IGBTs S_{k2}, and S_{k3}, the switching losses of these IGBTs are excluded [31],[32].

Two standard modules will be compared in the same application with identical boundary conditions, as described in the following table 3.8. The modules used in this study are Semikron SKM 200MLI066T and Infineon F31 200R07PE4.

Table 3.8 – Converters characteristics

IGBT blocking voltage	Ic @ Ts=80 C	U_f @ 50 A	Eon+Eoff @Ic=200 A , Rg=3,6 ohm	Rthj-s
SKM 200MLI066T				
600 V	210 A	1,45 V	11,3 mJ	0,21 K/W
F31 200R07PE4				
600 V	200 A	1,55 V	15,3 mJ	0,22 K/W

The parameters needed in calculation are taken from the data-sheet of the respective converters. It should be mentioned that the parameters of turn-on and turn-off losses are not given directly there, however sometimes these values can be given by manufacturers in datasheets.

It should be kept in mind that obtained parameters correspond to the toughest conditions. In other words, it is assumed that inverter performs at high ambient temperature or without cooling, thus junction temperature of the device is T=150°C, as it can be seen from the figure 3.12 taken from the converters data-sheet.

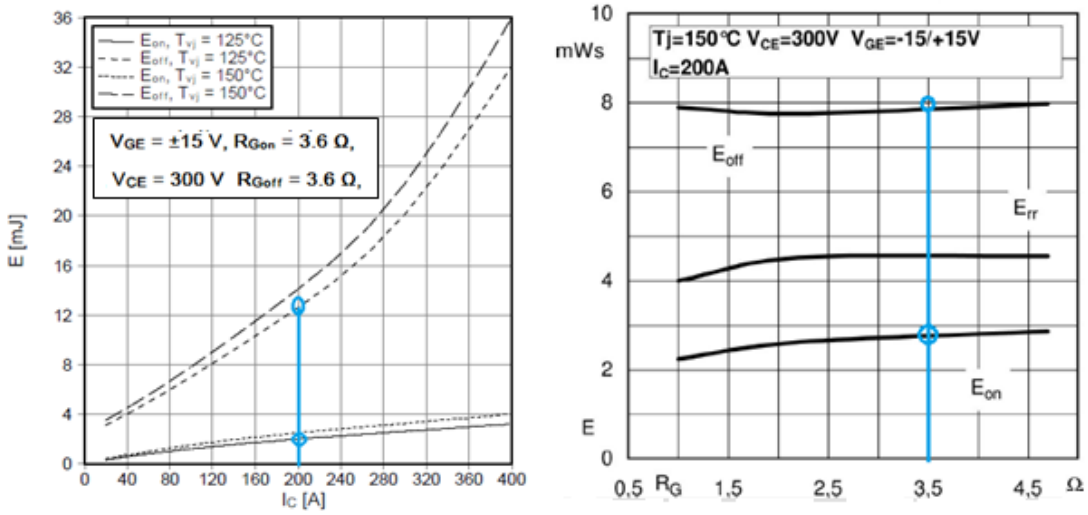

Figure 3.12 – Switching losses. Left) *SKM* **Right)** *F31*

Table 3.9 – Loss results for 10 kHz switching frequency

Fsw = 10 kHz		*SKM 200MLI066T*			*F31 200R07PE4*		
Modulation index		0,7	0,8	0,9	0,7	0,8	0,9
IGBT							
Conduction losses	T1/T4	61,92469	70,77107	79,61746	67,37361	76,99841	86,62321
	T2/T3	111,1648	108,7891	106,4133	124,0971	121,9098	119,7225
Switching losses	T1/T4	35,96893	35,96893	35,96893	48,7013	48,7013	48,7013
	T2/T3	neglegible	neglegible	neglegible	neglegible	neglegible	neglegible
IGBT							
Total losses per IGBT	T1/T4	97,89362	106,74	115,5864	116,0749	125,6997	135,3245
	T2/T3	111,1648	108,7891	106,4133	124,0971	121,9098	119,7225
Total losses per arm		418,1169	431,0581	443,9994	480,344	495,219	510,094
Clamped Diodes							
Conduction losses	D5/D6	101,0705	97,25264	93,43483	112,5194	108,6781	104,8369
Switching losses	D5/D6	12,73237	12,73237	12,73237	7,957729	7,957729	7,957729
Clamped Diodes							
Total losses per diode		113,8028	109,985	106,1672	120,4771	116,6359	112,7946
Clamped diodes total losses		227,6056	219,97	212,3344	240,9542	233,2717	225,5892
Total losses per arm		645,7225	651,0282	656,3338	721,2982	728,4907	735,6832
Total losses per inverter		1937,168	1953,084	1969,001	2163,895	2185,472	2207,05

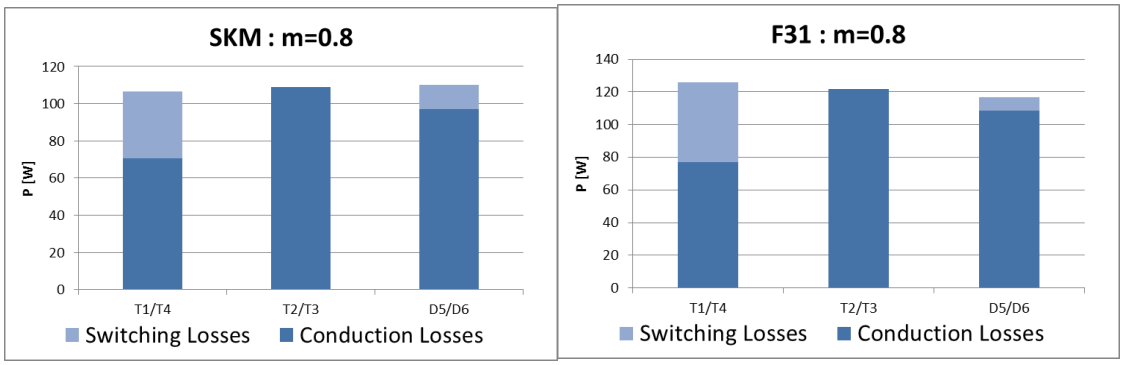

Figure 3.13 – Switching losses vs conduction losses for switching frequency=10 kHz

Table 3.10 - Loss results for 15 kHz switching frequency

Fsw = 15 kHz		*SKM 200MLI066T*			*F31 200R07PE4*		
Modulation index		0,7	0,8	0,9	0,7	0,8	0,9
IGBT							
Conduction losses	T1/T4	61,92469	70,77107	79,61746	67,37361	76,99841	86,62321
	T2/T3	111,1648	108,7891	106,4133	124,0971	121,9098	119,7225
Switching losses	T1/T4	53,9534	53,9534	53,9534	73,05195	73,05195	73,05195
	T2/T3	neglegible	neglegible	neglegible	neglegible	neglegible	neglegible
IGBT							
Total losses per IGBT	T1/T4	97,89362	124,7245	133,5709	140,4256	150,0504	159,6752
	T2/T3	111,1648	108,7891	106,4133	124,0971	121,9098	119,7225
Total losses per arm		418,1169	467,0271	479,9683	529,0453	543,9203	558,7953
Clamped Diodes							
Conduction losses	D5/D6	101,0705	97,25264	93,43483	112,5194	108,6781	104,8369
Switching losses	D5/D6	19,09855	19,09855	19,09855	11,93659	11,93659	11,93659
Clamped Diodes							
Total losses per diode		120,169	116,3512	112,5334	124,456	120,6147	116,7735
Clamped diodes total losses		240,338	232,7024	225,0668	248,912	241,2294	233,5469
Total losses per arm		658,4549	699,7294	705,0351	777,9573	785,1497	792,3422
Total losses per inverter		1975,365	2099,188	2115,105	2333,872	2355,449	2377,027

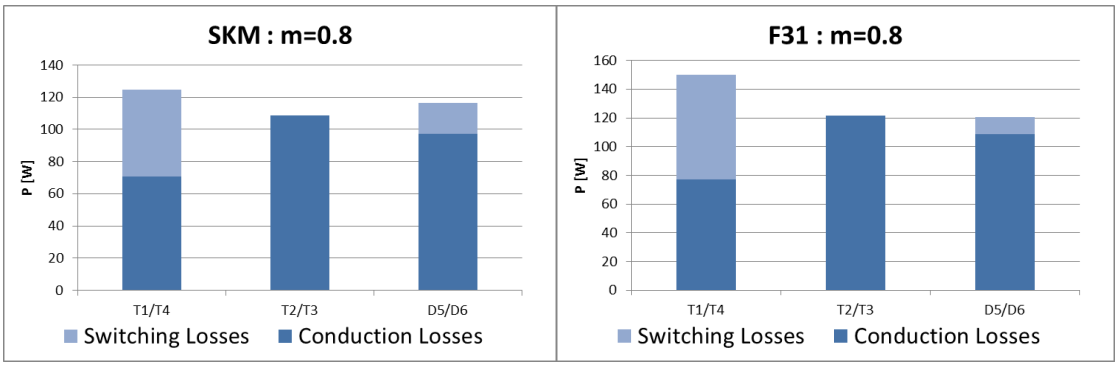

Figure 3.14 – Switching losses vs conduction losses for switching frequency=15 kHz

Table 3.11 - Loss results for 20 kHz switching frequency

Fsw = 20 kHz		*SKM 200MLI066T*			*F31 200R07PE4*		
Modulation index		0,7	0,8	0,9	0,7	0,8	0,9
IGBT							
Conduction losses	T1/T4	61,92469	70,77107	79,61746	67,37361	76,99841	86,62321
	T2/T3	111,1648	108,7891	106,4133	124,0971	121,9098	119,7225
Switching losses	T1/T4	71,93787	71,93787	71,93787	97,4026	97,4026	97,4026
	T2/T3	negligible	negligible	negligible	negligible	negligible	negligible
IGBT							
Total losses per IGBT	T1/T4	97,89362	142,7089	151,5553	164,7762	174,401	184,0258
	T2/T3	111,1648	108,7891	106,4133	124,0971	121,9098	119,7225
Total losses per arm		418,1169	502,996	515,9372	577,7466	592,6216	607,4966
Clamped Diodes							
Conduction losses	D5/D6	101,0705	97,25264	93,43483	112,5194	108,6781	104,8369
Switching losses	D5/D6	25,46473	25,46473	25,46473	15,91546	15,91546	15,91546
Clamped Diodes							
Total losses per diode		126,5352	122,7174	118,8996	128,4348	124,5936	120,7523
Clamped diodes total losses		253,0704	245,4347	237,7991	256,8697	249,1872	241,5047
Total losses per arm		671,1873	748,4307	753,7364	834,6163	841,8088	849,0013
Total losses per inverter		2013,562	2245,292	2261,209	2503,849	2525,426	2547,004

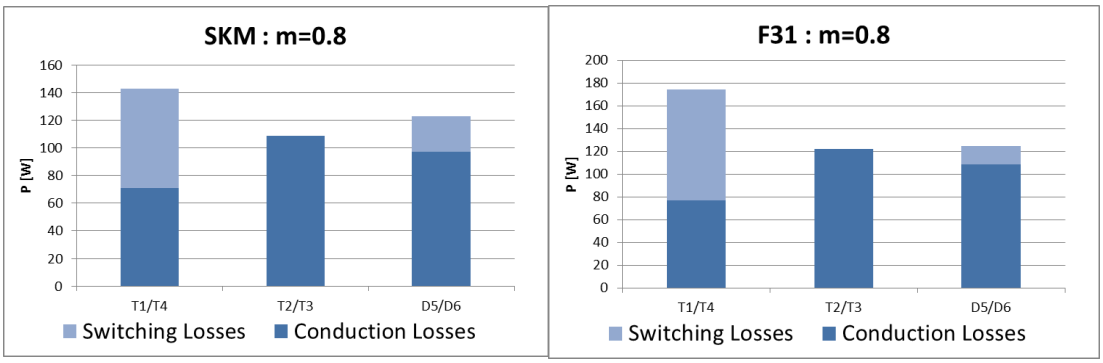

Figure 3.15 – Switching losses vs conduction losses for switching frequency=20 kHz

Taking a closer look at the switching versus conduction losses figures (3.13-3.15), selecting a device that offers high switching frequencies through lower switching losses will result in higher conduction losses. This in turn requires a larger heatsink, which adds system cost and creates space issues. Alternatively, a device with lower conduction losses is most efficiently operated at lower frequencies, which may introduce audible noise due to coil vibration.

Table 3.12 – Total loss results

Modulation index	Total inverter losses [W]		
	Fsw = 10kHz	*Fsw = 15kHz*	*Fsw = 20 kHz*
SKM 200MLI066T			
0.7	1937,17	2083,27	2229,38
0.8	1953,08	2099,19	2245,29
0.9	1969	2115,11	2261,21
F31 200R07PE4			
0.7	2163,89	2333,87	2503,85
0.8	2185,47	2355,45	2525,43
0.9	2207,05	2377,03	2547,01

It is clear through the analysis of table 3.12 that in both of the converters in study that the increase of the total inverter losses is proportional to the switching frequency, in the other hand it is inversely proportional to the modulation index.

As expected, selecting the switching frequency for an application is a tradeoff between high frequency in order to guarantee harmonic distortion and switching losses.

Regarding the converters in analysis, considering the obtained results the SKM manages to achieve minor total losses when operating in the same conditions that the F31.

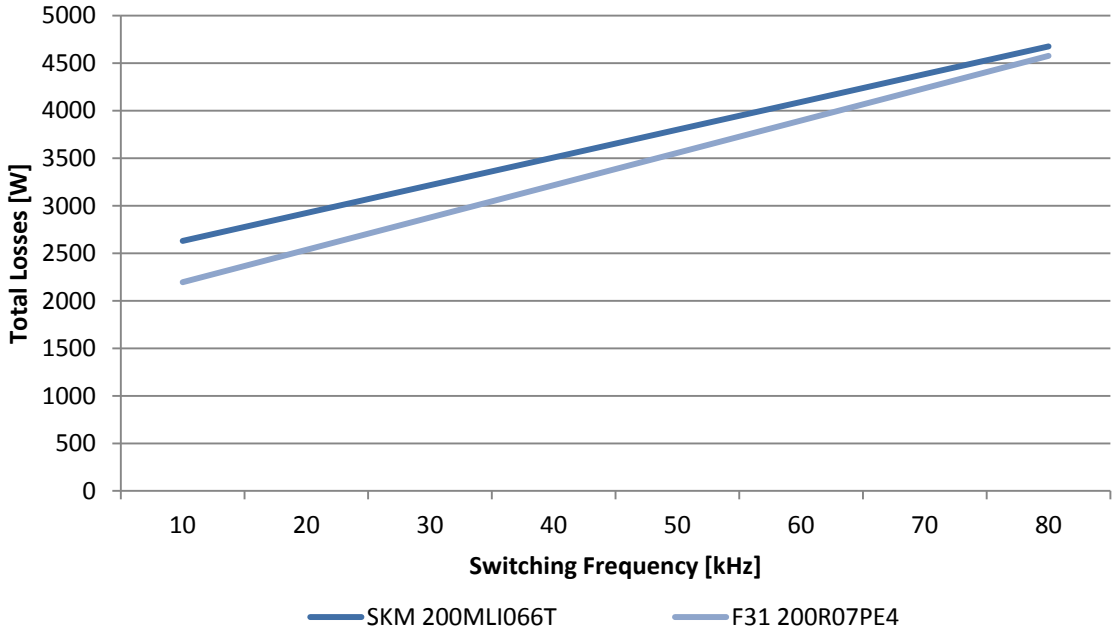

Figure 3.16 – Total losses vs Switching frequency

This chapter was focused on the calculus of total losses of two different 3L-NPC converters. Total conduction and switching losses have been calculated for each of these structures. Also, the study emphasized certain relations between the conduction and switching losses in power devices.

Achieving a higher PWM frequency will reduce ripple current and as a consequence the required filters can be made smaller because the output waveform is closer to the desired waveform.

4

CONTROL OF INDUCTION MACHINE

This chapter is devoted to the modeling and control of the induction motor.

The main task of the control block is to follow demand reference speed by motor and provide proper operation in static and dynamic states without any instability. This is ensured through suitable generated gate signals for the IGBT transistor inside of the inverter.

4.1 Mathematical Model

The model of the induction motor, suitable for designing the controller must incorporate all the dynamic effects of the induction motor operation in both steady and transient state.

The validity of the model is demonstrated against changes in voltage and current for any arbitrary instant time and with the ability to describe its operation under various operating conditions. The theory of spatial vectors is very close to the theory of coordinate transformation (biphasic-dq coordinates) of induction motors, but with the advantage of its simplicity and its ease for graphing and analysis. This chapter will represent the magneto motive forces, currents, voltages and flux linkages space vectors with their mathematical and physical considerations. Finally the dynamic equations of the three-phase induction motor are represented with the help of spatial vectors.

For simplicity it is assumed that IM has three-phase winding, winding symmetrical and smooth poles. It is considered that the permeability of iron is infinite and the flux density is radial in the gap, on the other hand, the effect of the slits and the effect of iron losses are neglected.

The coordinate systems used in this chapter are: the fixed dq reference system on the stator, and the fixed α-β reference system on the rotor.

4.1.1 Space Vectors of Stator Current and Magnetomotive Forces

If the stator windings are fed by a balanced three-phase current ias (t), ibs (t) and ICs (t), and considering that neutral is isolated, then the zero sequence current of the stator is zero, i.e. :

$$i_{0s}(t) = i_{as}(t) + i_{bs}(t) + i_{cs}(t) = 0 \tag{4.1}$$

The distribution of *mmf* produced by the currents do not have a sinusoidal shape, however, for purposes of analysis considers only the fundamental component derived from the series Fourier therefore the higher order spatial harmonics are ignored, then the winding real is replaced by a solenoid, which produces a magnetomotive force sinusoid whose amplitude is equal to the amplitude of the fundamental component of the real magnetomotive force. Whenever a reference is made to the distribution of mmf, the author is referring to their fundamental component.

The *mmf*, $f_{as}(\theta,t)$ produced by each of the three phases is a sine wave stationary in space, where their amplitude is equal to the instantaneous value of the current flowing through the winding, then the mmf has a pulsing behavior, each of the three *mmf* are spatially staggered by 120 degrees, that is:

$$f_{as}(\theta,t) = \frac{4}{\pi} \times \frac{N_{se}}{p} \times i_{as}(t) \times \cos(\theta) \tag{4.2}$$

$$f_{bs}(\theta,t) = \frac{4}{\pi} \times \frac{N_{se}}{p} \times i_{as}(t) \times \cos(2\pi/3 - \theta) \tag{4.3}$$

$$f_{as}(\theta,t) = \frac{4}{\pi} \times \frac{N_{se}}{p} \times i_{as}(t) \times \cos(4\pi/3 - \theta) \tag{4.4}$$

From these equations one can calculate the magnetomotive force in each of the three phases for an arbitrary spatial angle, θ, and time, t. Whereas p is the number of poles of the machine and N_{se} is the effective number of turns. Considering that the stator windings has an equal number of effective turns per phase. The sum of the three magnetomotive forces results in the magnetomotive force, fs, which moves spatially at a speed ωs, where ωs is the synchronous angular velocity.

The mmf present in each phase can be represented in the following way:

$$f_{as}(\theta,t) = \frac{4}{\pi} \times \frac{N_{se}}{p} \times Re\left[i_{as}(t) \times e^{j\theta}\right] \tag{4.5}$$

$$f_{bs}(\theta,t) = \frac{4}{\pi} \times \frac{N_{se}}{p} \times Re\left[i_{bs}(t) \times e^{j2\pi/3} \times e^{-j\theta}\right] \tag{4.6}$$

$$f_{cs}(\theta,t) = \frac{4}{\pi} \times \frac{N_{se}}{p} \times Re\left[i_{cs}(t) \times e^{j4\pi/3} \times e^{-j\theta}\right] \tag{4.7}$$

Moreover, the three windings represented by three fictitious solenoids are offset by 120 degrees, and by convention is considered that the three magnetic axes are situated at angles 0, 120 and 240 degrees respectively.

Then the space vector of magnetomotive force acting on each magnetic axis of the respective phases are:

$$f_{as}(\theta,t) = \frac{4}{\pi} \times \frac{N_{se}}{p} \times i_{as}(t) \times e^{0} \tag{4.8}$$

$$f_{bs}(\theta,t) = \frac{4}{\pi} \times \frac{N_{se}}{p} \times i_{bs}(t) \times e^{j2\pi/3} \tag{4.9}$$

$$f_{cs}(\theta,t) = \frac{4}{\pi} \times \frac{N_{se}}{p} \times i_{cs}(t) \times e^{j4\pi/3} \tag{4.10}$$

The interaction between the three mmf, results in the spatial vector of the mmf of the stator:

$$f_{as}(\theta,t) = \frac{4}{\pi} \times \frac{N_{se}}{p} \times \left\{ i_{as}(t) \times e^{0} + i_{bs}(t) \times e^{j2\pi/3} + i_{cs}(t) \times e^{j4\pi/3} \right\} \quad (4.11)$$

The magnetomotive force, $f_{as}(\theta,t)$ operates in the phase of the magnetic axis which coincides with the real axis of the stationary reference system forming an angle of zero degrees, e^{0}. The magnetomotive force, $f_{bs}(\theta,t)$, acts on the magnetic axis of b which forms a phase angle of 120 degrees with the real axis of the stationary reference system, $e^{j2\pi/3}$. The magnetomotive force, $f_{cs}(\theta,t)$, acts on the magnetic axis of step c to form an angle of 240 degrees with the real axis of the stationary reference system, $e^{j4\pi/3}$.

Each of these three mmf's are stationary spatial vectors (non-rotating) and act solely in their respective magnetic axes varying their amplitudes proportional to their current.

From equation (4.11) the stator current spatial vector is defined as:

$$\vec{\imath}_s(t) = \frac{2}{3} \times \left[i_{as}(t) \times 1 + i_{bs}(t) \times a + i_{cs}(t) \times a^2 \right] = |\vec{\imath}_s| \times e^{j\alpha_s} \quad (4.12)$$

The equation (4.12) represents the stator current of the spatial vector, in the stationary reference system, whereas $a = e^{j2\pi/3}$e $a^2 = e^{j4\pi/3}$ are spatial operators. On the other hand, $|\vec{\imath}_s|$ is the absolute value of the stator current vector and, α_s, is the angle relatively to the real axis of the stationary system.

The stator current spatial vector can be expressed in the d-q frame as:

$$\vec{\imath}_s = i_{ds} + j i_{qs} \quad (4.13)$$

In symmetrical machines, the biphasic stator currents in the real axis $i_{ds}$and in the imaginary axis i_{qs}in relation with the triphasic currents are expressed by:

$$i_{ds} = \frac{2}{3} \times \left[i_{as} - \frac{1}{2} \times i_{bs} - \frac{1}{2} \times i_{cs} \right] \quad (4.14)$$

$$i_{qs} = \frac{\sqrt{3}}{3} \times (i_{bs} - i_{cs}) \quad (4.15)$$

4.1.2 Space Vectors of Rotor Current and Magnetomotive Forces

Similarly to equation (4.11) the distribution of the rotor mmf, is represented by:

$$f_r(\alpha,t) = \frac{4}{\pi} \times \frac{N_{re}}{p} \times [i_{ar}(t) \times \cos(\alpha) + i_{br}(t) \times \cos(2\pi/3 - \alpha) + \\ + i_{cr}(t) \times \cos(4\pi/3 - \alpha)] \quad (4.16)$$

In the complex frame the equation (4.16) is written as:

$$f_r(\alpha,t) = \frac{3}{2} \times \frac{4}{\pi} \times \frac{N_{re}}{p} \times Re\left\{\frac{2}{3} \times [i_{ar}(t) + i_{br}(t) \times a + i_{ar}(t) \times a^2] \times e^{-j\alpha}\right\} \quad (4.17)$$

In the equation (4.18) is presented the spatial vector of the rotor current expressed in the fixed reference system.

$$i_r(t) = \frac{2}{3} \times [i_{ar}(t) + i_{br}(t) \times a + i_{ar}(t) \times a^2] = \left|\vec{i}_r\right| \times e^{j\alpha_r} \quad (4.18)$$

Where $|\vec{i}_r|$ is the spatial vector magnitude of the rotor current, and α_r is the angle relative to the reference system fixed in the rotor. Following the same reasoning made for obtaining the equations (4.14) and (4.15), we observe that:

$$i_{\alpha r} = \frac{2}{3} \times \left[i_{ar}(t) - \frac{1}{2} \times i_{br}(t) - \frac{1}{2} \times i_{cr}(t)\right] \quad (4.19)$$

$$i_{\alpha r} = \frac{\sqrt{3}}{3} \times [i_{br}(t) - i_{cr}(t)] \quad (4.20)$$

4.1.3 Space Vectors of Linkage Flux

In this section the concept of spatial vector is extended for the representation of both the stator as the rotor flux linkages, starting from the definition of the flux present in each phase.

4.1.3.1 Space Vectors of Stator's Linkage Flux

Similarly to the spatial vector definition of the stator and the rotor current, one can define the space vector of the stator flux linkage as a function of the instantaneous flux values in each phase. The space vector's stator flux in the stationary reference system is:

$$\vec{\psi}_s = \frac{2}{3} \times [\psi_{as} + \psi_{bs} \times a + \psi_{cs} \times a^2] \quad (4.21)$$

Since the instantaneous values of the flux linkage depends on the stator and rotor currents, then:

$$\vec{\psi}_s = L_s \times \vec{i}_s + L_m \times \vec{i}_r \times e^{j\theta_r} = L_s \times \vec{i}_s + L_m \times \overrightarrow{i_r'} \quad (4.22)$$

L_s is the inductance of all three phases of the stator and L_m is the magnetizing inductance of the three phases.

In equation (4.22) is two spatial components of the vector of the stator flux linkage, the first, $L_s \times \vec{\imath}_s$, is the space vector of the self-flux linkage of phase stator currents produced by the stator, the second component, $L_m \times \overrightarrow{\imath_r'}$, is the space vector of mutual flux linkage generated by the rotor currents expressed in the stationary reference system.

Moreover, the stator flux linkage space vector in terms of its components on the real axis $\psi_{ds}$and the imaginary ψ_{qs} is:

$$\vec{\psi}_s = \psi_{ds} + j\psi_{qs} \tag{4.23}$$

Unfolding the expression (4.23) in terms of its components on the real and imaginary axis:

$$\psi_{ds} = L_s \times i_{ds} + L_m \times i_{dr} \tag{4.24}$$
$$\psi_{qs} = L_s \times i_{qs} + L_m \times i_{qr} \tag{4.25}$$

In the above expression currents i_{ds}, i_{qs}, i_{dr} and $i_{qr}$are instantaneous values of the currents in the real and imaginary axis stator and rotor respectively.

4.1.3.2 Space Vectors of Rotor's Linkage Flux

The spatial vector of the rotor flux linkage, expressed in their natural reference system (reference system fixed in the rotor) which is rotating at a speed ωr, is represented as follows:

$$\vec{\psi}_r = \frac{2}{3} \times [\psi_{ar} + \psi_{br} \times a + \psi_{cr} \times a^2] \tag{4.26}$$

Since ψ_{ar},$\psi_{br}$and $\psi_{cr}$are the instantaneous values of the rotor flux linkage in the three phases. These instantaneous values of the currents depend on the stator and rotor:

$$\vec{\psi}_r = L_r \times \vec{\imath}_r + L_m \times \overrightarrow{\imath_s'} \tag{4.27}$$

Where L_r is the total inductance of the three phases in the rotor, L_m is the magnetization inductance of the rotor three phases and $\overrightarrow{\imath_s'}$ is the space vector of the stator current expressed in the fixed reference system. Equation (4.27) can be expressed in terms of its components ($\psi_{\alpha r}$ and $\psi_{\beta r}$), i.e.:

$$\vec{\psi}_r = \psi_{\alpha r} + j\psi_{\beta r} \tag{4.28}$$

Unfolding the expression (4.28) in their components, results:

$$\psi_{\alpha r} = L_s \times i_{\alpha r} + L_m \times i_{ds}{}' \tag{4.29}$$
$$\psi_{\beta r} = L_s \times i_{\beta r} + L_m \times i_{qs}{}' \tag{4.30}$$

Variables $i_{\alpha r}$, $i_{\beta r}$, $i_{ds}{}'$ and $i_{qs}{}'$ are the components in the real and imaginary axis of the rotor and stator currents respectively.

4.1.4 Rotor and Stator Voltage Space Vectors

The space vector of the stator and rotor voltages may be defined similarly as the magnitudes above. Thus the stator voltage space vector in the stationary reference system and the rotor voltage space vector in the fixed reference system can be written as:

$$\overrightarrow{u_s} = \frac{2}{3} \times [u_{as}(t) + u_{bs}(t) \times a + u_{cs}(t) \times a^2] = u_{ds} + j u_{qs} \tag{4.31}$$

$$\overrightarrow{u_r} = \frac{2}{3} \times [u_{ar}(t) + u_{br}(t) \times a + u_{cr}(t) \times a^2] = u_{\alpha r} + j u_{\beta r} \tag{4.32}$$

In equations (4.31) and (4.32), $u_{as}(t), u_{bs}(t), u_{cs}(t), u_{ar}(t), u_{br}(t)$ and $u_{cr}(t)$ are the instantaneous values of the stator and rotor voltages respectively, while u_{ds}, u_{qs} and $u_{\alpha r}$, $u_{\beta r}$are the real and imaginary axis components. The tri-phasic voltage is related to its biphasic components as follows:

$$\overrightarrow{u_{ds}} = Re\left\{\frac{2}{3} \times [u_{as}(t) + u_{bs}(t) \times a + u_{cs}(t) \times a^2]\right\} = \\ = \frac{2}{3} \times \left[u_{as} - \frac{1}{2} \times u_{bs} - \frac{1}{2} \times u_{cs}(t)\right] \tag{4.33}$$

$$\overrightarrow{u_{qs}} = Im\left\{\frac{2}{3} \times [u_{as}(t) + u_{bs}(t) \times a + u_{cs}(t) \times a^2]\right\} = \\ = \frac{2}{3} \times \left[u_{as} - \frac{1}{2} \times u_{bs} - \frac{1}{2} \times u_{cs}\right] \tag{4.34}$$

Proceeding similarly for the rotor voltage, one obtains:

$$\overrightarrow{u_{\alpha r}} = \frac{2}{3} \times \left[u_{ar} - \frac{1}{2} \times u_{br} - \frac{1}{2} \times u_{cr}\right] \tag{4.35}$$

$$\overrightarrow{u_{\beta r}} = \frac{2}{3} \times [u_{br} - u_{cr}]/\sqrt{3} \tag{4.36}$$

Space vectors do not contain the zero sequence components, when necessary to represent the zero sequence voltages will need to consider them separately, then:

$$\overrightarrow{u_{0s}} = \frac{1}{3} \times [u_{as}(t) + u_{bs}(t) + u_{cs}(t)] \tag{4.37}$$

$$\overrightarrow{u_{0r}} = \frac{1}{3} \times [u_{ar}(t) + u_{br}(t) + u_{cr}(t)] \tag{4.38}$$

Rewriting the equations (4.33) (4.34) and (4.37) in a matrix arrangement:

$$\begin{bmatrix} u_{0s} \\ u_{ds} \\ u_{qs} \end{bmatrix} = \frac{2}{3} \times \begin{bmatrix} \frac{1}{2} & \frac{1}{2} & \frac{1}{2} \\ 1 & -\frac{1}{2} & -\frac{1}{2} \\ 0 & \frac{\sqrt{3}}{2} & -\frac{\sqrt{3}}{2} \end{bmatrix} \times \begin{bmatrix} u_{as} \\ u_{bs} \\ u_{cs} \end{bmatrix} \tag{4.39}$$

4.1.5 Dynamic Equations of an Induction Machine in Space Vectors

In this section are presented the equations governing the dynamic behavior of three-phase induction motor, in the form of space vector. These equations show the relationship between the flux linkages and the currents the voltages on both the stator and the rotor.

With the help of the spatial definition of the vectors of the voltages, equations (2.61) and (2.75), the spatial vectors of currents, equations (2.22) and (2.36), and the vectors of spatial flux linkages, equations (2.40) and (2.49) , stator and rotor respectively have that:

$$\overrightarrow{u_s} = R_s \times \overrightarrow{i_s} + \frac{d\overrightarrow{\psi_s}}{dt} \tag{4.40}$$

$$\overrightarrow{u_r'} = R_r \times \overrightarrow{i_r'} + \frac{d\overrightarrow{\psi'_r}}{dt} - j\omega\overrightarrow{\psi'_r} \tag{4.41}$$

$$\overrightarrow{\psi_s} = L_s \times \overrightarrow{i_s} + L_m \times \overrightarrow{i_r'} \tag{4.42}$$

$$\overrightarrow{\psi'_r} = L_s \times \overrightarrow{i_r'} + L_m \times \overrightarrow{i_s} \tag{4.43}$$

The first term of Equations (4.40) and (4.41) represents the drop in resistance of the stator and rotor respectively, and the second term represents the change in electromotive force, which is the first derivative of the space vector of the concatenated stator flux and rotor, finally the term $j\omega\overrightarrow{\psi'_r}$ represents the rotational electromotive force produced by the rotation of the rotor.

In symmetrical three-phase induction motor, one way to represent the instantaneous electromagnetic torque is via the cross product between vectors of spatial flux linkage and stator current.

$$T_{em} = \frac{3}{2} \times p \times \overrightarrow{\psi_s} \times \overrightarrow{i_s} \tag{4.44}$$

Given that $\overrightarrow{\psi_s}$ and $\overrightarrow{i_s}$ are the flux linkage and stator current space vector respectively, and P the number of pole pairs.

Considering that $\alpha_s$and ρ_s are the angles of the flux linkage and the stator current real axis in relation to the stationary reference system, then from equation (4.44), it follows that:

$$T_{em} = \frac{3}{2} \times p \times \left|\overrightarrow{\psi_s}\right| \times \left|\overrightarrow{i_s}\right| \times \sin(\alpha_s - \rho_s) = \frac{3}{2} \times p \times \left|\overrightarrow{\psi_s}\right| \times \left|\overrightarrow{i_s}\right| \times \sin(\alpha) \tag{4.45}$$

Whereas $\alpha = \alpha_s - \rho_s$ is the angle between the vectors of the spatial flux linkage and stator current.

If appropriate voltage is applied on the stator in such a way to keep the stator flux constant and the same voltage could change the angle ρ_s, then the electromagnetic torque will also vary. If the angle increases the electromagnetic torque produced is positive, while if the angle is decreased produced then a reduction in the electromagnetic torque is obtained. In conclusion to control the stator flux (magnitude and angle) it is necessary to generate the appropriate voltage vector through the inverter that feeds the IM.

4.2 Direct torque control

The direct torque control is principally a non-linear control in which the inverter switching states are imposed through a separate control of stator flux and electromagnetic torque of the motor. The inverter command is instantaneous and it replaces then the decoupling through the vector transformation. One of the most important characteristics of the DTC is the nonlinear regulation of stator flux and electromagnetic torque with variables structures or by hysteresis [23],[27].

The flux regulation is imperative for an efficient control of the induction machine torque and in the DTC, the stator flux regulation is chosen because it's easier to estimate, and partly it has a faster dynamics than the rotor flux. By adjusting the stator flux, the rotor flux is also adjusted.

As in the other control methods, which use a direct regulation of the flux, the flux nominal value is imposed as a constant reference, for speeds lower than the nominal value. For higher speeds, a flux reference value, decreasing proportionally with speed is imposed. On the other hand, the quality of rotation speed, and/or position, control of the modern actuators depends directly on the toque control.

It can be seen that once one has the estimated and reference instantaneous values of electromagnetic torque and stator flux, the following step is to calculate the error between them; these errors are used as inputs for the hysteresis controllers, which aim to maintain the torque and flux errors within upper and lower limits allowed.

The output levels achieved in this stage of the control are input signals to the block that is responsible for finding the right vector to reduce the speed error. This procedure is made for each sampling instant to drive the IM to the desired speed value [33],[34].

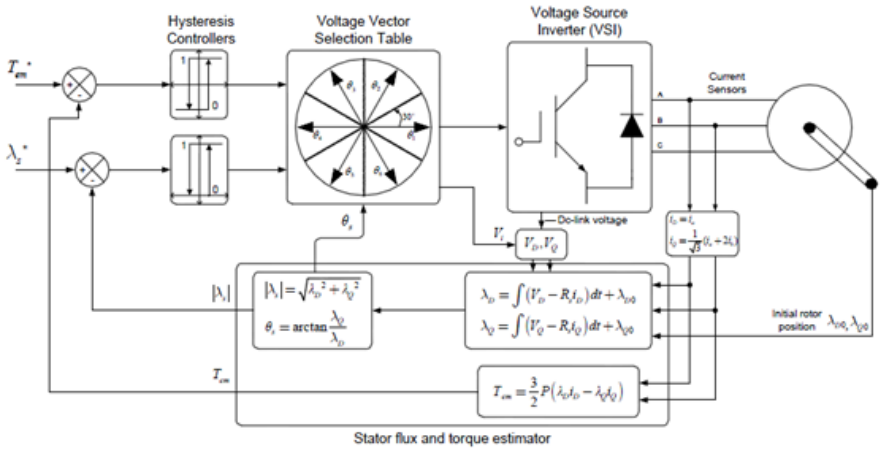

Figure 4.1 – DTC model

4.2.1 Stator flux and torque control

As stated before, the motor torque control is achieved with two hysteresis controllers, one for stator flux magnitude error and the other for the torque magnitude error. The selection of one switching vector per sampling time depends on the sign of these two controllers without inspections of the magnitude of the errors produced in the transient and dynamic situations per sampling time and level of the applied stator voltage.

The stator flux hysteresis bandwidth

This value is the total bandwidth distributed symmetrically around the flux set point (Wb). The following figure illustrates a case where the flux set point is flux_ref and the torque hysteresis bandwidth is set to dFlux.

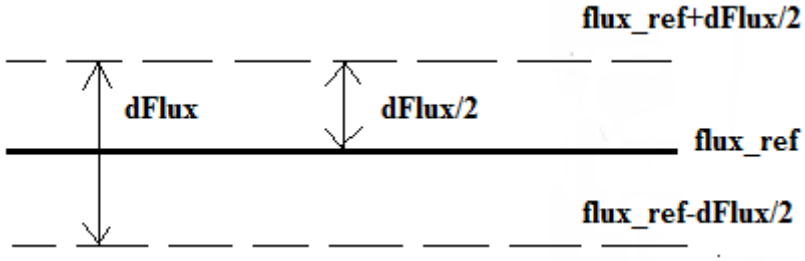

Figure 4.2 – Flux hysteresis interval

The torque hysteresis bandwidth

This value is the total bandwidth distributed symmetrically around the torque set point (N.m). The following figure illustrates a case where the torque set point is Te_ref and the torque hysteresis bandwidth is set to dTe.

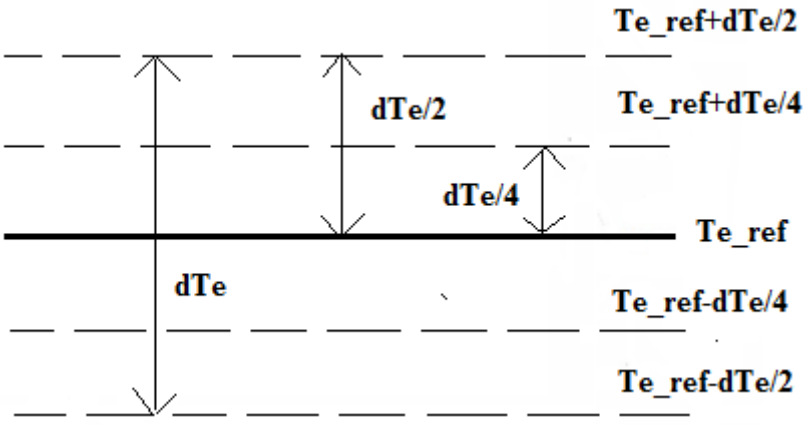

Figure 4.3 – Torque hysteresis interval

4.2.2 Torque and flux estimator

Flux estimation is an important task in implementation of high-performance DTC motor drives. Vector control method of IM drive needs knowledge about actual value of the stator flux magnitude and position as well electromagnetic torque.

Many different techniques have been developed for IM flux estimation. Generally, they may be divided into two groups: open loop estimators and closed loop estimators/observers. Most of these methods are based on so called “current model” or “voltage model”. In fact closed loop estimators/observers are based on the current or voltage model with an error correction loop, which drives error between two flux models to zero in steady state. However, an observer has his own dynamics, is sensitive to parameter changes, and has to be carefully designed for individual drives. Therefore, is very complicated and impractical.

Voltage model based flux estimator with ideal integrator

The stator flux linkage can be obtained by using terminal voltages and currents. It is the integral of terminal voltages minus the resistance voltage drop:

$$\frac{d\psi_{sd}}{dt} = (U_{sd} - R_s \times I_{sd}) \tag{4.46}$$

$$\frac{d\psi_{sq}}{dt} = \left(U_{sq} - R_s \times I_{sq}\right) \tag{4.47}$$

However, at low speed (frequencies) some problems arise, when this technique is applied, since the stator voltage becomes very small and the resistive voltage drops become dominant, requiring very accurate knowledge of the stator resistance R_s and very accurate integration.

Also, the stator resistance can vary due to temperature changes. The overall accuracy of the estimated flux linkage vector will also depend on the accuracy of the monitored voltages and currents.

The most know classical voltage model obtains the flux components in stator coordinates by integrating the motor back electromotive force. The method is sensitive for only one motor parameter, stator resistance Rs. However, the application of pure integrator is difficult because of dc drift and initial value problems.

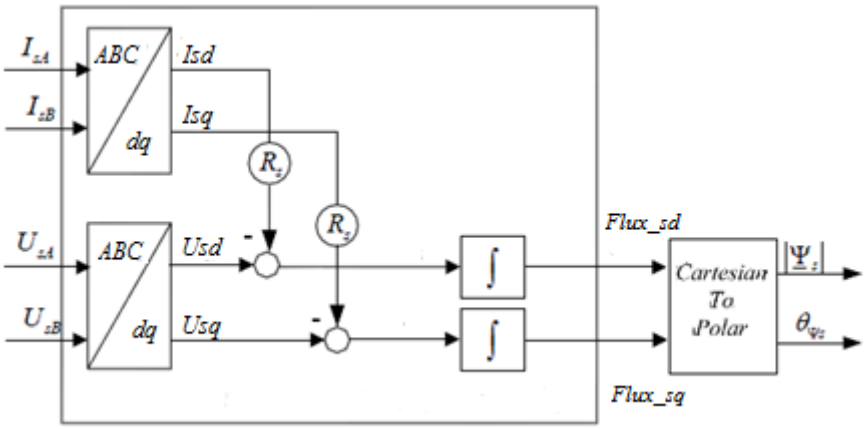

Figure 4.4 – Voltage model based estimator with ideal integrator

Electromagnetic torque estimation

The IM motor output torque is calculated based on the equation (4.48) presented latter in this Chapter, which for stator oriented coordinate system can be written as follows:

$$T_{em} = \frac{3}{2} \times p \times \left(\Psi_{sd} \times I_{sq} + \Psi_{sq} \times I_{sd}\right) \quad (4.48)$$

It can be seen that the calculated torque is dependent on the current measurement accuracy and the stator flux estimation method.

Simulink implementation

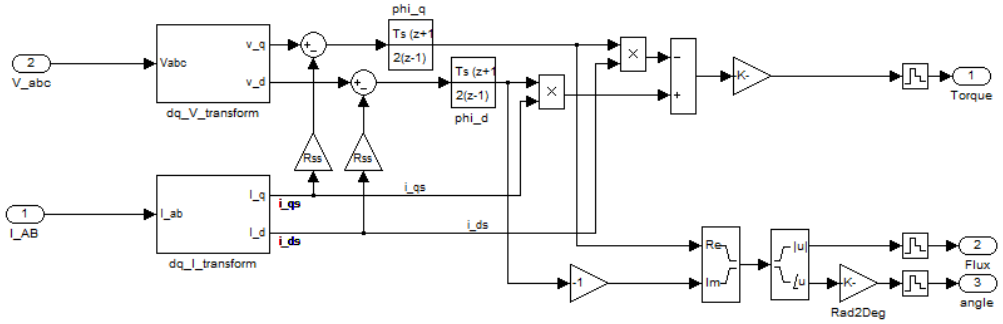

Figure 4.5 – Simulink model of flux and electromagnetic torque estimator

In this particular case, a three level inverter is used in the command of the DTC, what allows having a higher level of output voltage and can contribute to reducing harmonics and torque ripple. In this case, the voltage space is subdivided into six sectors by adopting a technique which employs only twelve active voltage space vectors, corresponding to the small and large vectors and consequently without using the zero or the middle space vectors.

Table 4.1 – Switching states and respective voltage vector

Switching State	*Sa Sb Sc*	*Voltage Vector*	*Vector Type*	*Switching State*	*Sa Sb Sc*	*Voltage Vector*	*Vector Type*
S1	000	V0	Zero Vector	S15	212	V6	Small Vector
S2	111	V0	Zero Vector	S16	210	V7	Middle Vector
S3	222	V0	Zero Vector	S17	120	V8	Middle Vector
S4	100	V1	Small Vector	S18	021	V9	Middle Vector
S5	110	V2	Small Vector	S19	012	V10	Middle Vector
S6	010	V3	Small Vector	S20	102	V11	Middle Vector
S7	011	V4	Small Vector	S21	201	V12	Middle Vector
S8	001	V5	Small Vector	S22	200	V13	Large Vector
S9	101	V6	Small Vector	S23	220	V14	Large Vector
S10	211	V1	Small Vector	S24	020	V15	Large Vector
S11	221	V2	Small Vector	S25	022	V16	Large Vector
S12	121	V3	Small Vector	S26	002	V17	Large Vector
S13	122	V4	Small Vector	S27	202	V18	Large Vector
S14	112	V5	Small Vector				

4.2.3 Selection of voltage vectors for the control of the stator flux amplitude

When the stator flux vector is in a sector, the control of the flux and the torque can be assured by selecting one of the possible voltage vectors stated in table 4.1. The difference between each of the inverter states that generate the same voltage vectors is in the way the load is connected to the DC bus. The analysis of the inverter states show that:

• The large vectors correspond to only the positive and negative rails of the DC bus are used and consequently have no effect on the neutral point potential;

• In the case of the medium vectors, the load is connected to the positive rail, neutral point and negative rail. The effect on the neutral point depends on the load current;

• There are two possible states of each of the small voltage vectors which can be used to control the neutral point voltage.

Depending on the stator flux position (sector) and the values of the outputs of torque and flux controllers, the optimal vector is selected, from all available vectors.

4.2.4 Switching table

The elaboration of the command structure is based on the hysteresis controller output relating to the variable flux, the variable torque and the sector N corresponding to the stator flux vector position.

The exploitation of the first degree of freedom of the inverter, is made by the choice of vectors to apply to the machine among the 12 possibilities, during a sampling period.

For the rebalancing of the capacitive middle point, the phase level sequence is chosen among all the possibilities associated with every voltage vector adopted. This establishes the second degree of freedom which must be necessarily used.

4.2.5 Control scheme for DC link capacitor voltages balancing

This control scheme, which uses only twelve active voltage space vectors corresponding to the sections with small and large vectors and without using the null and medium space vectors, is a natural extension of classical DTC for a two level inverter.

The author considered the case where stator flux is achieved by using two-level hysteresis comparator and electromagnetic torque by using 4-level hysteresis. So the inputs at the command structure will be sector, the outputs of the hysteresis controllers relating to the flux and torque.

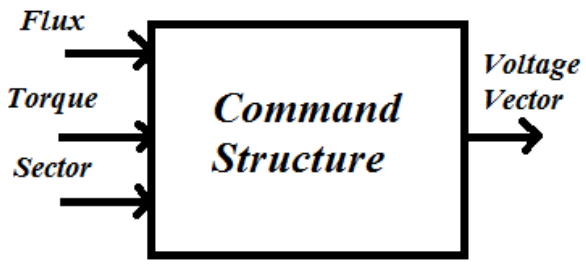

Figure 4.6 – Command structure input/output signals

The command structure consists on a series of look-up tables, which contain for each sector the necessary voltage vector to apply at the multilevel inverter, depending of the values returned by the hysteresis controllers.

Table 4.2 – Command structure look-up tables

Sector I		
flux	***torq***	***voltage vector***
1	**2**	V2h
	1	V2l
	-1	V6l
	-2	V6h
-1	**2**	V3h
	1	V3l
	-1	V5l
	-2	V5h

Sector III		
Flux	***Torque***	***Voltage Vector***
1	**2**	V4h
	1	V4l
	-1	V2l
	-2	V2h
-1	**2**	V5h
	1	V5l
	-1	V1l
	-2	V1h

Sector V		
Flux	***Torque***	***Voltage Vector***
1	**2**	V6h
	1	V6l
	-1	V4l
	-2	V4h
-1	**2**	V1h
	1	V1l
	-1	V3l
	-2	V3h

Sector II		
flux	**torq**	**voltage vector**
1	**2**	V3h
	1	V3l
	-1	V1l
	-2	V1h
-1	**2**	V4h
	1	V4l
	-1	V6l
	-2	V6h

Sector IV		
Flux	**Torque**	**Voltage Vector**
1	**2**	V5h
	1	V5l
	-1	V3l
	-2	V3h
-1	**2**	V6h
	1	V6l
	-1	V2l
	-2	V2h

Sector VI		
Flux	**Torque**	**Voltage Vector**
1	**2**	V1h
	1	V1l
	-1	V5l
	-2	V5h
-1	**2**	V2h
	1	V2l
	-1	V4l
	-2	V4h

Further analysis on table 4.2 reveals that the output as one of the following structures, *Vxl* or *Vxh*, where letters “l” and “h” stand for low and high, respectively. The reason for implementing this structure is because of the second degree of freedom stated before.

One of the conclusions reached when the analysis of the multilevel inverter states was made previously on this chapter, is that there are two possible states of each of the small voltage vectors which can be used to control the neutral point voltage.

Table 4.3 – DTC available voltage vectors

Voltage Vector	**1**	**2**	**3**	**4**	**5**	**6**
High	200	220	020	022	002	202
Low	*Negative Phase Current*					
	211	110	121	011	112	101
	Positive Phase Current					
	100	221	010	122	001	212

The principal reason for the neutral point unbalance is due to the current flow from/to the neutral point. As mentioned above, the NPC three-level inverter has redundant states. Thus, some discrete voltage level can be obtained by more than one switching state. As the voltage evolution for a given capacitors will be different for each state as shown in this section, this redundancy permits to control the capacitors voltages while the requested vector voltage is supplied.

The large vectors and the zero vectors do not change the voltage of neutral point. The line current flows through the neutral point for a given vector and the NPP is then affected. The compensation of voltage capacitor balance has to be given to the next small vector because this vector could flow opposite current from the capacitor bank.

Table 4.4 – Small vectors current flow

Switching State	*Sa Sb Sc*	*Voltage Vector*	*iNP*	*Vector Type*
S4	100	V1	iSA	Small Vector
S5	110	V2	-iSC	Small Vector
S6	010	V3	iSB	Small Vector
S7	011	V4	-iSA	Small Vector
S8	001	V5	iSC	Small Vector
S9	101	V6	-isB	Small Vector
S10	211	V1	-iSA	Small Vector
S11	221	V2	iSC	Small Vector
S12	121	V3	-isB	Small Vector
S13	122	V4	iSA	Small Vector
S14	112	V5	-iSC	Small Vector
S15	212	V6	iSB	Small Vector

Based on this property, a control strategy is presented and applied to a three level NPC VSI. Thus, using as inputs the required voltage vector, the actual state of the capacitor voltages and the current direction in the neutral point, a simple control algorithm is defined. Then, the inverter will be controlled by the switching state assuming the requested discrete voltage vector and the needed capacitor voltage evolutions. The diagram of the control algorithm is shown at figure 4.7.

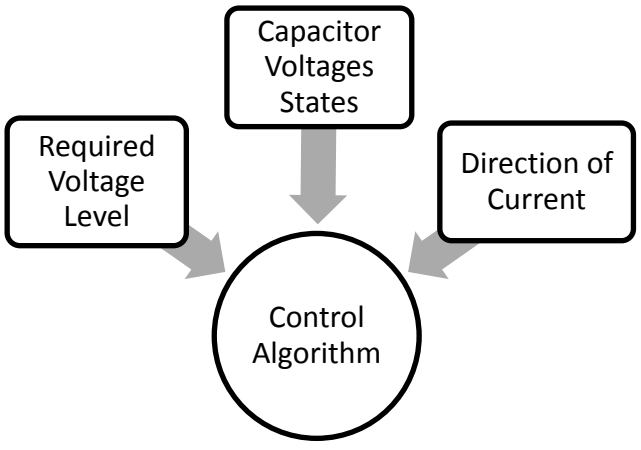

Figure 4.7 – Neutral point voltage control algorithm

This simple control algorithm consists on comparing the sign of the current provided by de DC link with the one of the last instant when a small vector had been applied and, if the sign of the current does not change, then the other available switching pattern type for is selected to permit the capacitors voltage to be balanced.

The following figure shows the selected voltage vector for each sector to maintain the stator flux in the hysteresis bound.

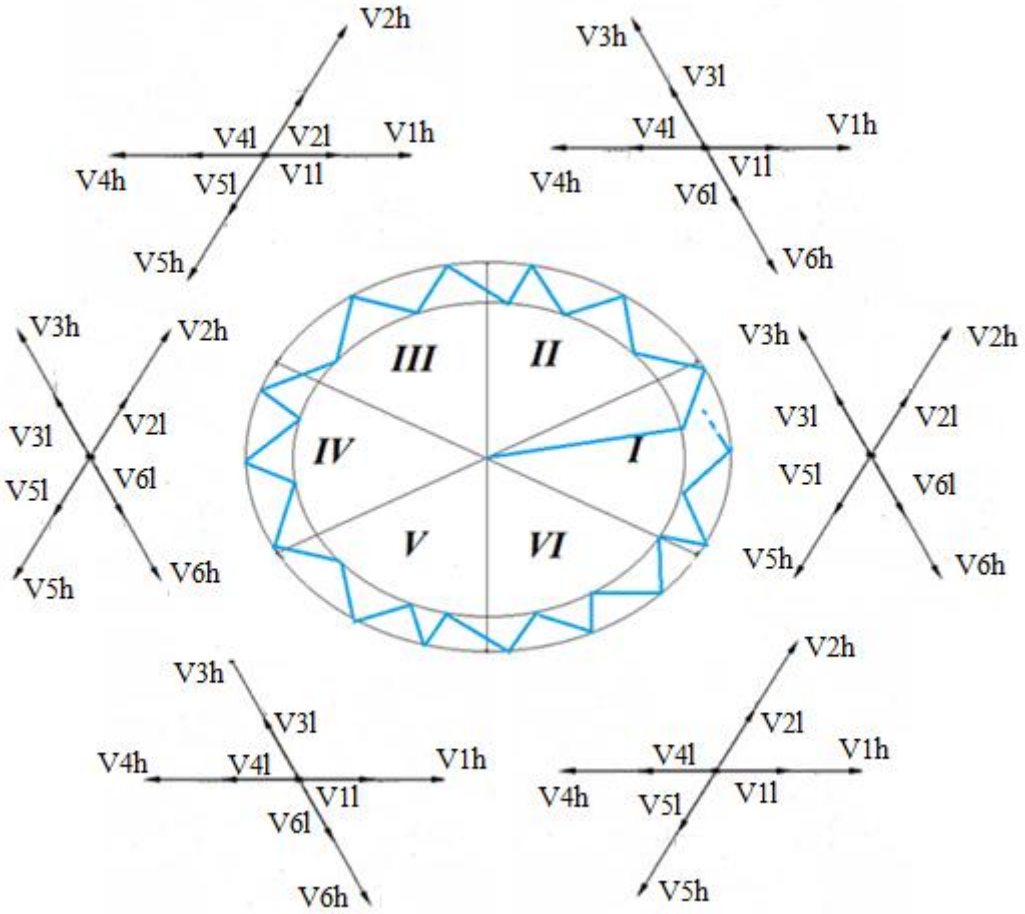

Figure 4.8 – DTC available voltage vectors

Simulink implementation

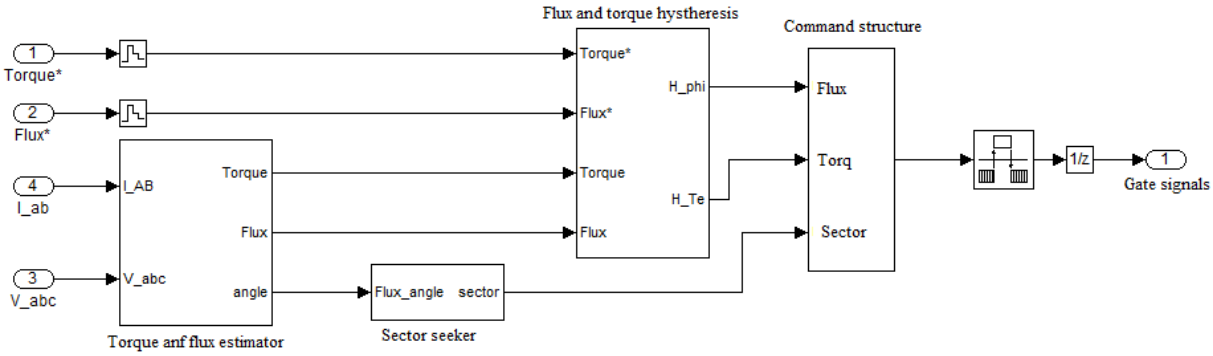

Figure 4.9 – Simulink model of DTC

4.3 Direct Torque Control with Space Vector Modulation

SVM is used to synthesize a required voltage vector that has been calculated by the controller in the DTC scheme. By using a space vector modulator, the torque ripple is reduced and the switching frequency of the component is constant. When extending the classic DTC-SVM scheme to the multilevel inverter, the inverter is capable of generating more available voltage vectors proportional to its voltage levels.

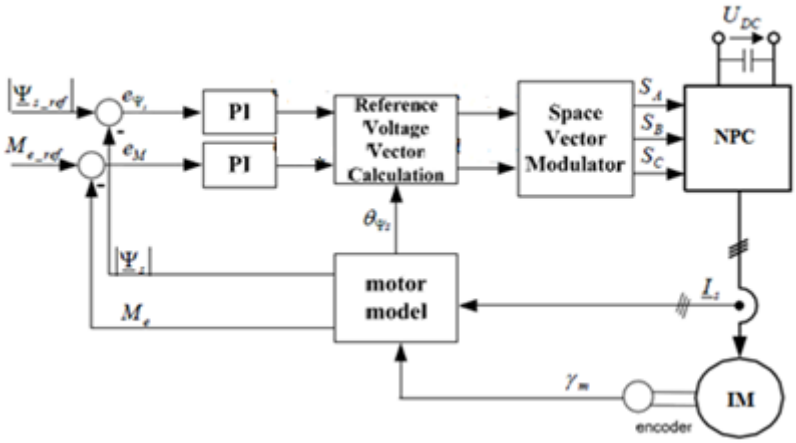

Figure 4.10 – DTC-SVM model

A combination of DTC and Space Vector Modulation (SVM) avoids the use of look-up tables in selecting the voltage vector and although using the same torque and flux estimators, the torque and flux hysteresis controllers and the switching table used in basic DTC are replaced by a PI torque and flux controllers [20],[22].

As it is in DTC, in the SVM there are eighteen “active states” which produce different voltage vectors (some of them can be realized by two combinations of transistor states) and three switching states which produce zero voltages at the load phases. These “zero voltage vectors” are active when either all upper, center or lower transistors are switched on.

As stated previously, a three-phase three-level converter provides twenty seven vectors:

- 3 zero (000, 111, 222),
- 12 internal (100, 211, 110, 221, 010, 121, 011, 122, 001, 112, 101, 212),
- 6 middle (210, 120, 021, 012, 102, 201)
- 6 external (200, 220, 020, 022, 002, 202).

External vectors divide plane into six sectors (figure 4.11). Voltage angle α can also be used to determine the sector, since each section encloses in 60º. In each sector calculations carried out to achieve vectors duration times are the same and the difference is only in power switch selection for the gating signal. Thus, the reference vector is normalized to the first sector and after evaluation of vectors switching times a proper transistor switching sequence, for reference position, is created [25].

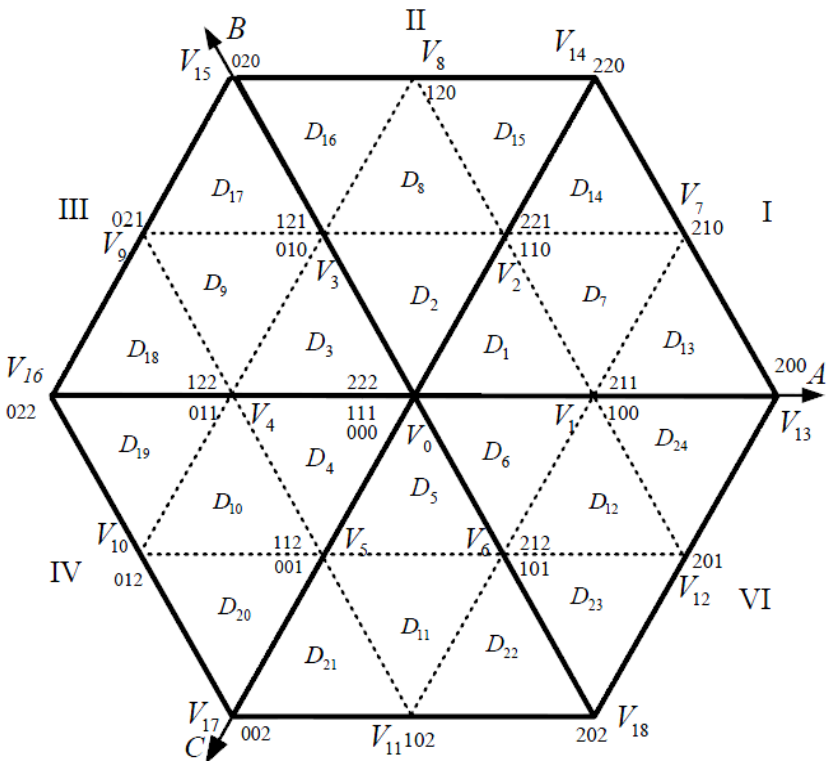

Figure 4.11 – Space vector

According to the space voltage vectors representation of the inverter, the voltage diagram can be divided into six sectors as shown in figure 4.11, and each sector is divided into four triangles or regions. The SVM technique is based on the modulation of a vector reference using the three voltage vectors that construct the region where the end of the reference vector resides.

4.3.1 Proposed method

It is the task of the modulator to decide which position the switches should assume (switching state), and the duration needed (duty cycle) in order to synthesize the reference voltage vector. In other words, it is the task of the modulator to approximate the reference vector, computed by the controller, using the PWM of several switching vectors. Arguably, the best way to synthesize the voltage reference vector is by using the nearest three vectors.

Because the control loops are implemented in the rotating reference frame, and because the conversion from rotating reference frame to the stationary polar reference frame requires computation of the arctangent function to determine the angle *q* of the reference vector, the α, β reference frame is perhaps a better choice.

After the reference vector is calculated the modulator needs to identify the NTVs[2], which is really to determine the region (small triangle) in which the tip of the reference vector is located, so that their corresponding duty cycles can be calculated.

[2] Nearest three vectors

Finally, in the last step the switching sequence is elaborated in order to better synthesize the voltage reference vector, and at the same time to keep the neutral point balanced. The sequence of actions to perform the proposed method of space vector modulation is displayed in figure 4.12.

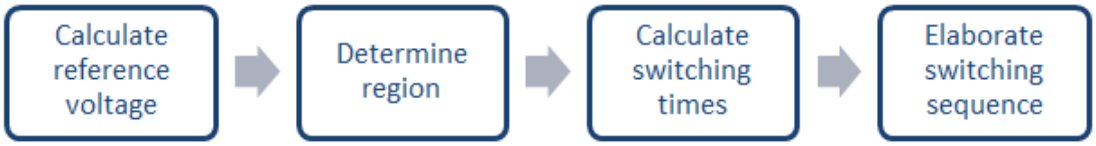

Figure 4.12 – Proposed SVM method steps

1) Calculate reference voltage

In this control scheme the reference stator flux magnitude and reference electromagnetic torque are compared with estimated values, respectively. The flux and torque errors are delivered to PI controllers, which generate command value the stator voltage components in stator flux coordinates. This voltage signals are transformed to stationary coordinates using the stator flux position angle.

The control scheme shown in figure 4.13, has two control loops, one for the stator flux and one for the electromagnetic torque. The output of the PI controller, whose input is the error of the electromagnetic torque, provides the voltage needed to minimize the error of electromagnetic torque.

On the other hand, the output of PI controller, whose input is the error of the stator flux, provides the necessary voltage value to minimize the error of the stator flux. The resulting voltage from the processing block is modulated by spatial modulation vectors (SVM) to finally be synthesized by the inverter.

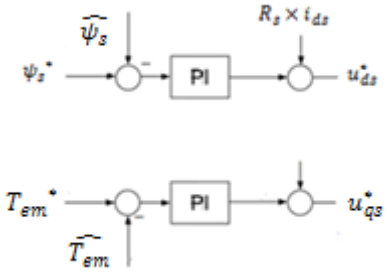

Figure 4.13 – Torque and flux PI controllers for reference vector determination

The vector of the stator flux space which rotates with an angular speed ωs, can be represented in terms of dq components, namely:

$$\overrightarrow{\psi_s} = \psi_{ds} + j\psi_{qs} \tag{4.49}$$

Whereas $\overrightarrow{\psi_s} = \psi_{ds}$ and $\psi_{qs} = 0$ it follows that the components of the real axis and the imaginary stator voltage, in the reference system aligned with the stator flux are given by:

$$u_{ds} = R_s \times i_{ds} + \frac{d\psi_s}{dt} \tag{4.51}$$

$$u_{qs} = R_s \times i_{qs} + \omega_s \times \psi_s \tag{4.51}$$

Since R_s is the stator resistance, i_{ds} and i_{qs} axis are the current in the real and imaginary stator respectively. The electromagnetic torque is given by the expression in the reference system aligned with the stator flux:

$$T_{em} = \frac{3}{2} \times P \times \psi_s \times i_{qs} \leftrightarrow$$
$$\leftrightarrow i_{qs} = \frac{2}{3 \times P} \times \frac{T_{em}}{\psi_s} \tag{4.52}$$

Replacing (4.52) in (4.51), then:

$$u_{qs} = R_s \times \frac{2}{3 \times P} \times \frac{T_{em}}{\psi_s} + \omega_s \times \psi_s \tag{4.53}$$

So through the error of the stator flux and the electromagnetic torque is possible to produce uncoupled reference values, of the real and imaginary components of the space vector of stator voltage across the PI controllers in order to minimize errors stator flux and the electromagnetic torque.

It can be observed from equation (4.51) that the stator flux is controlled by the real component of the space vector u_{ds}stator voltage. For each sampling period T_s, equation (4.51) can be approached by:

$$u_{ds} = R_s \times i_{ds} + \Delta\psi_s / T_s \tag{4.54}$$

For the case when IM operates at high speeds $R_s \times i_{ds}$ can be neglected and the voltage can become proportional to the change of flow stator $\Delta\psi_s$ and the switching frequency $1/T_s$. However, at low speeds $R_s \times i_{ds}$ is not negligible. Then, to avoid the use of a coordinate transformation to calculate the current in the reference system aligned with the stator flux estimate and the drop in the stator resistance, a PI controller is used for the control loop of the stator flux, then in the continuous domain:

$$u_{ds}^* = \left(K_{P_\psi} + K_{I_\psi}/s\right) \times \left({\psi_s}^* - \widehat{\psi_s}\right) \tag{4.55}$$

Discretizing equation (4.55) using backward difference ($s = \frac{z-1}{T_s \times z}$) method then:

$$u_{ds}^* = \left(K_{P_\psi} + K_{I_\psi}\right) \times \frac{z - \frac{K_{P_\psi}}{K_{P_\psi} + K_{I_\psi}}}{z-1} \times \left({\psi_s}^* - \widehat{\psi_s}\right) \tag{4.56}$$

In equation (3.67) has that the imaginary component of the space vector of stator voltage u_{qs}, if the term $\omega_s \times \psi_s$is de-coupled, controls the electromagnetic torque.

A simple way to accomplish the decoupling is to add the term $\omega_s \times \psi_s$ speed-dependent controller output to the electromagnetic torque, ie:

$$u_{qs}^{*} = (K_{PTem} + K_{ITem}/s) \times \left(T_{em}{}^{*} - \widehat{T_{em}}\right) + \omega_s \times \psi_s \quad (4.57)$$

The transfer function for PI controller in discrete system using backward difference method for discretization is expressed as:

$$u_{qs}^{*} = (K_{PTem} + K_{ITem}) \times \frac{z - \frac{K_{PTem}}{K_{PTem}+K_{ITem}}}{z-1} \times \left(T_{em}{}^{*} - \widehat{T_{em}}\right) + \omega_s \times \psi_s \quad (4.58)$$

Simulink implementation

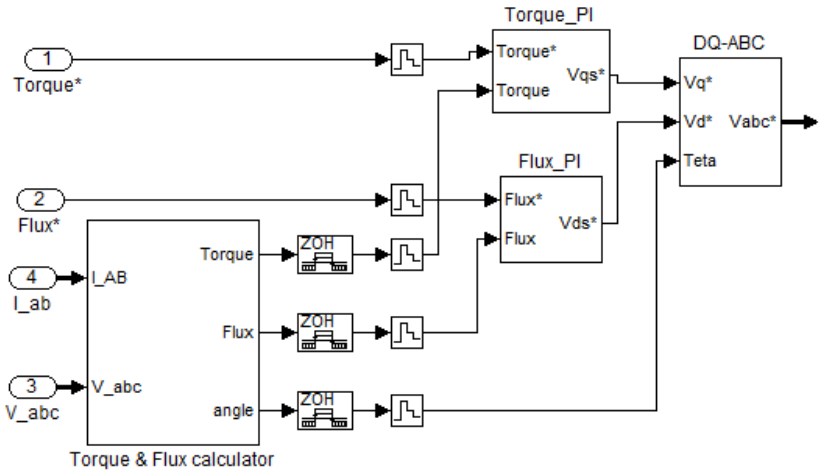

Figure 4.14 – Simulink model of reference vector determination

2) Determine region

The entire vector space is divided into 24 triangle sections (D1 to D24). The essence of the SVM is to compound the command voltage vector Vref using the nearest three vectors in which region (triangle section) the Vref locates.

From the real and imaginary components of the estimated stator flux the angle of the stator flux with the real axis of the stationary reference system is calculated, i.e.:

$$\theta_{\psi_s} = \tan^{-1}\left(\psi_{qs}/\psi_{ds}\right) \quad (4.59)$$

Given that θ_{ψ_s}, ψ_{qs} and $\psi_{ds}$are the angle and the real and imaginary components of the stator flux represented in the stationary reference system. With the obtained angle it is possible to establish the sector where the reference voltage is situated, like it is demonstrated in table 4.5.

Table 4.5 – Space vector sectors

Angle	*Sector*	*Areas*
$0<\theta_{\psi_s}\leq 60$	I	D1 D7 D13 D14
$60<\theta_{\psi_s}\leq 120$	II	D2 D8 D15 D16
$120<\theta_{\psi_s}\leq 180$	III	D3 D9 D17 D18
$180<\theta_{\psi_s}\leq 240$	IV	D4 D10 D19 D20
$240<\theta_{\psi_s}\leq 300$	V	D5 D11 D21 D22
$300<\theta_{\psi_s}\leq 360$	VI	D6 D12 D23 D24

Through the analysis of Figure 4.15 it is verified that there are four different voltage levels for the “q” component of the space vector. So it is necessary to determine at which of this four levels the reference voltage is positioned through basic trigonometric calculations. The first step is to define the limits of each level; then performing a series of comparisons between these levels and the “q” component of the reference vector will allow to determine where the reference is situated.

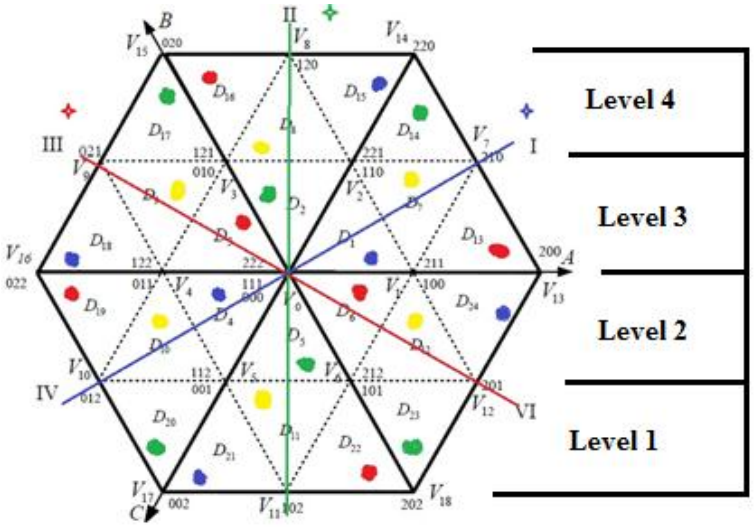

Figure 4.15 – Proposed SVM – Space vector

The easier way to explain this process is through an example, so considering, for demonstration reasons, that the reference voltage is situated somewhere in region D1 (Sector I), it is necessary to determine the sector and the level on which the reference voltage is located. Thus, in the green axis, the reference is present in the third level and in the first sector, as it is demonstrated in figure 4.16. Performing the algorithm associated to this axis, which is present in the same figure, the obtained value is 0.

```
switch (level) {
        case 1:  if (sector == 4) return D20
                 else if (sector == 6) return D23
                 else return 0;
        case 2:  if (sector == 5) return D5
                 else return 0;
        case 3:  if (sector == 2) return D2
                 else return 0;
        case 4:  if (sector == 1) return D14
                 else if (sector == 3) return D17
                 else return 0;
}
```

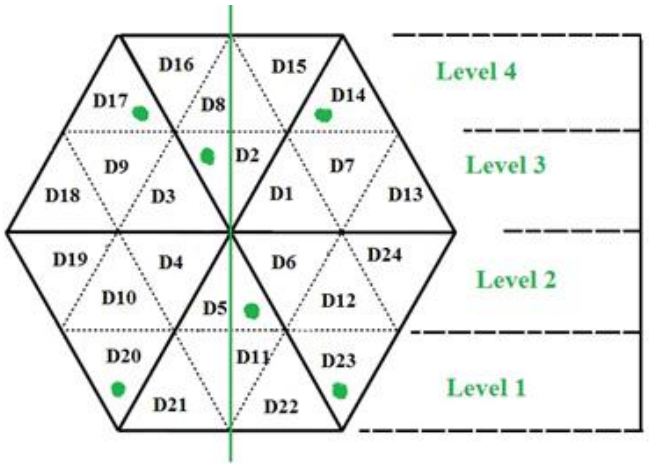

Figure 4.16 – Green pseudo code

Since the region wasn't detected with the previous algorithm, it is necessary to rotate the d-q axis -pi/3 radians, as it is displayed in figure 4.17. Changing the level and sector where the reference voltage lays. In the case at study (Region D1), the reference is now at the second level on the sector VI. Again, performing the algorithm the region is not determined, because any of the conditions is verified.

```
switch (level) {
        case 1:  if (sector == 4) return D22
                 else if (sector == 6) return D13
                 else return 0;
        case 2:  if (sector == 5) return D6
                 else return 0;
        case 3:  if (sector == 2) return D3
                 else return 0;
        case 4:  if (sector == 1) return D16
                 else if (sector == 3) return D19
                 else return 0;
}
```

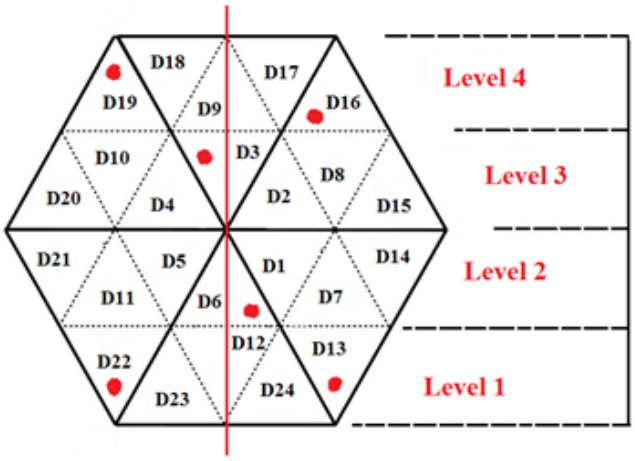

Figure 4.17 – Red pseudo code

Similarly to the red algorithm, it is necessary to perform a rotation on the d-q axis, however in this case, is pi/3 radians. After the level and sector relative to this reference are calculated, the blue algorithm is applied. The reference voltage in analysis now is on the third level of the sector II. And finally, algorithm conditions are verified thus returning the region D1.

```
switch (level) {
        case 1:  if (sector == 4) return D21
                 else if (sector == 6) return D18
                 else return 0;
        case 2:  if (sector == 5) return D4
                 else return 0;
        case 3:  if (sector == 2) return D1
                 else return 0;
        case 4:  if (sector == 1) return D24
                 else if (sector == 3) return D15
                 else return 0;
}
```

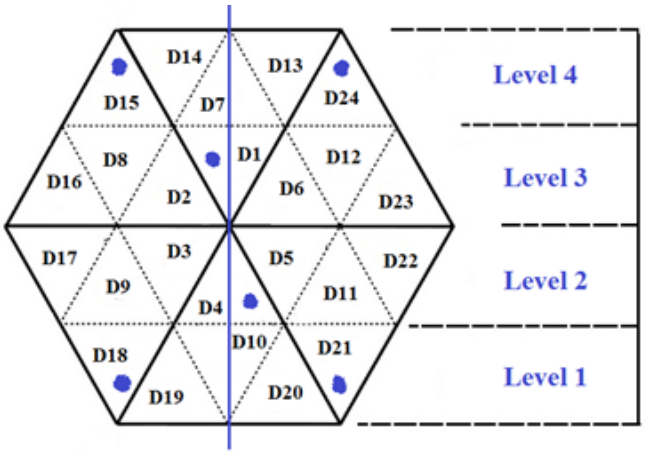

Figure 4.18 – Blue pseudo code

In the case that the previous algorithms doesn´t obtain the region, than the reference voltage is situated in one of the middle regions (D7/D8/D9/D10/D11/D12), so in this step only the reference sector is necessary to determine the respective region.

```
if (sector == 1) return D8
else if (sector == 2) return D9
else if (sector == 3) return D10
else if (sector == 4) return D11
else if (sector == 5) return D12
else return D7
```

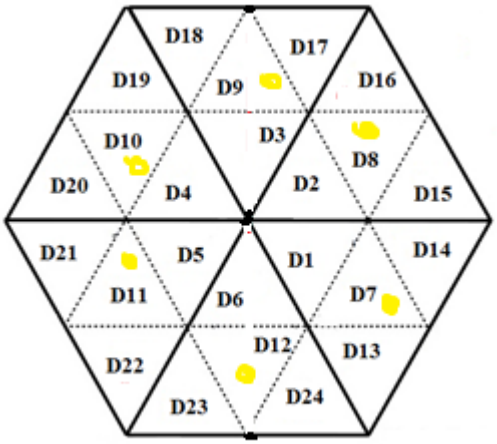

Figure 4.19 – Yellow pseudo code

The algorithmic description of the implementation shows its simplicity. The flowchart of the proposed region detection algorithm is displayed in Figure and respective Simulink model in Figure .

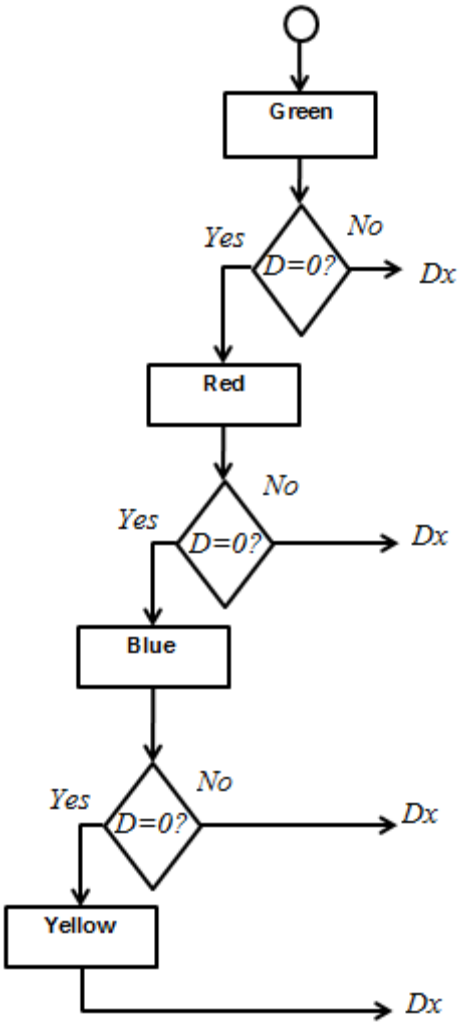

Figure 4.20 – Flowchart of proposed region detection algorithm

Simulink implementation

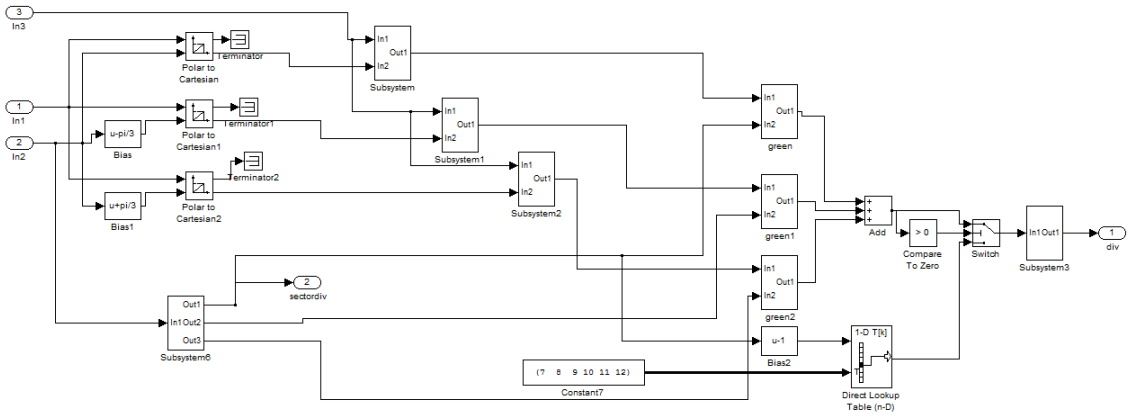

Figure 4.21 – Simulink model of region detection algorithm

3) *Calculate vector switching times*

The reference vector is obtained by switching on (for proper time) three adjacent vectors in each region, but it can be realized by different on/off sequences, which will have influence on the performance of the modulator. The three vectors are imposed to the motor terminals successively in such away less harmonics components of the output voltage and current are produced.

The required on-duration of each vector in a specified triangle is determined by the equations (4.70), these specify that the demand vector is the geometric sum of the chosen three vectors multiplied by their on-durations. To each voltage vector it is associated a respective on-duration type (Ta, Tb or Tc), which is presented in table 4.6.

Table 4.6 -Time– Vectors associated

Voltage Vector	*Tx*	*Voltage Vector*	*Tx*
V0	b	V10	B
V1	a	V11	B
V2	c	V12	B
V3	a	V13	C
V4	c	V14	A
V5	a	V15	C
V6	c	V16	A
V7	b	V17	C
V8	b	V18	A
V9	b		

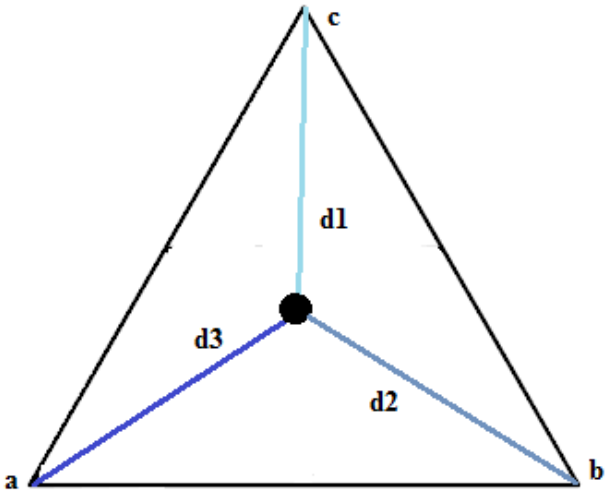

Figure 4.22 – Dwell time

$$d_1 + d_2 + d_3 = d_t \leftrightarrow$$

$$\leftrightarrow \frac{d_1}{d_t} + \frac{d_2}{d_t} + \frac{d_3}{d_t} = 1 \rightarrow D_1 + D_2 + D_3 = 1 \tag{4.60}$$

Multiplying equation (4.60) by the sampling time:

$$D_1 \times T_s + D_1 \times T_s + D_1 \times T_s = T_s \rightarrow t_a + t_b + t_c = T_s \tag{4.61}$$

Combining equations (4.60) and (4.61) the dwell time is determined.

$$\begin{cases} t_a = D_1 \times T_s = \frac{d_1}{d_t} \times T_s \\ t_b = D_2 \times T_s = \frac{d_2}{d_t} \times T_s \\ t_c = D_3 \times T_s = \frac{d_3}{d_t} \times T_s \end{cases} \tag{4.62}$$

Thus the reference voltage can be represented as (4.63):

$$V_{ref} \times T_s = v_x \times t_a + v_y \times t_b + v_z \times t_c \tag{4.63}$$

Simulink implementation

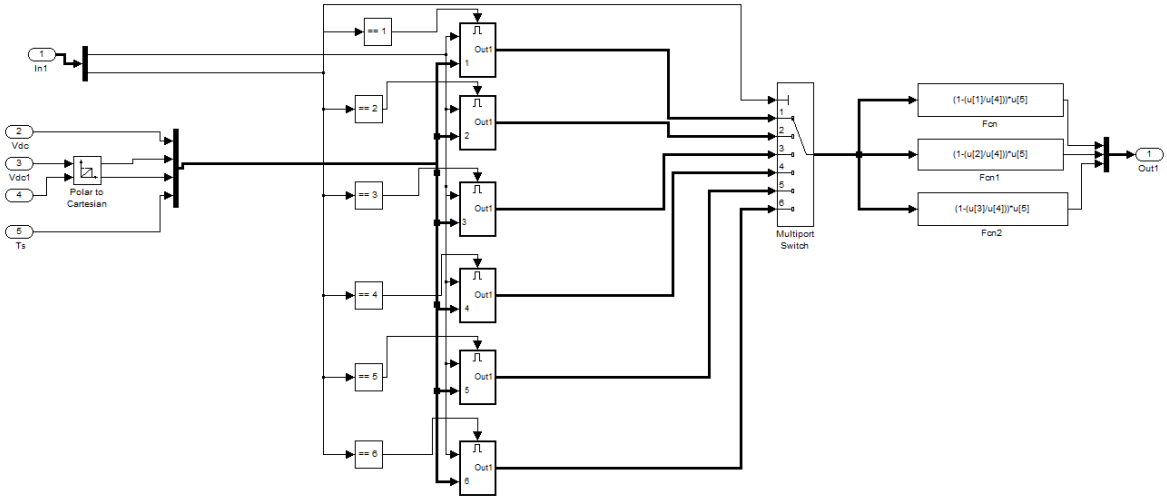

Figure 4.23 – Simulink model for duration times calculation

4) Switching sequence

The sequence of switching states Vx, Vy, Vz in one switching cycle is important because it affects the THD and switching loss during the SVM. In order to reduce the THD and switching loss, it is popular to (1) make the switching cycle symmetric; (2) to begin and end the cycle with the same switching state; (3) there is only one state change at a time.

Classical modulation for three-level converter uses symmetrical placement of zero and internal vectors. It means that time devoted to internal vectors is divided by two and each vector (e.g. 211 and 100) is switched on for half of the calculated time. This type of modulation provides good neutral point balance because of equal selection of small (redundant) vectors, which is followed by equal usage of DC link capacitors.

Although good voltage equalization in DC link and minimization of current and torque ripples thanks to high number of different voltage states in sampling, this modulation introduces high switching losses (all possible vectors are used).

By drawing pictures like the one in figure 4.24, the switching sequence for each switch can be easily determined, and applying the same procedure to the other regions, the switching time (duty ratio) can be decided with less effort. The switching sequences corresponding to each region are presented in the following tables.

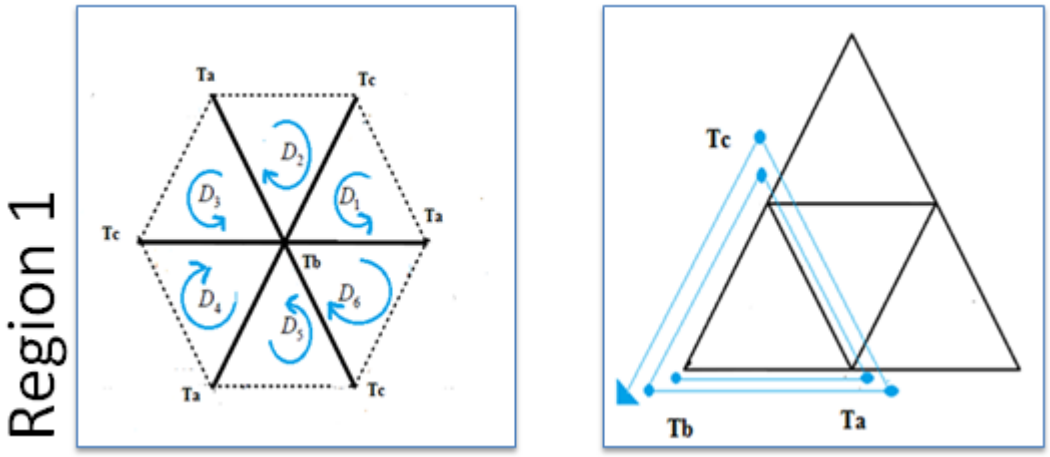

Figure 4.24 – Switching sequence – Region 1

Table 4.7 – Region 1 switching sequence

Index	*1*	*2*	*3*	*4*	*5*	*6*	*7*	*8*	*9*	*10*	*11*	*12*	*13*
Switching Times	Tb/4	Ta/2	Tc/2	Tb/2	Ta/2	Tc/2	Tb/2	Tc/2	Ta/2	Tb/2	Tc/2	Ta/2	Tb/4

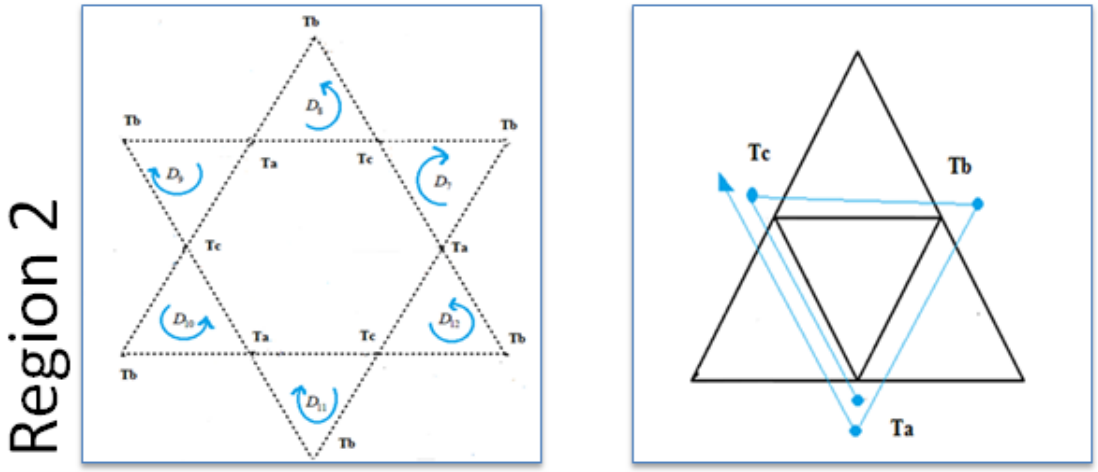

Figure 4.25 – Switching sequence – Region 2

Table 4.8 – Region 2 switching sequence

Index	*1*	*2*	*3*	*4*	*5*	*6*	*7*	*8*	*9*
Switching Times	Ta/2	Tc/2	Tb	Ta/2	Tc	Ta/2	Tb	Tc/2	Ta/2

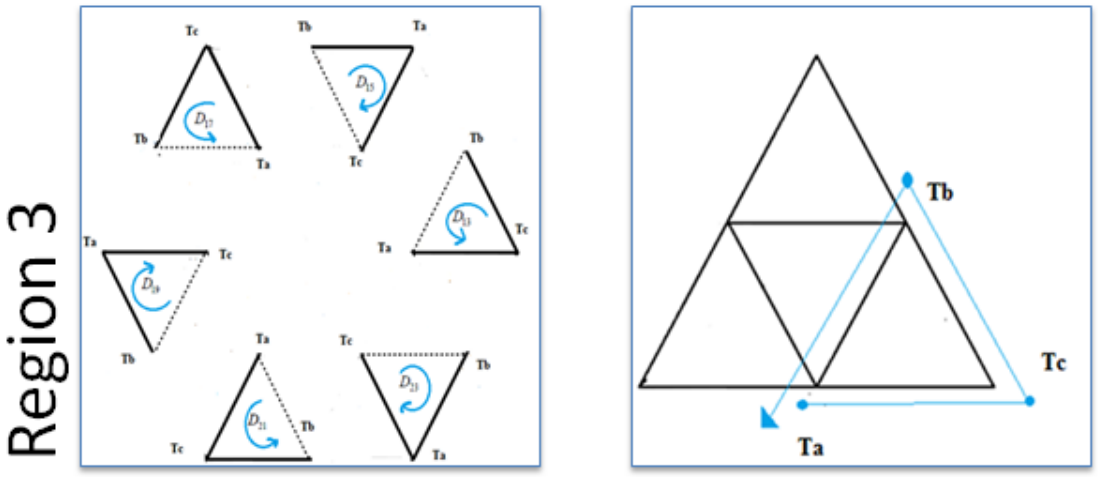

Figure 4.26 – Switching sequence – Region 3

Table 4.9 – Region 3 switching sequence

Index	***1***	***2***	***3***	***4***	***5***	***6***	***7***
Switching Times	Ta/2	Tc	Tb	Ta	Tb	Tc	Ta/2

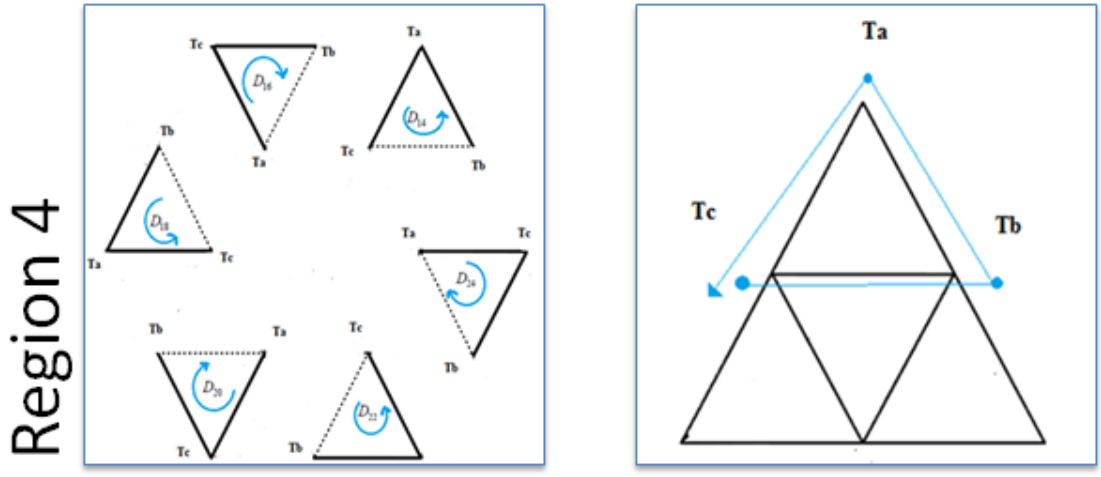

Figure 4.27 – Switching sequence – Region 4

Table 4.10 – Region 4 switching sequence

Index	***1***	***2***	***3***	***4***	***5***	***6***	***7***
Switching Times	Tc/2	Tb	Ta	Tc	Ta	Tb	Tc/2

Simulink implementation

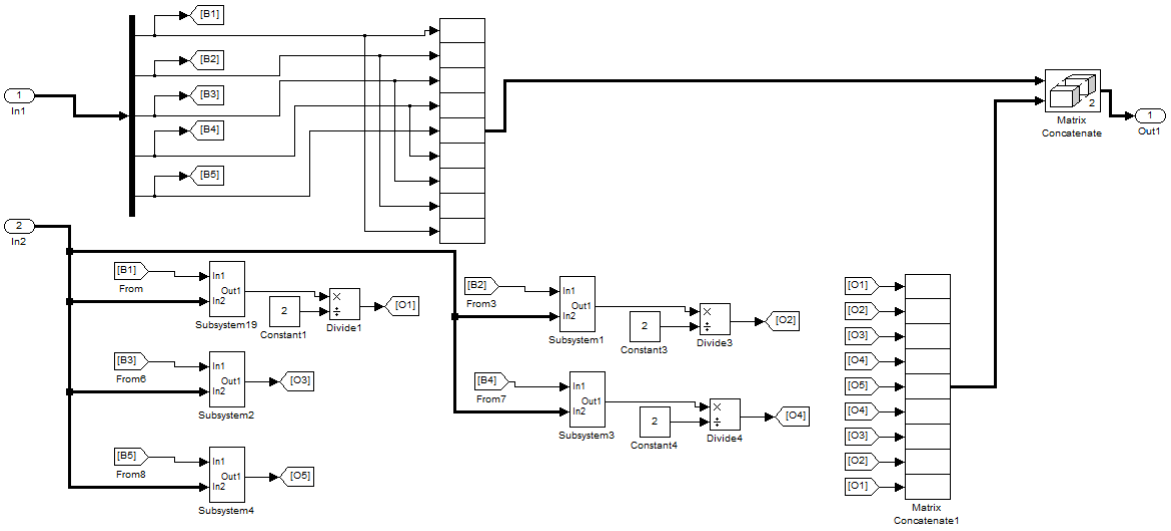

Figure 4.28 – Simulink model for switching sequence elaboration

This chapter introduces a new space vector algorithm for multilevel three-phase inverters. In addition, the efficiency and the ease of implementation of this algorithm makes it well suited for simulation on digital computers; it can become a very useful tool in further exploration of the properties of multilevel power converters.

The flexibility of SVM comes from the seemingly unlimited number of ways for its implementation. This is due to the degrees of freedom inherent to the SVM method and can be used as parameters for optimizing the modulation.

By exploiting these degrees of freedom built-in to SVM, appropriate switching sequences can be devised to obtain the desired waveform quality. The available degrees of freedom have been previously used to devise sequences that feature lower switching losses or harmonic content.

5

SIMULATION RESULTS

In this section are presented the results of simulations of both control schemes (DTC with and without SVM) proposed and studied for different operating conditions which are:

- Steady state behavior - setting a reference and load torque;
- Dynamic state behavior - applying a step change in the reference and load torque;
- Speed variation – applying variations in the speed reference and load torque.

Both control techniques were implemented with the three-level neutral point clamped presented previously in Chapter 3.

The simulations were realized in Matlab/Simulink software version R2010a. The sample time used in the control system is 2 μs in order to verify the efficiency of the proposed SVM scheme in with high sampling frequencies.

In order to assess the performance of both control systems, the torque standard deviation and stator flux standard deviation are calculated to evaluate the ripple of both variables. The expression for the standard deviation of a generic variable employed is as follows (being n the number of samples):

$$\sigma = \sqrt{\left(\frac{1}{n-1}\sum_{i=1}^{n}(x_i - \bar{x})^2\right)} \tag{5.1}$$

$$\bar{x} = \frac{1}{n}\sum_{i=1}^{n} x_i \tag{5.2}$$

The IM parameters were chosen for comparison reasons and are displayed in the following table.

Table 5.4 – IM parameters

Induction machine simulation parameters					
Nominal power	149,2	kW	Rotor resistance	9,30E-03	ohm
Pole pairs	2		Rotor inductance	3,03E-04	H
Stator resistance	1,49E-02	ohm	Mutual inductance	1,05E-02	H
Stator inductance	3,03E-04	H	Moment of inertia	3,10E+00	kg.m^2

5.1 Steady State Behavior

The objective of this test is to observe the capability of the control schemes stability and response time compared to a fixed torque reference.

In the first simulation engine running at no load was applied torque nominal, whereas in the second simulation the systems is in the presence of a load torque. In the following table are presented the respective reference values of torque and flux used in this operation condition.

Table 5.2 – Steady state behavior

Simulation	Reference Torque [N.m]	Reference Flux [Wb]	Load Torque [N.m]	Sampling Time [s]
I	300	0.8	0	2,00E-06
II	300	0.8	100	2,00E-06

5.1.1 Simulation I

5.1.1.1 Direct Torque Control

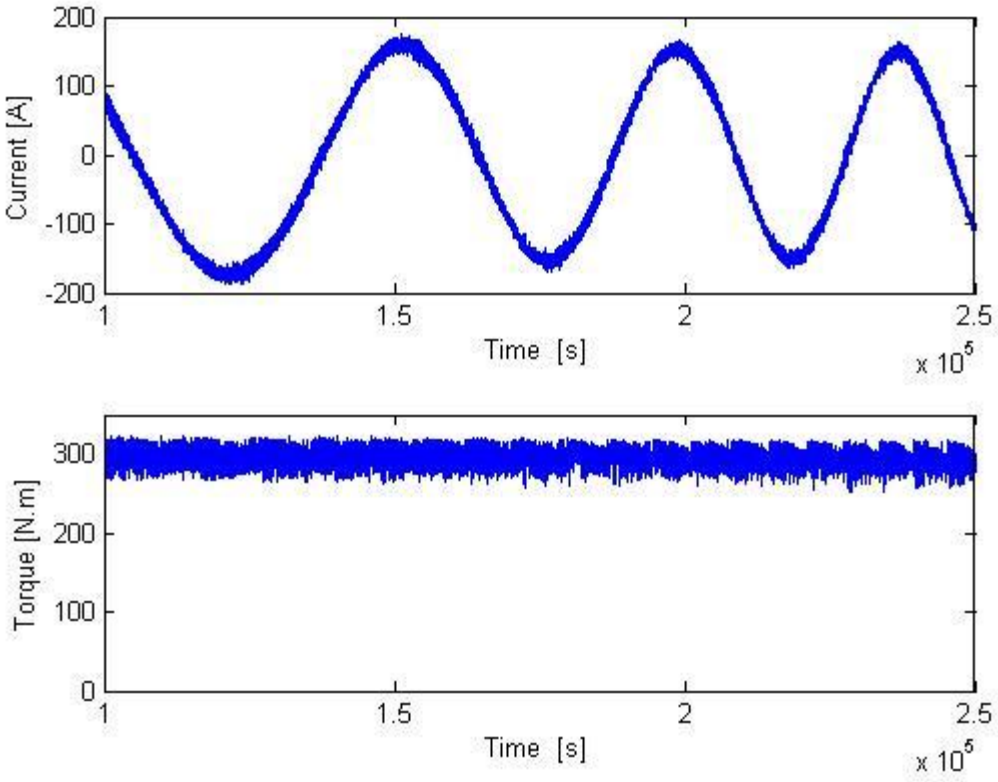

Figure 5.1 - Steady Behavior – Simulation I – DTC – Phase current and torque

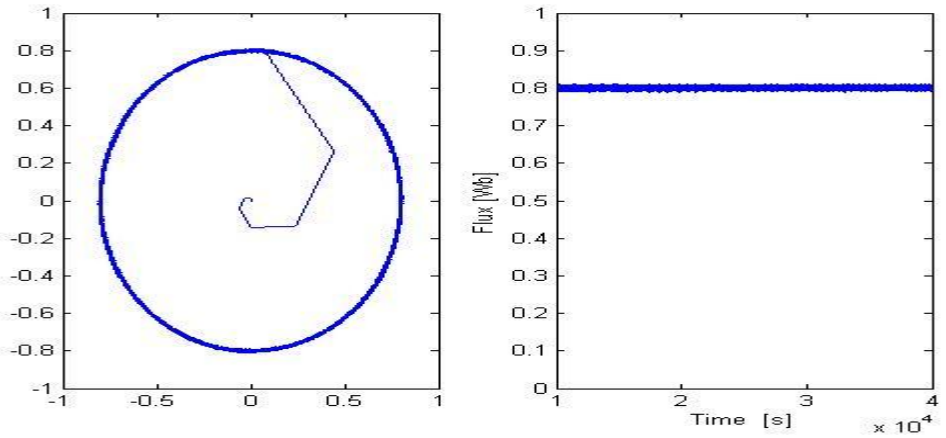

Figure 5.2 – Steady Behavior – Simulation I – DTC - Flux

5.1.1.2 Direct Torque Control with Space Vector Modulation

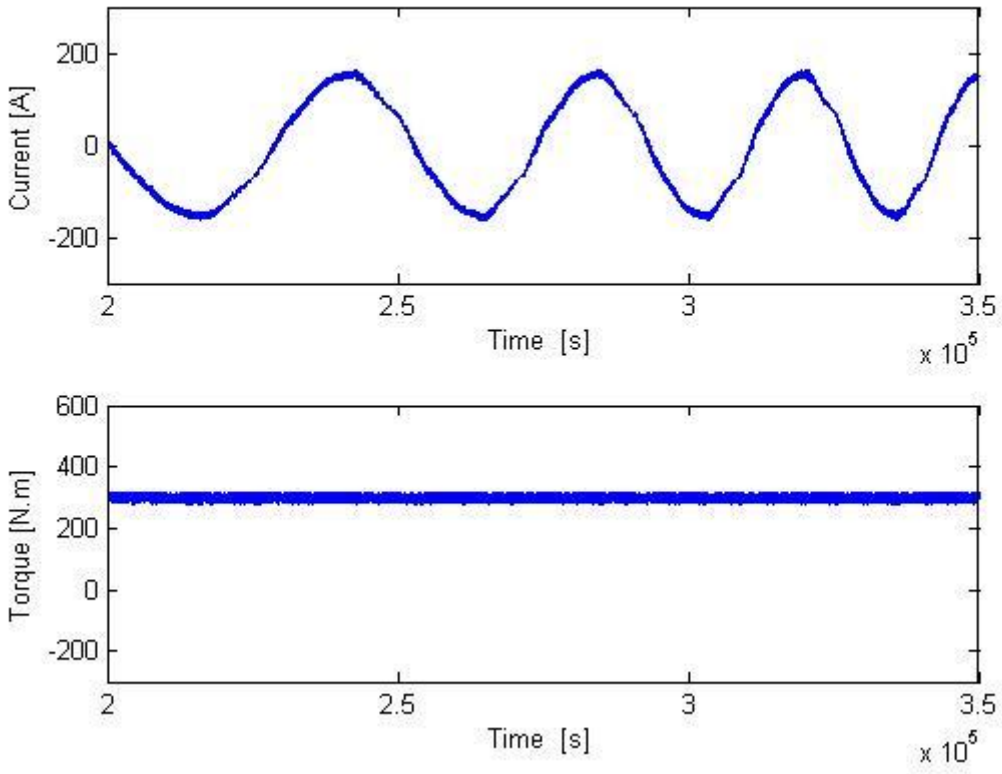

Figure 5.3 – Steady Behavihor – Simulation I – SVM - Phase current and Torque

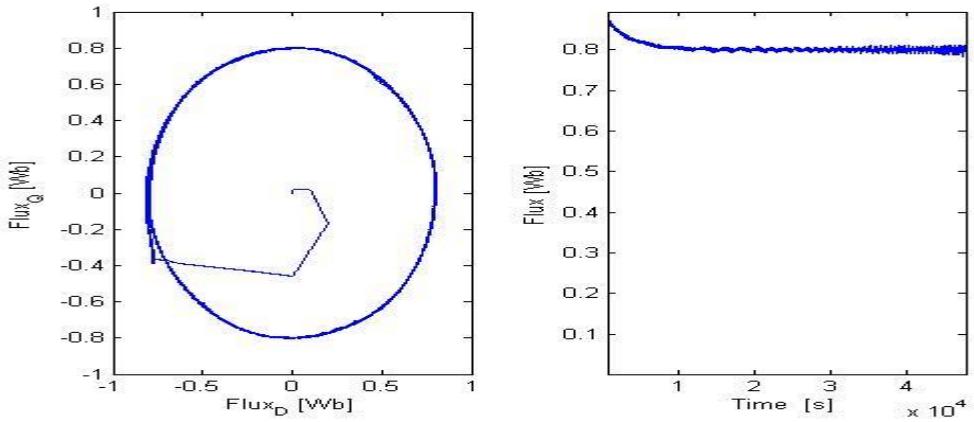

Figure 5.4 - Steady Behavior – Simulation I – SVM - Flux

In figures 5.1 and 5.3 the stator current in one phase is observed, and as expected in both DTC and SVM follows a sinusoidal behavior. As for the torque, in both control methods, it follows the reference; nevertheless in the space vector modulation it is visible that the torque ripple is lower.

In Figure 5.2 and 5.4 the flux remains constant during the application of the reference torque, the same behavior can be confirmed in the locus of the flux.

5.1.2 Simulation II

5.1.2.1 Direct Torque Control

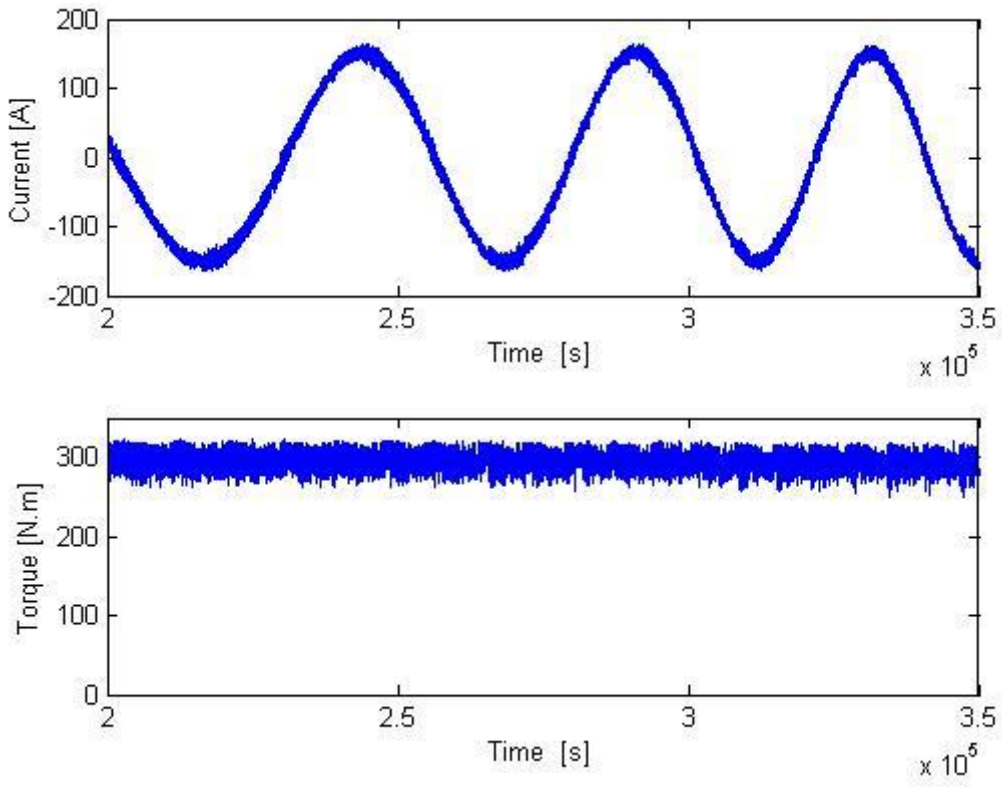

Figure 5.5 - Steady Behavior – Simulation II – DTC – Phase current and torque

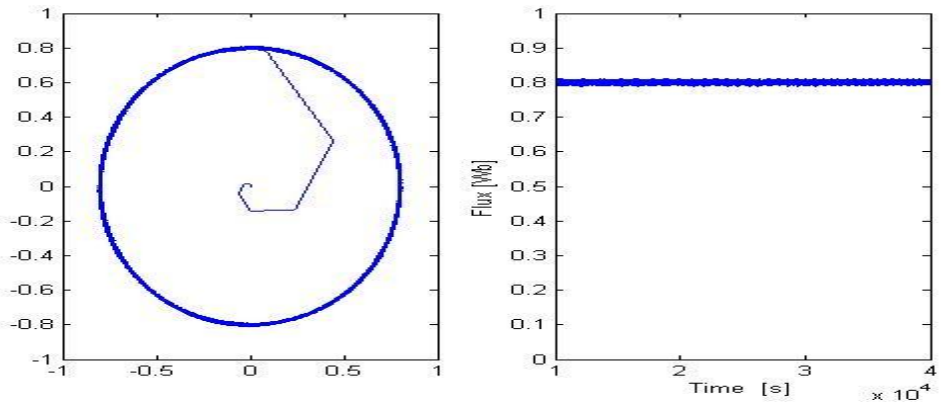

Figure 5.6 - Steady Behavior – Simulation II – DTC - Flux

5.1.2.2 Direct Torque Control with Space Vector Modulation

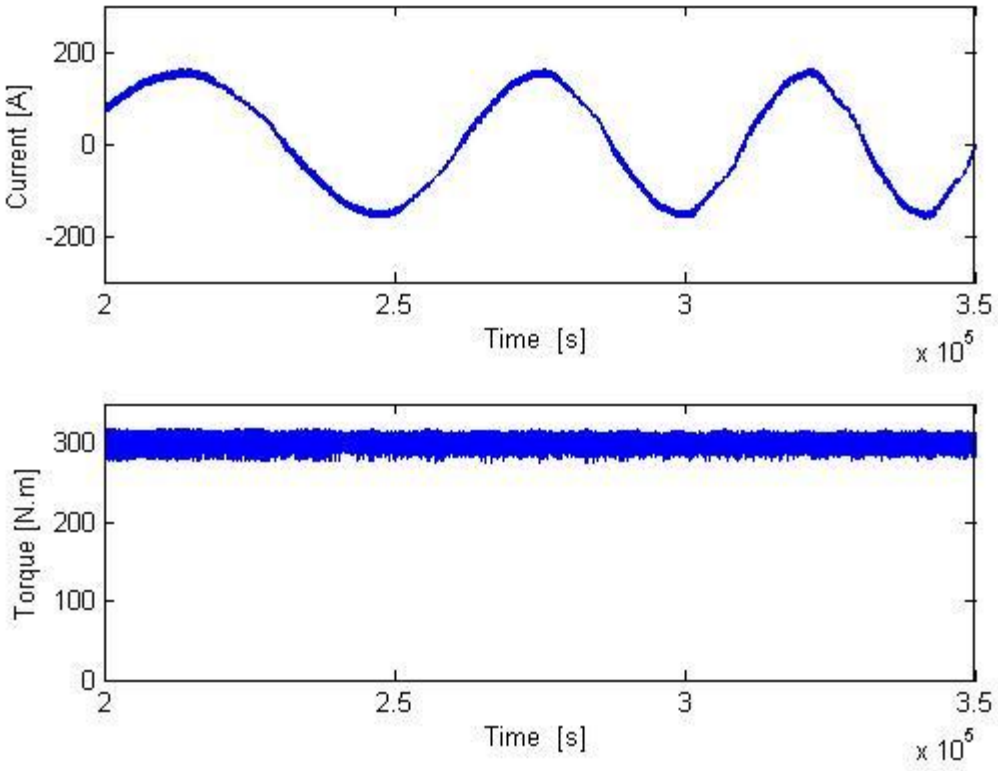

Figure 5.7 - Steady Behavior – Simulation II – SVM – Phase current and torque

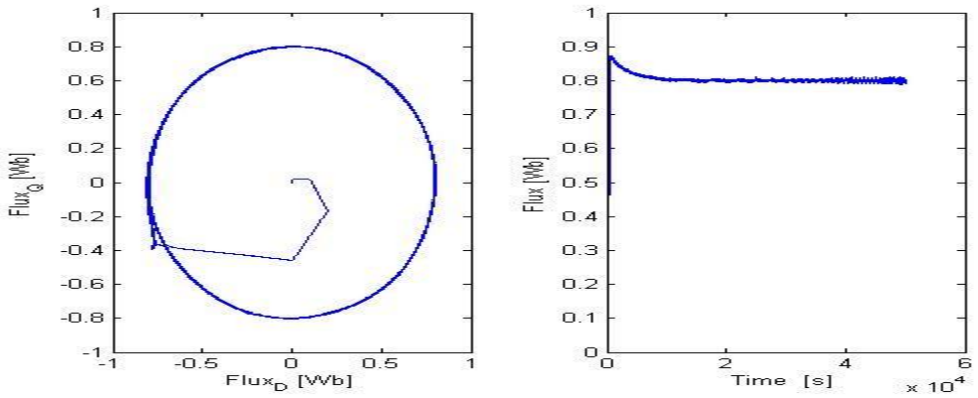

Figure 5.8 - Steady Behavior – Simulation II – SVM – Flux

Comparatively to the first simulation, where no load torque is applied, the results are very similar. Suggesting that the load torque of 150 N.m doesn't affect the performance of both control methods when applying a torque of 300 N.m. As expected, the phase current maintains sinusoidal in DTC and DTC-SVM, as well as the torque accomplished to follow the reference.

When analyzing the results obtained in these simulations (Table 5.3), it is visible that the torque and flux deviation are lower when the space vector modulation is implemented. Also, one can verify that when a load torque is applied the deviation torque in both control schemes increases. As for the flux, in the DTC decreases slightly, whereas in the SVM maintains approximately the same.

Table 5.3 – Steady state deviation results

Evaluation	DTC	DTC-SVM
Simulation I		
Torque Standard Deviation [N.m]	12,6835	8,0847
Flux Standard Deviation [Wb]	0,0619	0,0393
Simulation II		
Torque Standard Deviation [N.m]	13,0413	8,2269
Flux Standard Deviation [Wb]	0,0436	0,0396

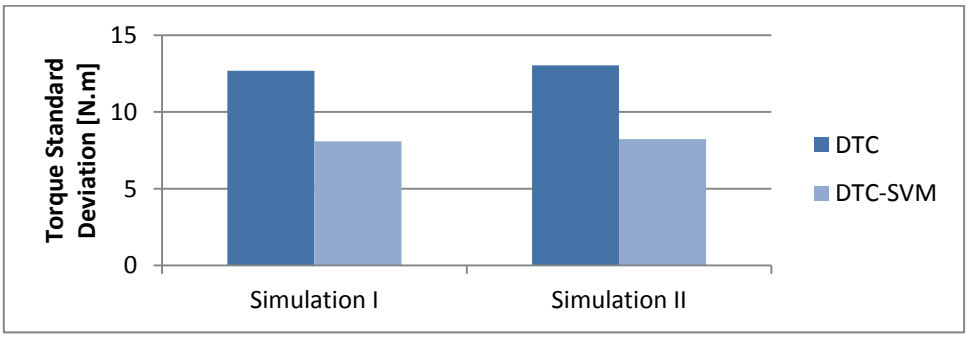

Figure 5.9 – Steady state – Torque standard deviation

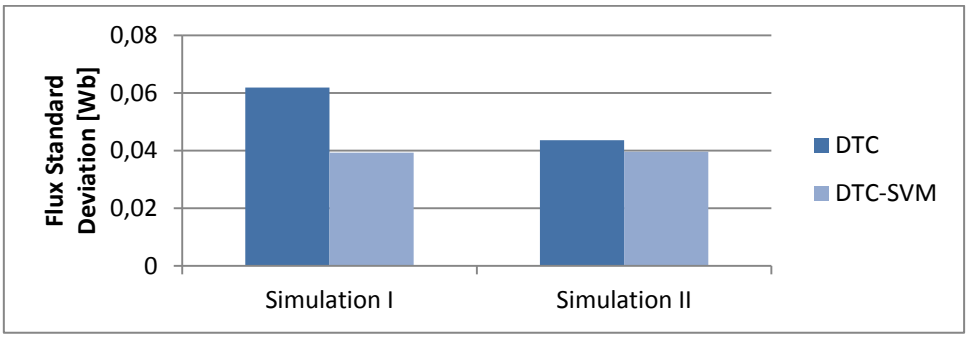

Figure 5.10 – Steady state – Flux standard deviation

5.2 Dynamic Behavior

The objective of this test is to analyze the dynamic response in the proposed control schemes for two different simulation conditions. In the first one is applied a sudden variation of the reference torque with no load torque. As for the second simulation, the same sudden variation of the reference torque is applied, however with a load torque of 50 N.m. The flux is maintained at 0.8 Wb.

Table 5.4 – Dynamic behavior simulation conditions

Simulation	Reference Torque [N.m]	Reference Flux [Wb]	Load Torque [N.m]	Sampling Time [s]
I	100→300	0.8	0	2,00E-06
II	100→300	0.8	50	2,00E-06

5.2.1 Simulation I

5.2.1.1 Direct Torque Control

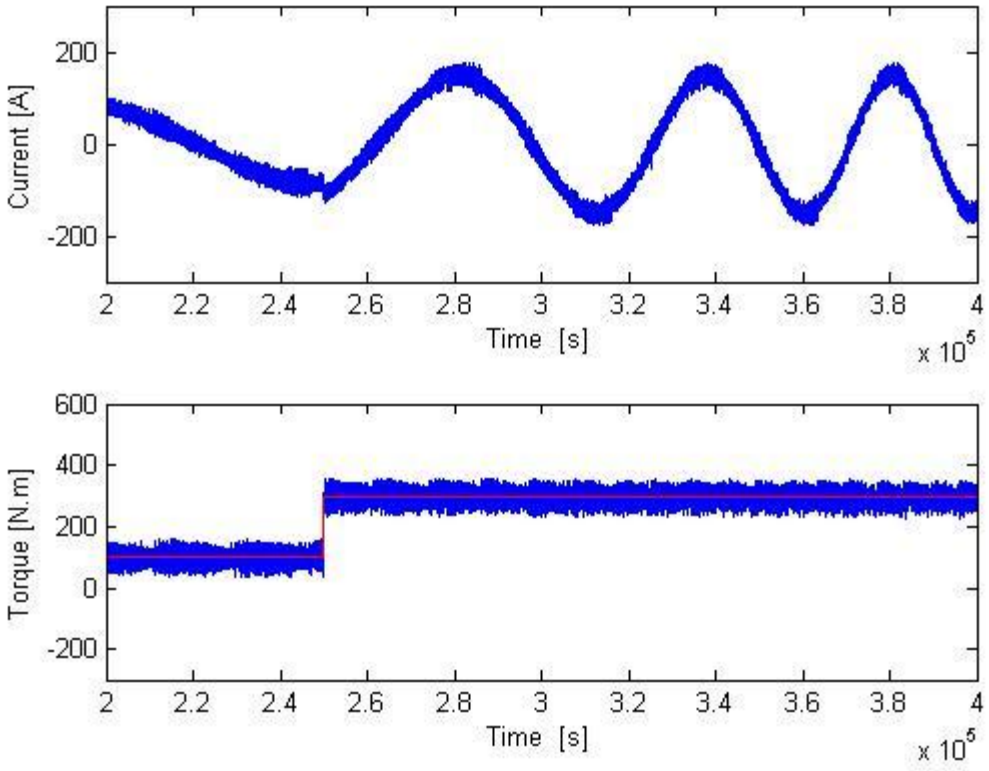

Figure 5.11 – Dynamic Behavior – Simulation I – DTC – Stator current and torque

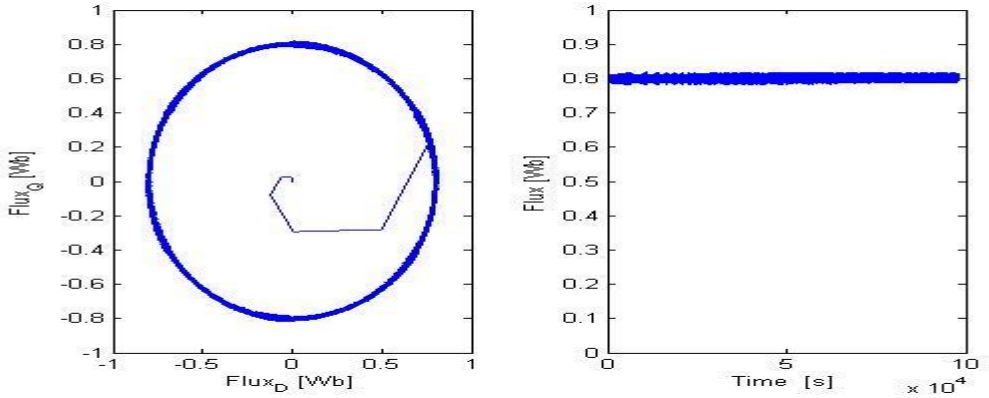

Figure 5.12 – Dynamic Behavior – Simulation I – DTC – Flux

5.2.1.2 Direct Torque Control with Space Vector Modulation

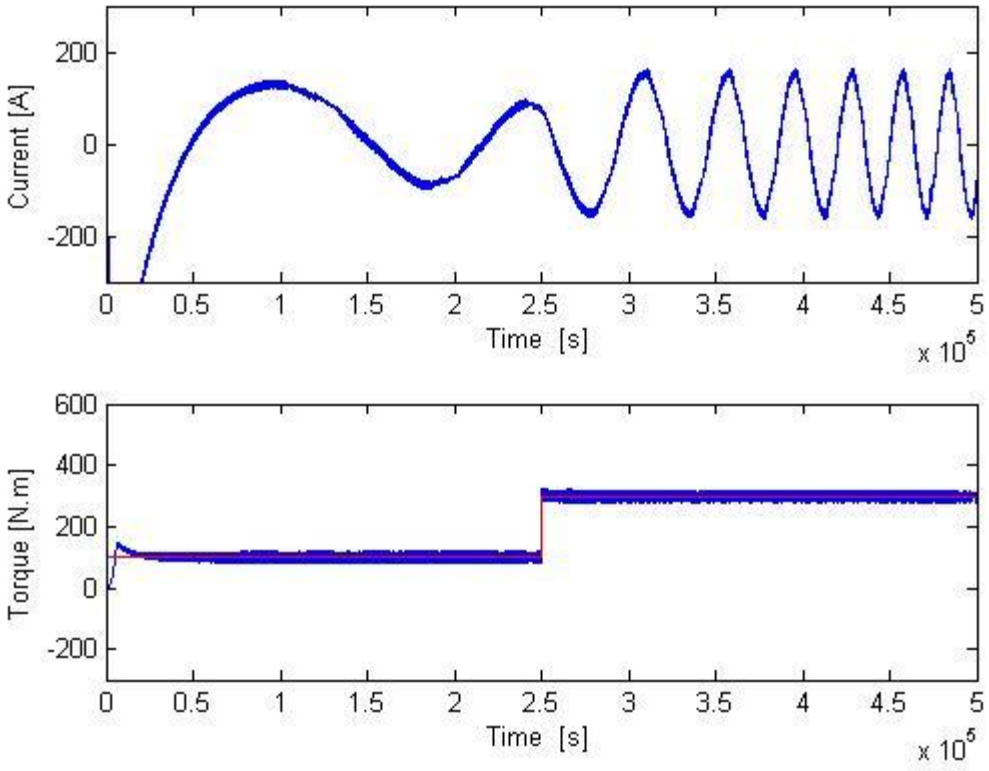

Figure 5.13 – Dynamic Behavior – Simulation I – SVM – Stator current and torque

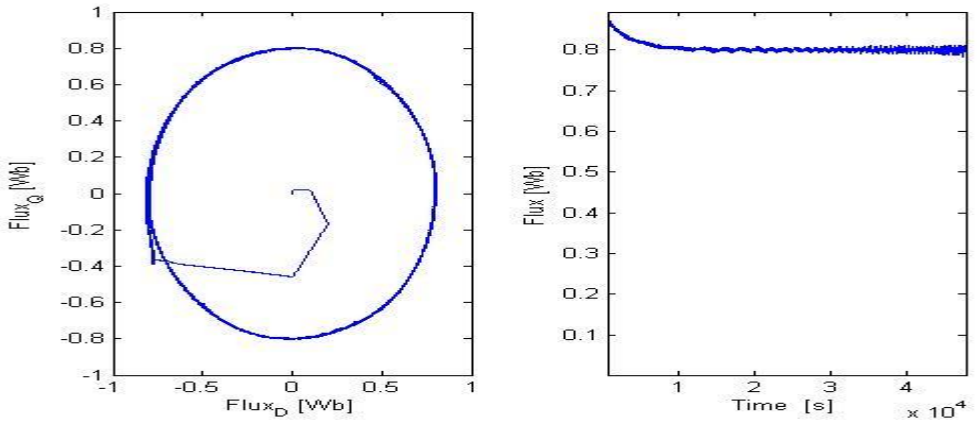

Figure 5.14 – Dynamic Behavior – Simulation I – SVM – Flux

In figures 5.11 and 5.13 the stator current in one phase is observed and, again, both follow a sinusoidal behavior. As expected, when the step on the reference torque is applied, it is visible the sudden variation on the current. This variation is due to the need of the drive to adjust the current in order to achieve the reference torque.

Through the analysis of figures 5.11 and 5.13, both DTC and DTC-SVM accomplish a good response time and stability when the variation in the torque is applied, at 2.5 seconds.

Considering the ripple in the current and in the torque, in the case of the DTC is higher. This result derives from the fact that this control scheme is implemented through hysteresis controllers, which depending upon the sampling frequency and the hysteresis bandwidth can vary. As previously stated, higher sampling frequencies it is expected to achieve a lower ripple.

5.2.2 Simulation II

5.2.2.1 Direct Torque Control

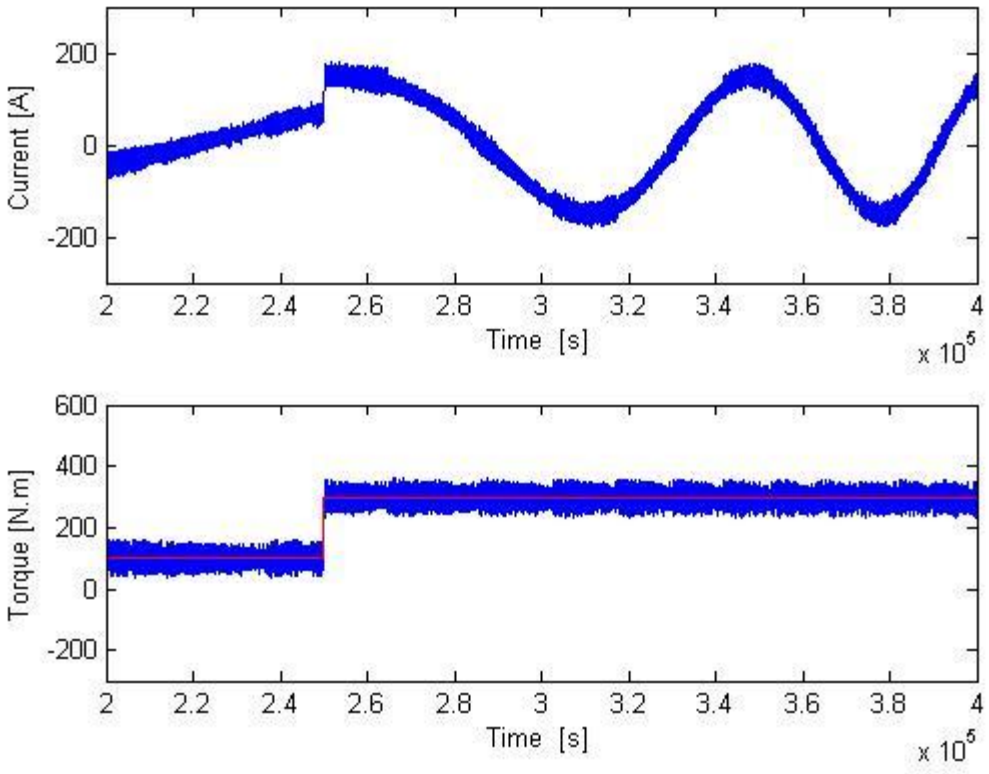

Figure 5.15 – Dynamic Behavior – Simulation II – DTC – Stator current and torque

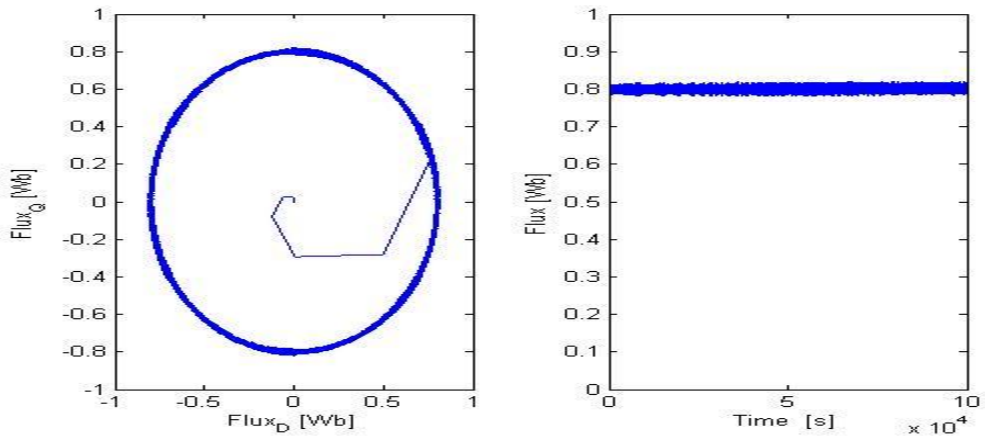

Figure 5.16 – Dynamic Behavior – Simulation I – DTC – Flux

5.2.2.2 Direct Torque Control with Space Vector Modulation

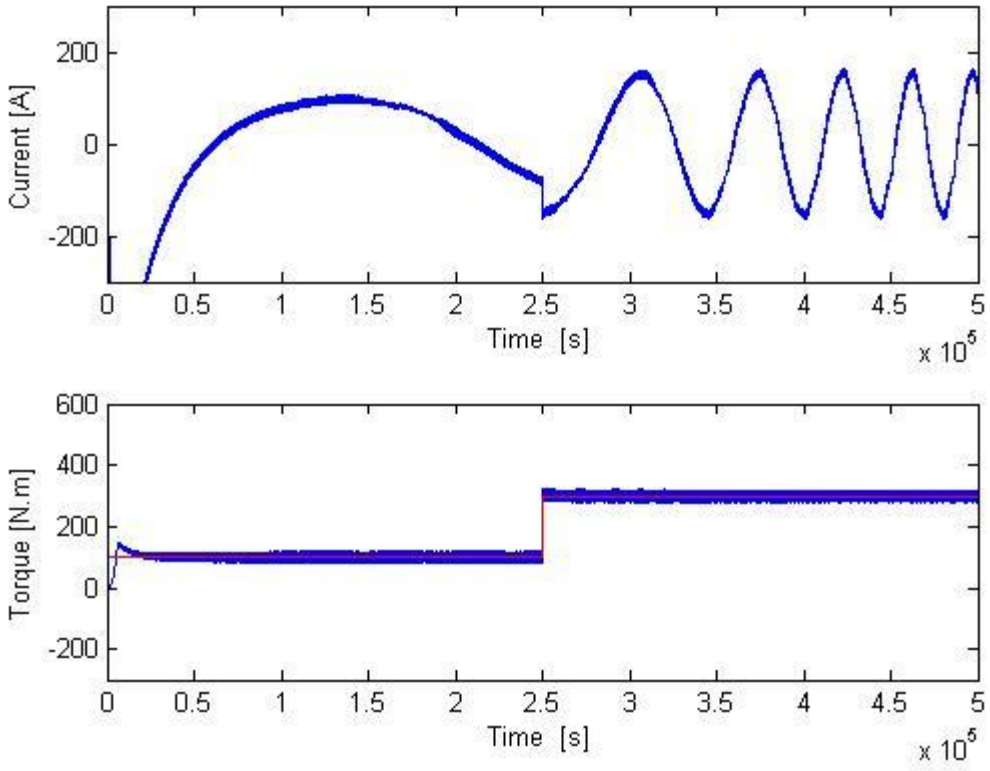

Figure 5.17 – Dynamic Behavior – Simulation II – SVM – Stator current and torque

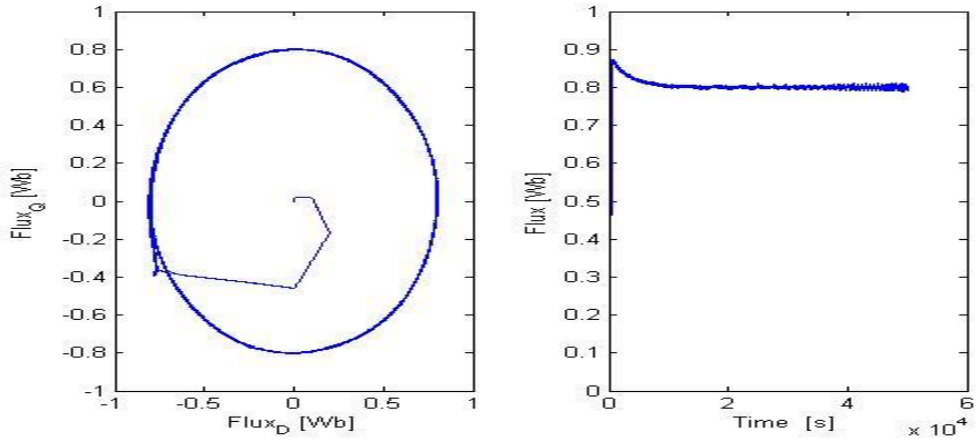

Figure 5.18 – Dynamic Behavior – Simulation II – SVM – Flux

In this simulation the trend of the results obtained in the previous simulations maintains. In both control schemes the reference torque is achieved with a good time response and the flux is maintained with the appropriate value. Again the variation in the current is present when the step in the reference voltage is applied.

From the experimental results presented in figure 5.14 to 5.18 it is apparent that the torque and flux ripple for the DTC-SVM utilizing a three-level VSI is considerably reduced when compared to DTC. This conclusion is reinforced with the deviations values obtained throughout the simulations.

Similarly to the simulation results obtained when operating in the steady state behavior, the standard torque and flux deviations are higher in DTC compared to SVM. However, the torque deviation maintains almost the same when operating with and without load torque.

Table 5.5 – Dynamic deviation results

Evaluation	DTC	DTC-SVM
Simulation I		
Torque Standard Deviation [N.m]	11,5252	8,2326
Flux Standard Deviation [Wb]	0,0619	0,0389
Simulation II		
Torque Standard Deviation [N.m]	11,7116	8,3278
Flux Standard Deviation [Wb]	0,0436	0,0396

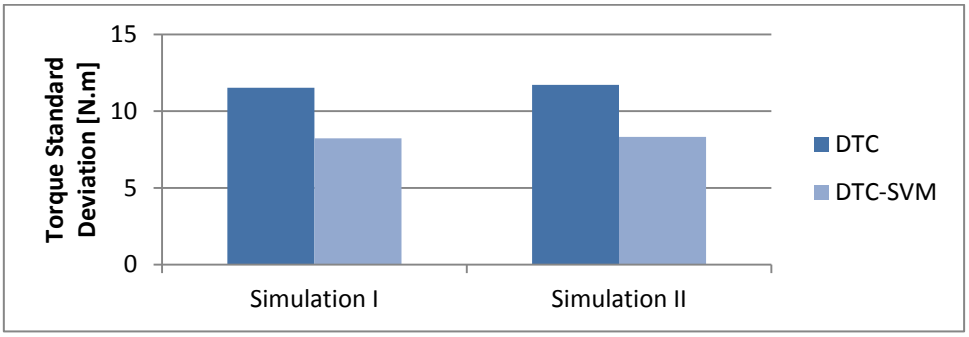

Figure 5.19 – Dynamic Behavior – Torque Standard Deviation

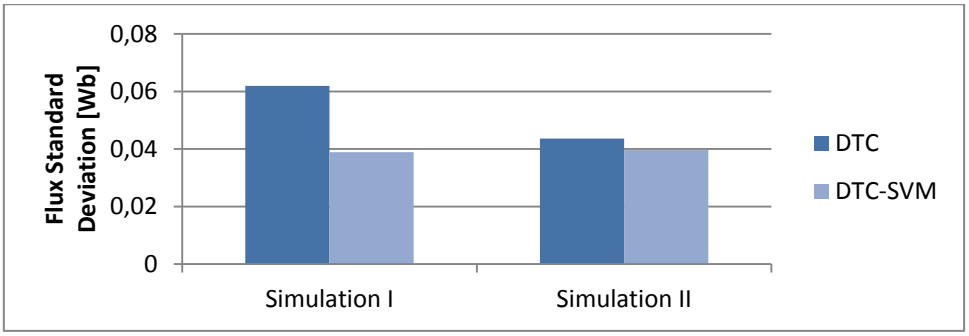

Figure 5.20 – Dynamic Behavior – Flux Standard Deviation

5.3 Speed Control

Resorting to a speed controller available in Matlab/Simulink based on a PI regulator, shown below in figure 5.21, a comparison between DTC and DTC-SVM is presented. The output of this regulator is the reference torque necessary to guarantee the speed set point.

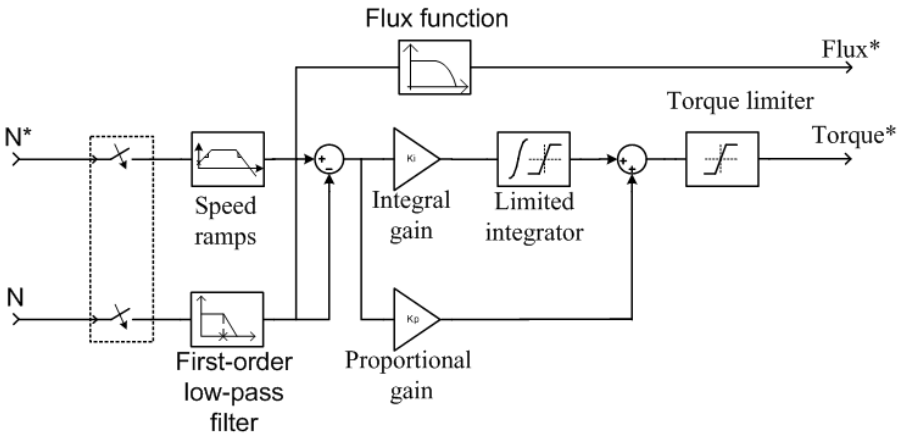

Figure 5.21 – Speed control model

5.3.1 Simulation I

In this simulation, a ramp variation is applied in the speed reference causing a reversal in the rotation. The objective of this test is to observe, among other factors, the dynamic of the slow characteristic of the control and the torque behavior.

The ramp reference presents a variation in the speed of 0 RPM up to +200 RPM in 0.1 seconds as shown in Figure 5.22 and 5.24. Once reached this level the speed reference remains stable for 0.4 seconds, then returns to a ramp with a variation in the opposite direction until the speed -200 RPM is achieved. The engine operates with no load torque

5.3.1.1 Direct Torque Control

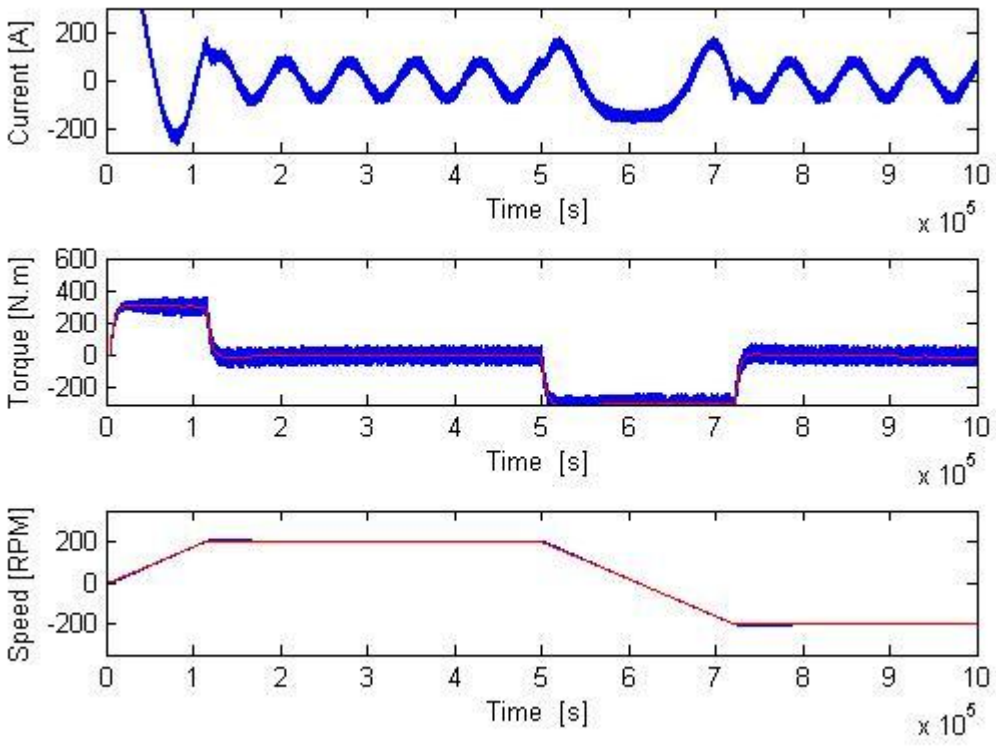

Figure 5.22 – Speed control– Simulation I – DTC – Stator current, torque and speed

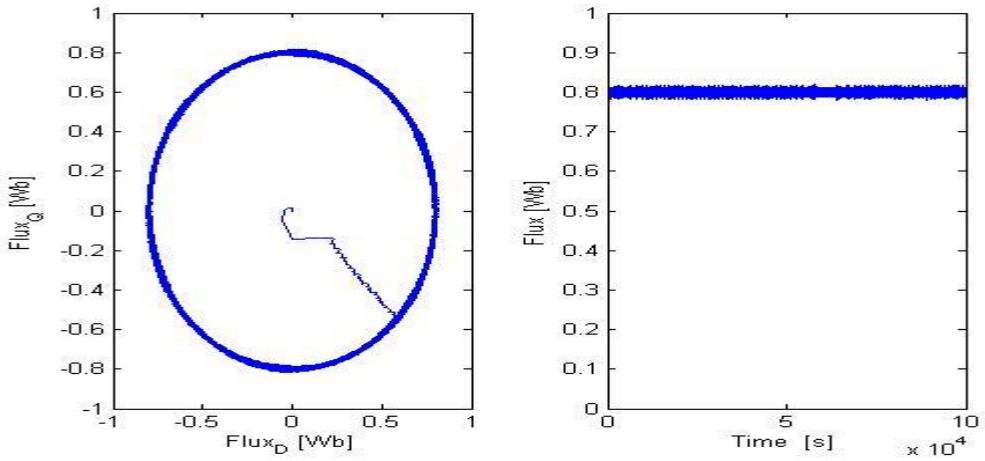

Figure 5.23 – Speed control– Simulation I – DTC – Flux

5.3.1.2 Direct Torque Control with Space Vector Modulation

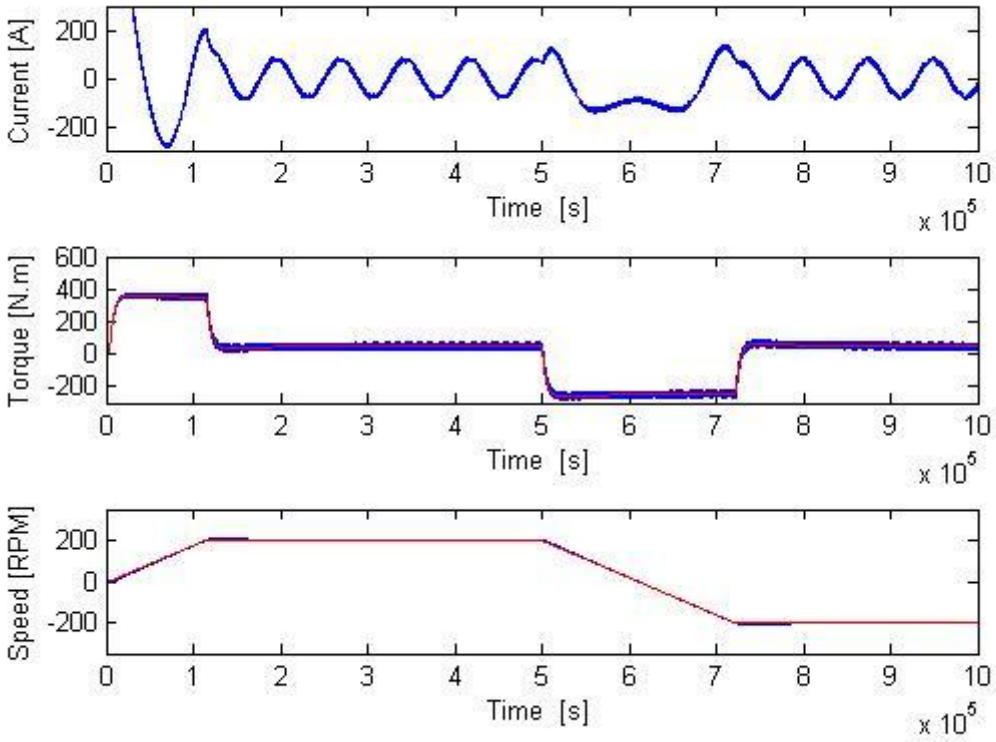

Figure 5.24 – Speed control– Simulation I – SVM – Stator current, torque and speed

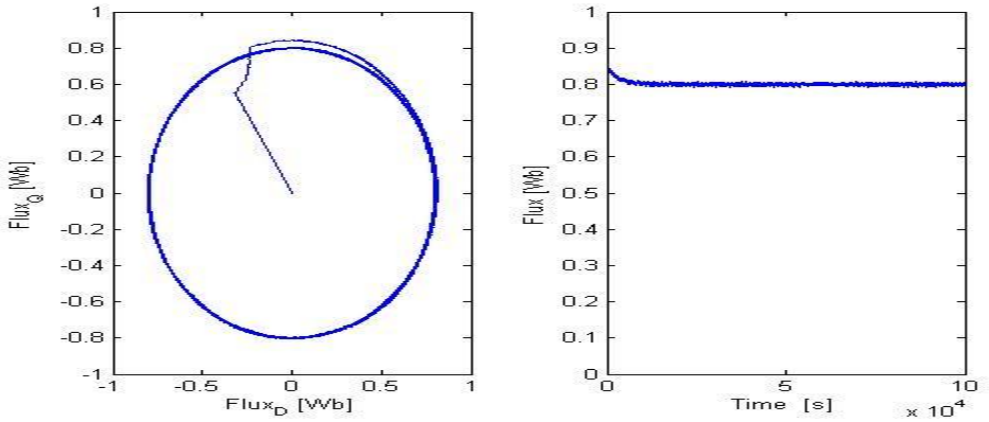

Figure 5.25 – Speed control– Simulation I – SVM – Flux

In both control schemes, one observes that between time instants 0 and 0.1 seconds, when the speed ramp is applied, the reference torque increases. This reaction is expected because, as thoroughly explained in the Chapter 4, the difference between the load and the electromagnetic torque has to be higher than zero in order to achieve an increase in the speed (or acceleration).

Thus, when the speed stabilizes (acceleration is equal to zero), the reference torque has to be equal to the load torque, as it is achieved in both control schemes. When a speed reversal is imposed, the opposite reaction in the torque is verified; ergo the reference torque is set to a negative value until the speed stabilizes.

5.3.2 Simulation II

In this final simulation, steady and transient states under different load scenarios are observed. In table 5.6 is presented the reference speed and load torque assigned at each instant.

Table 5.6 – Final simulation conditions

Time (s)	Reference Speed (RPM)	Load Torque (N.m)
0	100	0
0.5	100	100
1	200	100
1.5	200	-100
2	300	-100

5.3.2.1 Direct Torque Control

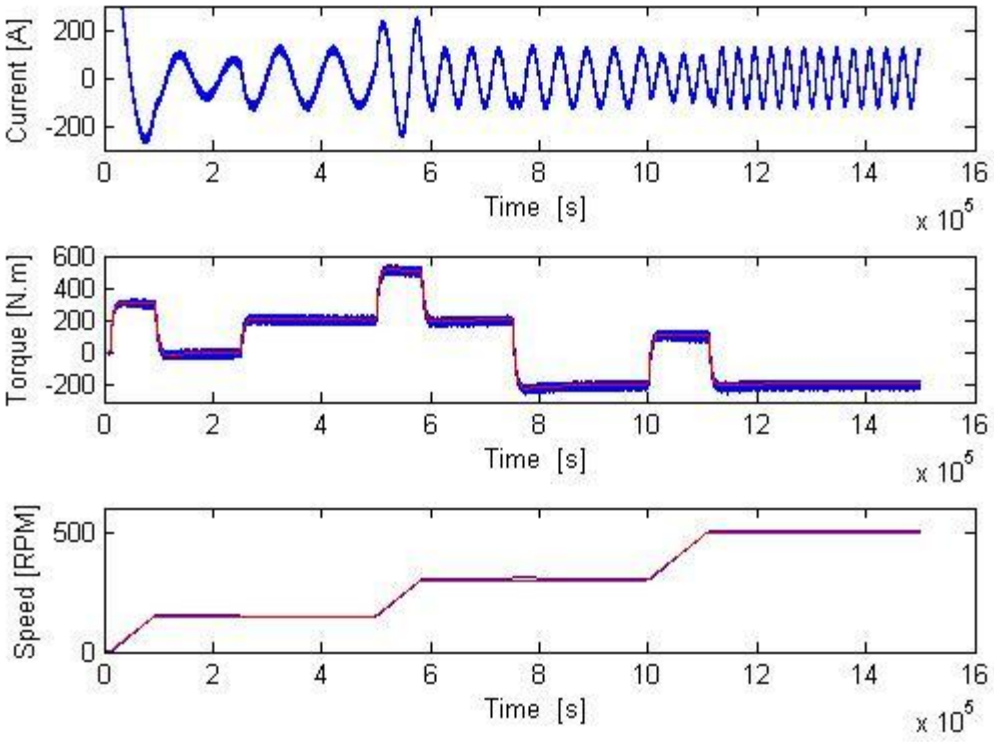

Figure 5.26 – Speed control– Simulation II – DTC – Stator current, torque and speed

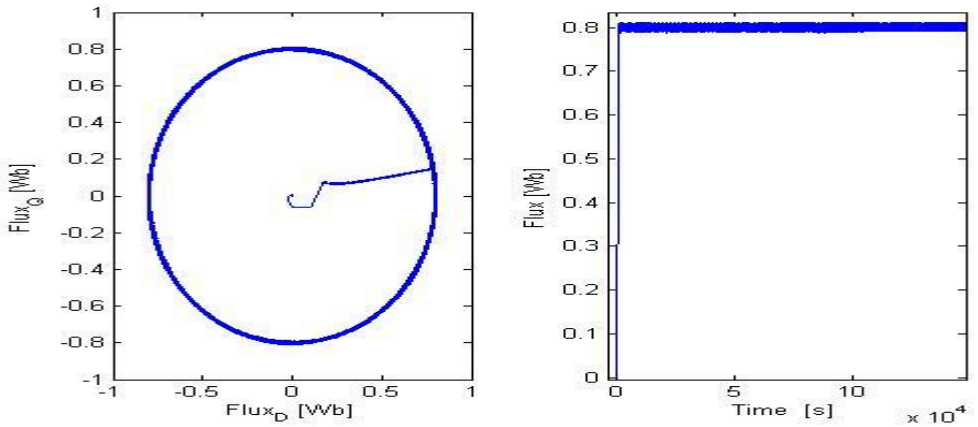

Figure 5.27 – Speed control– Simulation II – DTC – Flux

5.3.2.2 Direct Torque Control with Space Vector Modulation

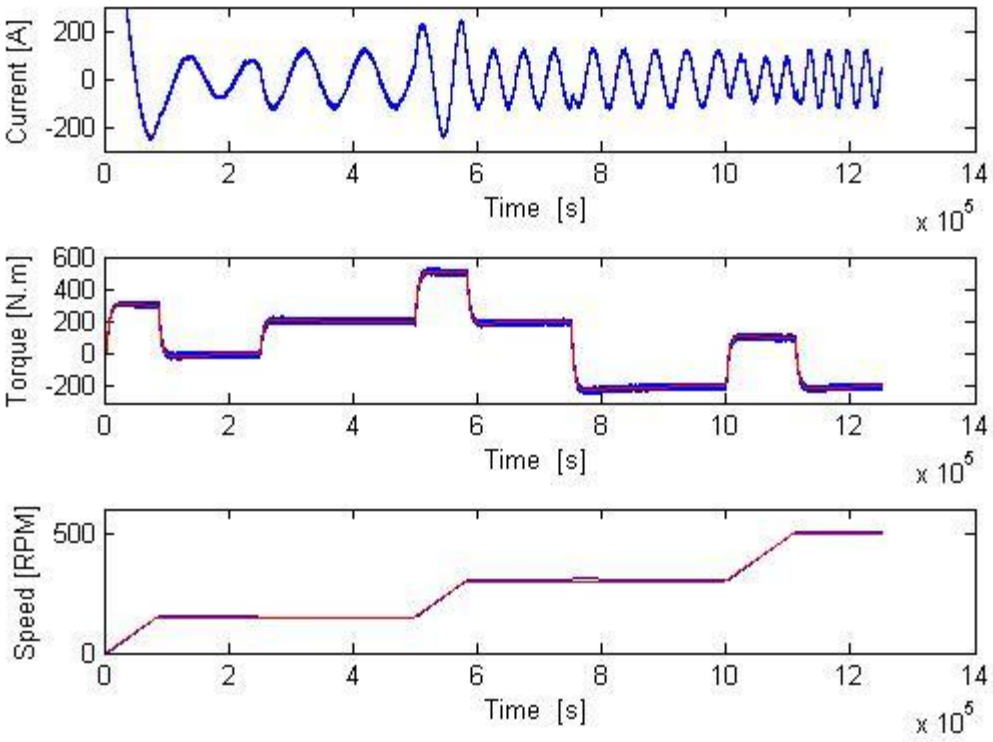

Figure 5.28 – Speed control– Simulation I – SVM – Stator current, torque and speed

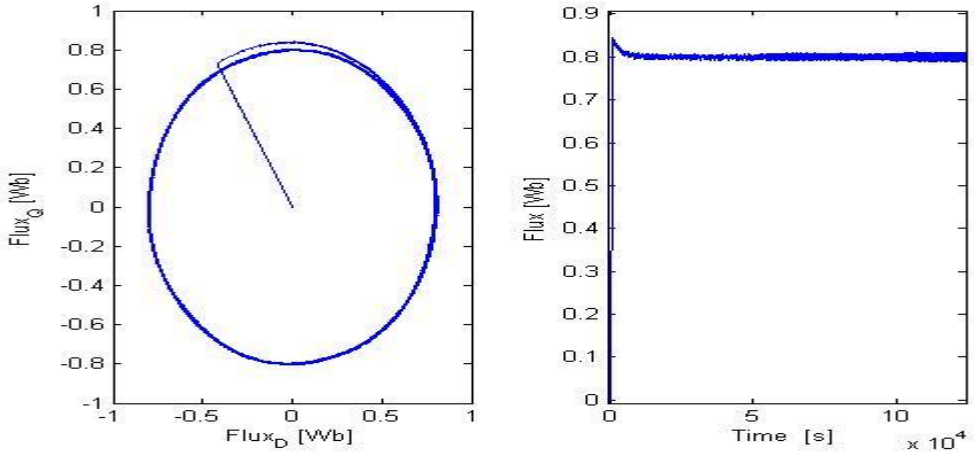

Figure 5.29 – Speed control– Simulation II – DTC – Flux

At time t = 0 s, the speed set point is 500 rpm. Observe that in both control schemes, the speed follows precisely the acceleration ramp.

At t = 0.5 s, a load torque is applied to the motor shaft while the motor speed is still ramping to its final value. This forces the electromagnetic torque to increase the user-defined maximum value and then to stabilize at 500 N.m once the speed ramping is completed and the motor has reached 200 rpm.

At t = 2 s, the speed set point is changed to 300 rpm. The speed increases to this value by following precisely the acceleration ramp even though the mechanical load is decreased abruptly, passing from 100 N.m to - 100 N.m, at t = 1.5 s. Shortly after, the motor speed stabilizes at 500 RPM.

Table 5.7 – Speed control deviation results

Evaluation	DTC	DTC-SVM
Simulation I		
Torque Standard Deviation [N.m]	10,6984	8,6146
Flux Standard Deviation [Wb]	0,0619	0,0387
Simulation II		
Torque Standard Deviation [N.m]	11,0736	8,6431
Flux Standard Deviation [Wb]	0,0623	0,0389

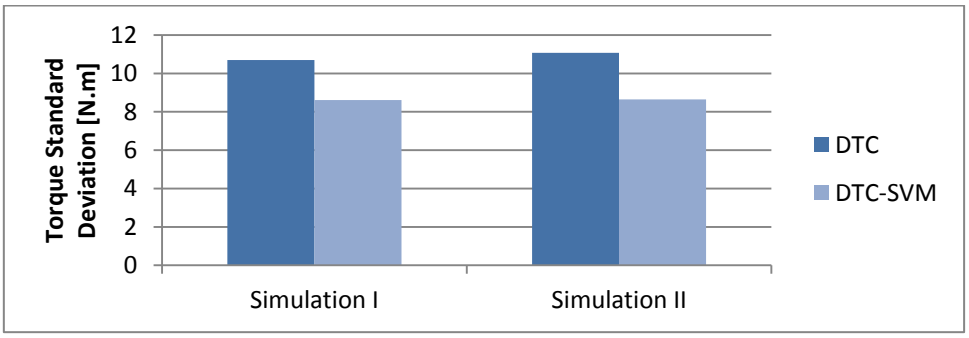

Figure 5.30 – Speed control – Torque Standard Deviation

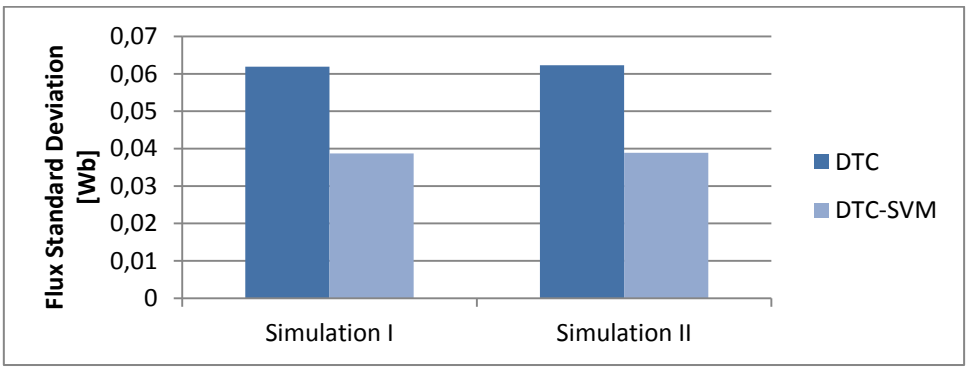

Figure 5.31 – Speed control – Flux Standard Deviation

The simulation results show that the proposed controller scheme for DTC-SVM has achieved a rapid response and a lower torque ripple relative to electromagnetic DTC. Also the results obtained for all schemes presented herein were shown to be consistent with the results reported in the literature.

6

CONCLUSION

This thesis studied basic problems related to topology solutions, investigation and simulation of an inverter-fed induction machine drive. System efficiency is an important consideration when inverters are used in motor drive applications. One approach to achieving improved efficiency is to replace the usually-used two-level inverters with a three-level configuration. Although three-level inverters have added complexity, partitioning the circuits in modules according to their power handling requirements can overcome circuit complexity disadvantages.

After review of basic three-level inverter topologies further considerations have been concentrated on Neutral Point Clamped (NPC) converter. When implementing multilevel converter, one of the most important tasks is selection of appropriate modulation strategy. Since 3L-NPC converters are mainly applied in high power systems; the problem of switching losses becomes extremely important. Thus, the author has evaluated and compared in detail two commercially available NPC topologies, regarding harmonic spectrum and converter losses.

The real benefit of multi-level level inverters is the reduced stress on the power switches, owing to the lower losses as well as the fact that the output voltage switches through three voltage levels. The resultant output-voltage waveform is almost sinusoidal with a reduced harmonic distortion, leading to the use of smaller output filters.

The primary contribution of this thesis work is the development, analysis and simulation of DTC and DTC-SVM on an induction motor. Its principles and basic concepts have been introduced and thoroughly explained. The simulations were performed using the software Matlab/ Simulink. In order to cover most of the situations that the motor would be exposed in real conditions, different operating conditions were set. When these tests were imposed on the induction motor, the proposed control methods (DTC and DCT-SVM) ensured a rapid response. However, the simulation results show that the proposed controller scheme for DTC-SVM has achieved a lower electromagnetic torque ripple. Also the results obtained for all schemes presented revealed to be consistent with the results reported in the literature.

From the analysis of these results the author establishes the following remarks:

1. Both control schemes achieve a rapid response.

2. The simulation results obtained with a three-level VSI illustrate a considerable reduction in torque ripple, flux ripple, distortion in stator currents and switching frequency when compared to the existing Classical DTC system utilizing switching table (due to the SVM control technique).

3. Constant switching frequency is obtained using SVM, resulting in lower converter losses.

6.1 Future work

Although this dissertation has covered many issues and challenges of the neutral point clamped multi-level inverter induction motor drives, additional work has been left for future research.

Some of those possible works are listed below:

- **Neutral point voltage control**

  Commercially available NPC inverters make it possible to construct medium voltage drives with high voltage IGBTs. But neutral point (NP) voltage issues make costly and bulky transformers necessary in commercial systems. Although the proposed approach to control NP potential was designed and simulated through this work, it needs further investigation. Also, NP voltage variation controlled through a buck-boost circuit by the method of controlling NP current could be a good topic investigated in future work.

- **Sensorless speed control**

  Many motion control applications require the use of a position transducer for speed or position feedback, such as an encoder or resolver. Some of systems utilize velocity transducer as well. These sensors add cost, weight, and reduce the reliability of the system. Also, a special mechanical arrangement needs to be made for mounting the position sensors. An extra signal wires are required from the sensor to the controller. Additionally, some type of position sensors are temperature sensitive and their accuracy degrades, when the system temperature exceed the limits. Therefore, the research in the area of sensorless speed control of IM could also be a good topic of investigation in the future, because of the elimination of the feedback wiring, reduced cost, and improved reliability.

- **Fault diagnosis in multilevel converters**

  Since a multilevel converter is normally used in medium to high power applications, the reliability of the multilevel converter system is very important. Thus faults should be detected as soon as possible after they occur, because if a motor drive runs continuously under abnormal conditions, the drive or motor may quickly fail.

REFERENCES

[1] M.E.H. Benbouzid et *al.*, Electric motor drive selection issues for HEV propulsion systems: A comparative study, *IEEE Trans. Vehicular Technology*, vol. 55, n°6, pp. 1756-1764, November 2006.

[2] Holtz, J. 1995. "The Representation of AC Machine Dynamics by Complex Signal Flow Graphs", in IEEE Trans. Ind. Appl., Vol. 42, No. 3, pp. 263-271.

[3] Guzinski, J *et al*.,Sensorless induction motor drive for electric vehicle application, International Journal of Engineering, Science and Technoology, 2010 pp.20-34

[4] Adam, Ali A., Gulez, Kayhan, Torque control of PMSM and associated harmonic ripples, Fatih Einversity, Electrical-Electronics Eng. Dept.

[5] Chin, Y.K., Soulard, J., A permanent magnet synchronous motor to traction applications of electric vehiclesm Royal Institute of Technology (KTH), Stockholm, Sweden

[6] Hassankhan, E., Khaburi, D., DTC-SVM scheme for induction motors with a three-level inverter, World Acafemy of Science, Engineering and Technology 2008.

[7] D. Casadei, F. Profumo, G. Serra, A. Tani, "FOC and DTC: two viable schemes for induction motors torque control", IEEE Transactions on Power Electronics, Vol. 17, Issue: 5, Sept. 2002,pp.779-787.

[8] D. Casadei, G. Serra, A. Tani, "Constant frequency operation of a DTC induction motor drive for electric vehicle", Proc. of ICEM Conf., Vol. 3, 1996, pp. 224-229.

[9] Tsung-Po Chen, Yen-Shin Lai, Chang-Huan Liu, "A new space vector modulation technique for inverter control" Power Electronics Specialists Conference, 1999. PESC 99. 30th Annual IEEE, Vol. 2, 27 June-1 July 1999, pp.777-782.

[10] Kantari, H. ,K direct torque control of induction motor using space vector modulation, International Journal of Modern Engineering Research, Vol.2, Issue5, Oct 2012

[11] Rodriguez,J. *et al*, Multilevel Voltage Source Converter Topologies for Industrial Medium Voltage Drives, IEEE Transactions on Industrial Electronics, Vol.54, 2007

[12] S. Bum-Seok, G. Sinha, M. D. Manjrekar, and T. A. Lipo, "Multilevel Power Conversion - An Overview Of Topologies And Modulation Strategies," in *Optimization of Electrical and Electronic Equipments, 1998. OPTIM '98. Proceedings of the 6th International Conference on*, 1998, pp. AD-11-AD-24.

[13] T. A. Meynard and H. Foch, "Multi-level conversion: high voltage choppers and voltage-source inverters," in *Power Electronics Specialists Conference, 1992. PESC '92 Record., 23rd Annual IEEE*, 1992, pp. 397-403 vol.1.

[14] J. Rodriguez, J. Pontt, P. Lezana, and S. Kouro, "Tutorial on Multilevel Converters," in *PELINCEC International Conference on Power Electronics and Intelligent Control for Energy Conservation*, Warsaw, 2005.

[15] Inti, V, Murthy,V.V., Modulation and simulation of multilevel inverter using switched/parallel DC voltage, Department of Electrical and Electronics ENg. JNT University, Kakinada, India

[16] J. S. Lai, F, Z. Peng, “Multilevel converters - a new breed of power converters,” IEEE Trans Indust~ Applications, vol. 32. no. 3, May 1996,pp. 509-517.

[17] Z. Tan, Y. Li, and M. Li, "A direct torque control of induction motor based on three-level NPCinverter," 2001.

[18] R. Zaimeddine, L. Refoufi, and E. M. Berkouk, "An Improved Direct Torque Control Strategy for Induction Motor Drive," International Journal of Electrical and Power Engineering, Medwell Journals, vol. 1, pp. 21 - 27, 2007.

[19] M. F. Escalante, J. C. Vannier, and A. Arzande, "Flying capacitor multilevel inverters and DTC motor drive applications," *IEEE Transactions on Industrial Electronics,* vol. 49, pp. 809-815, 2002.

[20] T. G. Habetler, F. Profumo, M. Pastorelli, and L. M. Tolbert, "Direct torque control of induction machines using space vector modulation," *IEEE Transactions on Industry Applications,* vol. 28, pp. 1045-1053, 1992.

[21] Nabea, I. Takahashi and H. Akagi, “ A New Neutral-Point-Clamped PWM Inverter”, IEEE Transactions on Industry Applications, Vol. IA-17, No. 5, September/October 1981, pp.518-523.

[22] Y. Wang, H. Li, and X. Shi, "Direct Torque Control with Space Vector Modulation for Induction Motors Fed by Cascaded Multilevel Inverters," 2006, pp. 1575-1579.

[23] R. Toufouti, S. Meziane, and H. Benalla, "Direct Torque Control for Induction Motor Using Intelligent Techniques," Journal of Theoretical and Applied Information Technology, 2007.
[24] Alonso, O.; Marroyo, L.; Sanchis, P.; Gubia, E.; Guerrero, A.; "*Analysis of neutral-point voltage balancing problem in three-level neutral-point-clamped inverters with SVPWM modulation*", IECON 02 [Industrial Electronics Society, IEEE 2002 28th Annual Conference of the, Volume 2, 5-8 Nov. 2002 Page(s):920 - 925 vol.2
[25] Busquets-Monge, S.; Bordonau, J.; Boroyevich, D.; Somavilla, S.; "The nearest three virtual space vector PWM - a modulation for the comprehensive neutral-point balancing in the threelevel NPC inverter", Power Electronics Letters, IEEE, Volume 2, Issue 1, March 2004 Page(s):11 – 15
[26] Bueno, E.J.; Garcia, R.; Marron, M.; Urena, J.; Espinosa, F.; "Modulation techniques comparison for three levels VSI converters", IECON 02 [Annual Conference of the Industrial Electronics Society, IEEE 2002 28th], Volume 2, 5-8 Nov. 2002 Page(s):908 – 913
[27] Buja, G.S.; Kazmierkowski, M.P.; „*Direct torque control of PWM inverter-fed AC motors – a survey*", IEEE Transactions on Industrial Electronics, Volume 51, Issue 4, Aug. 2004 Page(s):744 – 757
[28] Celanovic, N.; Boroyevich, D.; "A comprehensive study of neutral-point voltage balancing problem in three-level neutral-point-clamped voltage source PWM inverters", Power Electronics, IEEE Transactions on, Volume 15, Issue 2, March 2000 Page(s):242 – 249
[29] Martins, C.A.; Roboam, X.; Meynard, T.A.; Carvalho, A.S.; "Switching frequency imposition and ripple reduction in DTC drives by using a multilevel converter", IEEE Transactions on Power Electronics, Volume 17, Issue 2, March 2002 Pages:286 – 297
[30] Schibli N. P., Nguyen T., and Rufer A. C.; "A Three-Phase Multilevel Converter for High-Power Induction Motors", IEEE TRANSACTIONS ON POWER ELECTRONICS, VOL. 13, NO. 5, SEPTEMBER 1998, pp. 978-986
[31] Ikonen,M., *et al*,Two-level and three-level converter comparison in wind power application, Department of Electrical Engineering, Lappeenranta University of Technology
[32] Uwe Drofenik, Johann W. Kolar. "A General Scheme for Calculating Switching- and Conduction Losses of Power Semiconductors in Numerical Circuit Simulations of Power Electronic Systems." Proceedings of IPEC'05.
[33] Ch. French, P. Acarnley, "Direct Torque Control of Permanent Magnet Drivers", IEEE Transaction on Industrial Application, Vol. 32, No. 5, 1996, pp. 1080-1088.
[34] Zhiguo Pan; Fang Zheng Peng; Corzine, K.A.; Stefanovic, V.R.; Leuthen, J.M.; Gataric, S.; "*Voltage balancing control of diode-clamped multilevel rectifier/inverter systems*", IEEE Transactions on Industry Applications, Volume 41, Issue 6, Nov.-Dec. 2005 Pages:1698 – 1706